Control System Design

Richard Tymerski
and
Frank Rytkonen

ii

Preface

This is the preface.

Contents

Part I

Classical Control

Chapter 1

Compensators for the Buck Converter

1.1 Introduction

The buck converter is perhaps the simplest DC converter topology, yet one of the most useful. It is widely used in industry, it is a clear and simple example that is helpful in understanding the principles of switching converters, and it can be used to derive more complicated topologies. In light of this general usefulness, it is instructive to consider how one can use control systems to regulate the operation of such a converter. This serves not only to illustrate how switching converters can be controlled, but also results in a practical circuit for use in power supplies, voltage regulators, and so forth.

Since it is desirable to design an effective compensator for the buck converter, this chapter will consider the various properties of three different compensation schemes. The first section will present a basic discussion of the buck converter, its open-loop and uncompensated closed-loop behavior, and introduce an example converter that will be used for all the designs. The next section will present a basic attempt to counteract some of the undesirable properties of the buck converter with a proportional-integral compensator. The third section will detail a somewhat more sophisticated attempt to improve performance by use of a lead compensator. The last compensator discussed will be the combination of the lead and proportional-integral compensators to obtain the benefits of both. Each section will present the design of the compensator for the example converter given in the first section, derive an op-amp circuit to implement it, and evaluate the performance of the compensated system through simulation. The conclusion will summarize the results and compare the various designs.

1.2   The Uncompensated Buck Converter

The basic buck converter topology is shown in Figure 1.1. The function of this converter is transform a higher input DC voltage, V_g, into a lower output DC voltage, V. The conversion ratio, in steady-state, is $V = DV_g$, where D is the duty ratio of the switch. Thus, the output voltage is determined by both the input voltage and the switching duty cycle. In addition, non-ideal effects, most notably the discontinuous conduction mode, make the output voltage dependent on the load current. For this chapter, however, the controlled variable is considered to be the duty cycle, with variations in the input voltage considered to be disturbances, and the load current assumed to be constant, with the converter operating in the continuous conduction mode. The response of a buck converter operating in steady-state to a step change in the input voltage is shown in Figure 1.2. In open-loop, the converter exhibits large overshoot, large steady-state error, and excessive oscillations.
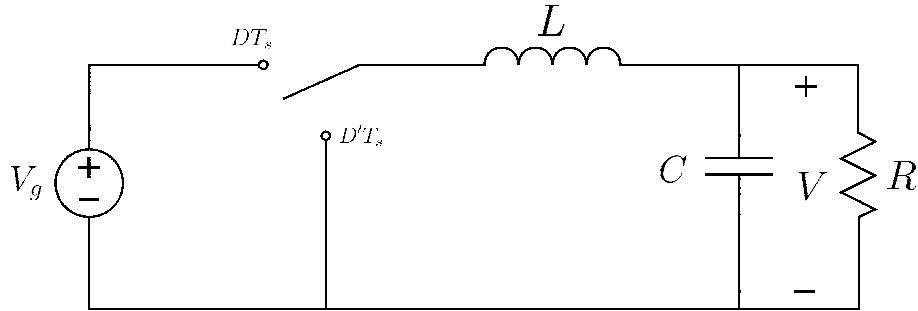
Figure 1.1: The ideal buck converter

Reference [1], Chapter 8 gives the small-signal averaged transfer function for the operation of the buck converter in the continuous conduction mode. This is the model that will be used in the following analysis. The model basically consists of two transfer functions, one which models the influence of the duty cycle on the output, $G_{vd}(s)$, and one which models the influence of the input voltage on the output, $G_{vg}(s)$. For the purposes of this chapter, the first will be considered the control input, while the second is a source of disturbances. The general forms of the these transfer functions are the same.

$$G_{vd}(s) = \frac{G_{d0}}{1 + \frac{s}{Q\omega_0} + \left(\frac{s}{\omega_0}\right)^2} \text{ and} \qquad (1.1)$$

$$G_{vg}(s) = \frac{G_{g0}}{1 + \frac{s}{Q\omega_0} + \left(\frac{s}{\omega_0}\right)^2} \; , \qquad (1.2)$$

where

$$G_{g0} = D, \quad G_{d0} = \frac{V}{D}, \quad \omega_0 = \frac{1}{\sqrt{LC}}, \quad \text{and} \quad Q = R\sqrt{\frac{C}{L}}$$

Figure 1.2: Response of open-loop buck converter to input voltage step

To correct the undesirable behavior demonstrated in response to a change in the input voltage, the buck converter can be placed in a control loop, as shown in Figure 1.3, where $H(s)$ is the gain of the output sensor, $G_c(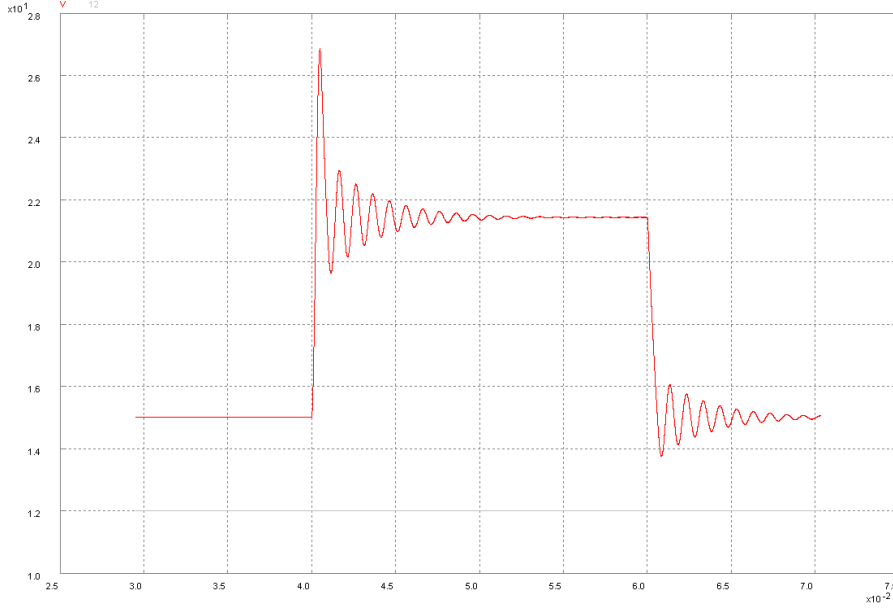s)$ is the transfer function of the compensator, and the $\frac{1}{V_m}$ factor is the transfer function of the pulse-width modulator used to drive the transistor that implements the ideal switch shown above. Usually, $H(s)$ and $\frac{1}{V_m}$ will be simple gains. One method in classical control theory to analyze systems and design controllers, and the method that will be used here, is by using the loop gain. For the control loop shown in Figure 1.3, the loop gain is

$$T(s) = \frac{G_c(s)G_{vd}(s)H(s)}{V_m} \tag{1.3}$$

This chapter will use an example converter to illustrate the design and effectiveness of the various compensators. Namely, the converter will have an input voltage $V_g = 28$ V, an output voltage $V = 15$ V, and a load of $R = 3$ Ω. The capacitor and the inductor values will be $C = 500$ μF and $L = 50$ μH, respectively. The peak-to-peak amplitude, V_m, of the sawtooth driving the modulator will be 4 V, the sensor gain will be $H = \frac{1}{3}$ and the switching frequency $f_s = 100$ kHz. The designs will be evaluated based on their gain and phase margins, and on how the converter responds to a input voltage step from 28 V to 40 V and back to 28 V. To have a basis of comparison for the compensated converter, the behavior of the buck in an uncompensated configuration must be examined.

Using the control-to-output transfer function given earlier, these values can
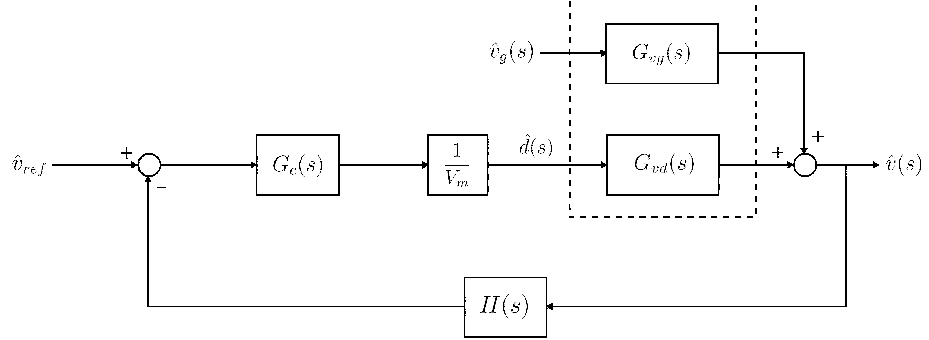
Figure 1.3: Buck converter control loop

be used to derive a more concrete expression for the loop gain. Since the loop is as yet uncompensated, $G_c(s) = 1$.

$$T(s) = \frac{G_c(s)G_{vd}(s)H(s)}{V_m} = \left(\frac{H}{V_m}\right) \frac{G_{g0}}{1 + \frac{s}{Q\omega_0} + \left(\frac{s}{\omega_0}\right)^2}$$

As can be seen, the uncompensated loop gain of the buck converter is a standard second-order system of the form

$$T(s) = \frac{T_o}{1 + \frac{s}{Q\omega_0} + \left(\frac{s}{\omega_0}\right)^2} \ , \tag{1.4}$$

where

$$T_o = \frac{G_{d0}H}{V_m} = \frac{28}{(3)(4)} = 2.33$$

$$\omega_0 = \frac{1}{\sqrt{LC}} = \frac{1}{\sqrt{(50 \ \mu H)(500 \ \mu F)}} = 2000\sqrt{10} \text{ rad/s} \Rightarrow f_0 = 1 \text{ kHz, and}$$

$$Q = R\sqrt{\frac{C}{L}} = 3 \ \Omega\sqrt{\frac{500 \ \mu F}{50 \ \mu H}} = 3\sqrt{10} = 9.49 \Rightarrow 19.5 \text{ dB}$$

A Bode plot of this loop gain is shown in Figure 1.4. The phase margin can be determined directly from the plot. In the asymptotic approximation, the closed-loop buck converter has a phase margin of $0°$. Since the phase asymptote reaches but does not cross $-180°$, the gain margin can be said to be infinite. Thus, without any compensator, the buck converter has an infinite gain margin but a $0°$ phase margin. Such a system is stable but will exhibit oscillations and other behavior that is generally considered undesirable. A plot of the step response of the converter in this configuration is shown in Figure 1.5. As can be seen, the oscillations in the output voltage present in the open-loop case are still present, though reduced in amplitude by the application of feedback, and there is still a steady-state error to a change in input voltage. Both of these issues will be addressed in the compensator designs that follow.
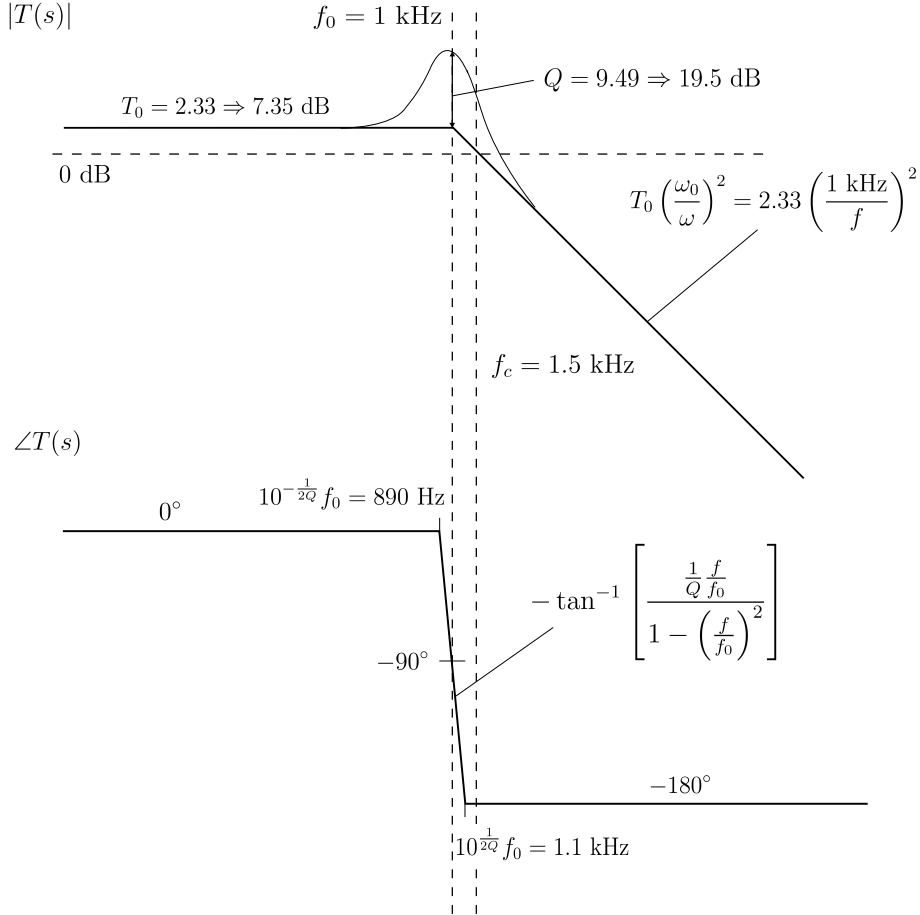
Figure 1.4: Uncompensated loop gain

1.3 Proportional-Integral Compensation

A simple but fairly effective way to improve the characteristics of the buck converter is to use a dominant-pole or integral compensator. This is simply a compensator with a single pole at $s = 0$ and a gain.

$$G_c(s) = \frac{G_{c0}}{s} \tag{1.5}$$

Although the plain integral compensator could be used for this purpose, it is difficult to obtain good performance using this type of compensator. It is more usual to use a proportional-integral or PI compensator, as discussed in Chapter 7 of [2] This is essentially the same as the integral compensator, but with a zero introduced at some higher frequency. The transfer function of the
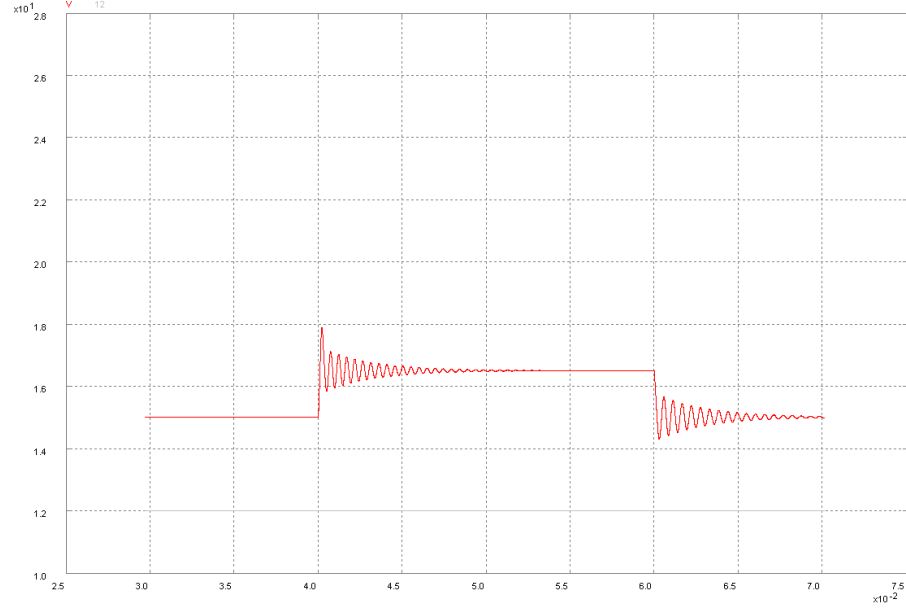
Figure 1.5: Step response of uncompensated buck converter

PI compensator is

$$G_c(s) = \frac{G_{c0}\left(1 + \frac{s}{\omega_z}\right)}{s} \tag{1.6}$$

As can be seen from the plot in Figure 1.6, this compensator provides a high gain at low frequencies, which falls off at -20 dB per decade and then levels out at the zero frequency, f_z. The phase is initially $-90°$, which increases by a rate of $45°$ per decade starting at $\frac{f_z}{10}$ to a maximum of $0°$ at $10f_z$. The benefit obtained by using a PI compensator is that the large low-frequency gain will eliminate steady-state error to step disturbances.

In general, however, this cannot be attained while still having acceptable gain and phase margins using a simple PI compensator. The design shown here will concentrate on low-frequency gain at the expense of gain and phase margins, although these are still a consideration. The unity-gain crossover frequency should be placed before the major phase downturn in the compensated loop. The design here will use $f_z = \frac{f_0}{10} = 100Hz$ and place the unity-gain crossover at this same frequency, to avoid too much interaction in the phase responses while still providing higher gains.

The loop gain of the buck converter with the PI compensator is shown in Figure 1.7, which can be expressed as

$$T(s) = T_0 G_{c0} \frac{1 + \frac{s}{\omega_z}}{s\left(1 + \frac{s}{Q\omega_0} + \left(\frac{s}{\omega_0}\right)^2\right)} \tag{1.7}$$
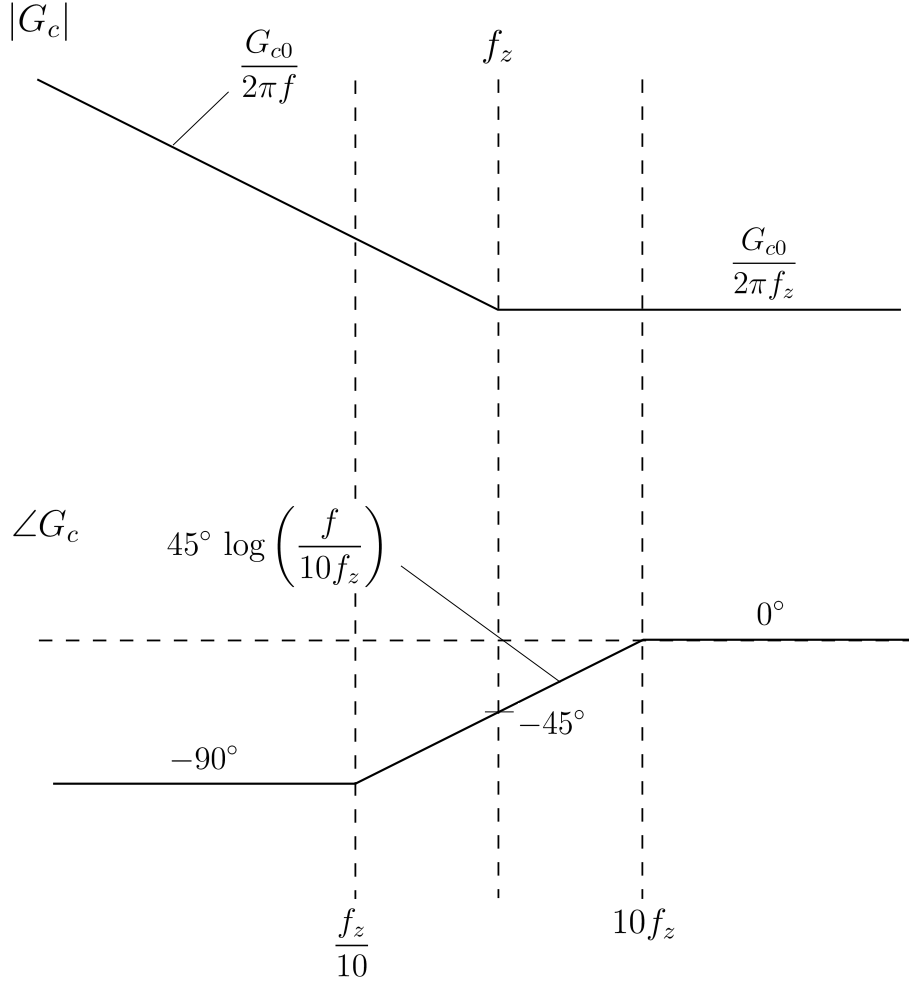
Figure 1.6: PI compensator transfer function

Using the expressions given on the Bode plot, the value of G_{c0} can be calculated. To find the low-frequency gain, one can simply use the gain expression at the new crossover frequency.

$$\frac{T_0 G_{c0}}{2\pi f_c'} = 0 \text{ dB} = 1$$

$$T_0 G_{c0} = 2\pi f_z$$

$$G_{c0} = \frac{2\pi \, (100 \text{ Hz})}{2.33}$$

$$G_{c0} = 270$$

$|T(s)|$

$f_z = f'_c = 100$ Hz $f_0 = 1$ kHz

$Q = 9.49 \Rightarrow 19.5$ dB

0 dB

$\dfrac{T_0 G_{c0}}{2\pi f}$

$\left(\dfrac{f_0}{f}\right)^2$

$\angle T(s)$ $45° \log\left(\dfrac{f}{f_0}\right)$ 890 Hz

$-90°$ $-\tan^{-1}\left[\dfrac{\frac{1}{Q}\frac{f}{f_0}}{1 - \left(\frac{f}{f_0}\right)^2}\right]$

$\dfrac{f_z}{10}$

$-180°$

1.1 kHz
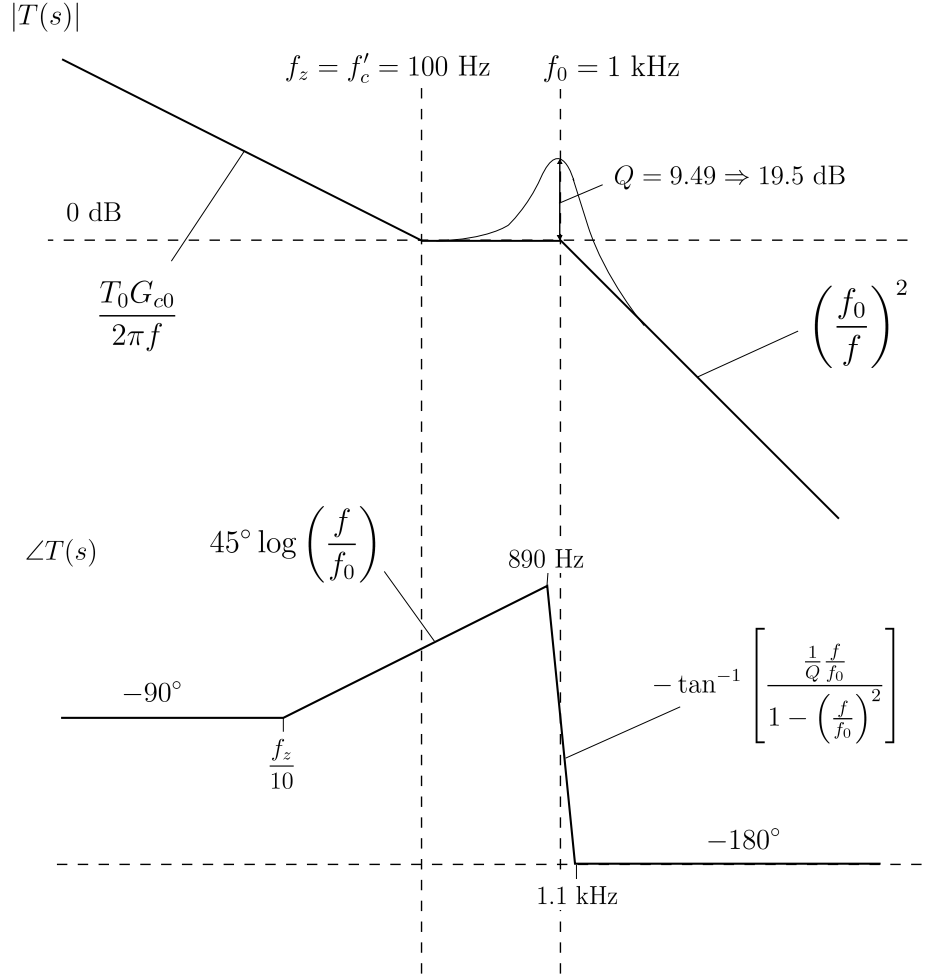
Figure 1.7: Loop gain with PI compensator

Since only G_{c0} and f_z are needed to specify the compensator, the design is complete. The phase margin of this design is the amount by which the phase at the crossover frequency is above $-180°$. This can be found by evaluating the gain asymptote at f_z.

$$\phi_M = 180° + 45° \log\left(\frac{f_z}{f_0}\right)$$

$$\phi_M = 180° + 45° \log\left(\frac{100 \text{ Hz}}{1 \text{ kHz}}\right)$$

$$\phi_M = 135°$$

This is actually a surprisingly high phase margin, which is only due to the asymptotic approximation. Due to the Q of the original circuit, the gain will rise above 0 dB and cross again after the phase downturn, so the actual phase margin is close to 0°. The gain margin, as in the uncompensated case, is actually infinite, since the phase never actually crosses $-180°$, although the asymptote reaches it. Thus, the PI compensated system has essentially the same gain and phase margins as the uncompensated system, and will show similarly undesirable transient characteristics. The presence of higher low-frequency gain, however, will eliminate the steady-state error seen in the uncompensated case.

To be able to simulate the behavior of the compensated buck converter, a control circuit must be derived to implement the PI compensator. Such a circuit is shown in Figure 1.8. This circuit implements the transfer function

$$G_c(s) = -\frac{R_2}{R_1}\left(\frac{R_2Cs+1}{R_2Cs}\right) \tag{1.8}$$

In this circuit, the second resistor and the capacitor set the zero frequency, while the first resistor in combination with these values sets the gain of the compensator. If a value of $R_2 = 100$ kΩ is assumed, then the capacitor value must be

$$\omega_z = \frac{1}{R_2C} \Rightarrow 2\pi\,(100\text{ Hz}) = \frac{1}{(100\text{ k}\Omega)\,C}$$

$$C = \frac{1}{2\pi\,(100\text{ Hz})\,(100\text{ k}\Omega)} \Rightarrow C = 15\text{ nF}$$

Likewise, the value of R_1 to set the gain to the proper value can be found from this value for C.

$$G_{c0} = \frac{1}{R_1C} \Rightarrow 270 = \frac{1}{R_1\,(15\text{ nF})}$$

$$R_1 = \frac{1}{270\,(15\text{ nF})} \Rightarrow R_1 = 240\text{ k}\Omega$$

The reference voltage on the non-inverting input of the opamp for this circuit can be simply 5 V, since there is no direct connection to the output.

The simulated response of the buck with this PI compensator to a step disturbance is shown in Figure 1.9. As would be expected from the phase margin, the system displays large oscillations in the output voltage, although not nearly as large as those of the open-loop converter. The presence of the pole at $s = 0$, however, which is the main purpose of using such a compensator, is quite effective in removing steady-state error. Thus, although some of the transient characteristics are undesirable, the PI compensator is effective in regulating the output to the proper voltage. A method to improve the transient characteristics is examined in the design of the next compensator.

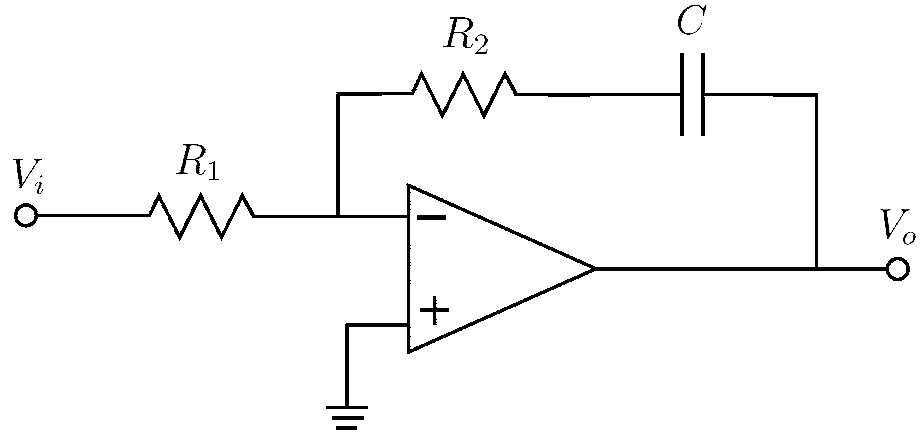Figure 1.8: Op-amp circuit implementation of PI compensator
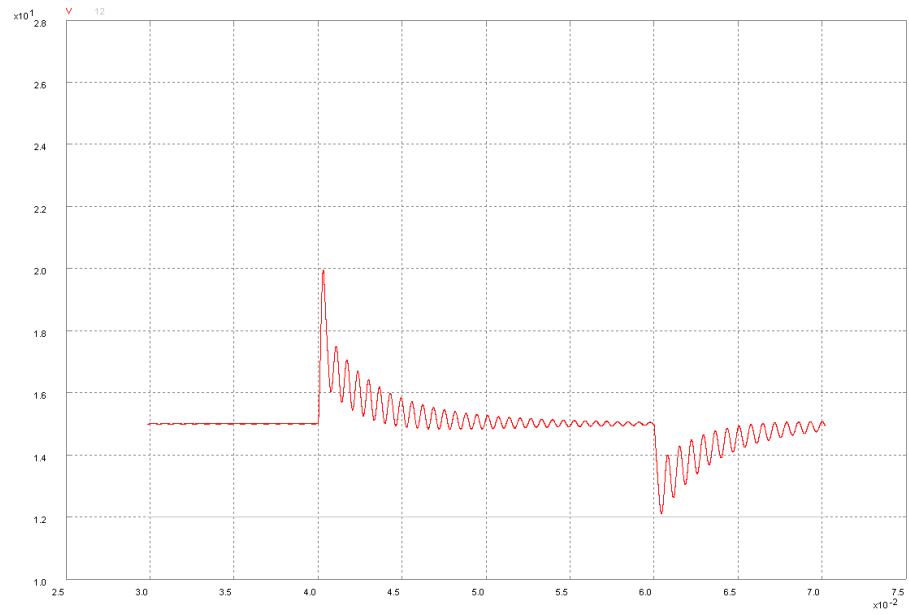
Figure 1.9: Step response of PI-compensated buck converter

1.4   Lead Compensation

A more sophisticated way to improve the performance of the buck converter is with a lead compensator. The transfer function of this compensator is

$$G_c(s) = G_{c0} \frac{\left(1 + \frac{s}{\omega_z}\right)}{\left(1 + \frac{s}{\omega_p}\right)} \ , \tag{1.9}$$

where $\omega_z < \omega_p$. As can be seen from the plot of the transfer function shown in Figure 1.10, the lead compensator provides both a phase boost that is adjustable based on the pole and zero frequencies, and a gain boost at higher frequencies that will result in a higher crossover frequency for the lead-compensated buck converter. Since the one of the most undesirable features of the uncompensated buck is its low phase margin, the phase boost should be chosen to improve the phase margin to an acceptable value. The new crossover frequency can be chosen arbitrarily. The design shown here will be to obtain a 45° phase margin and a crossover frequency of 5 kHz for the loop gain with a lead compensator.
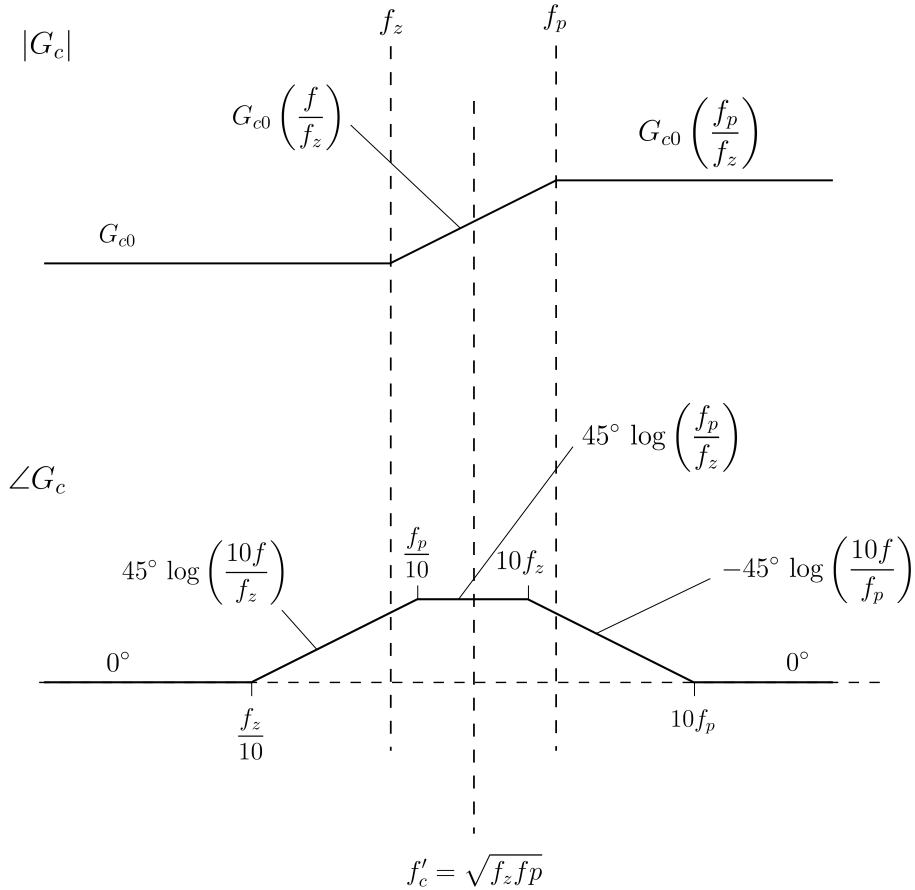
Figure 1.10: Lead compensator transfer function

When the compensator is placed in the loop, the loop gain of the buck
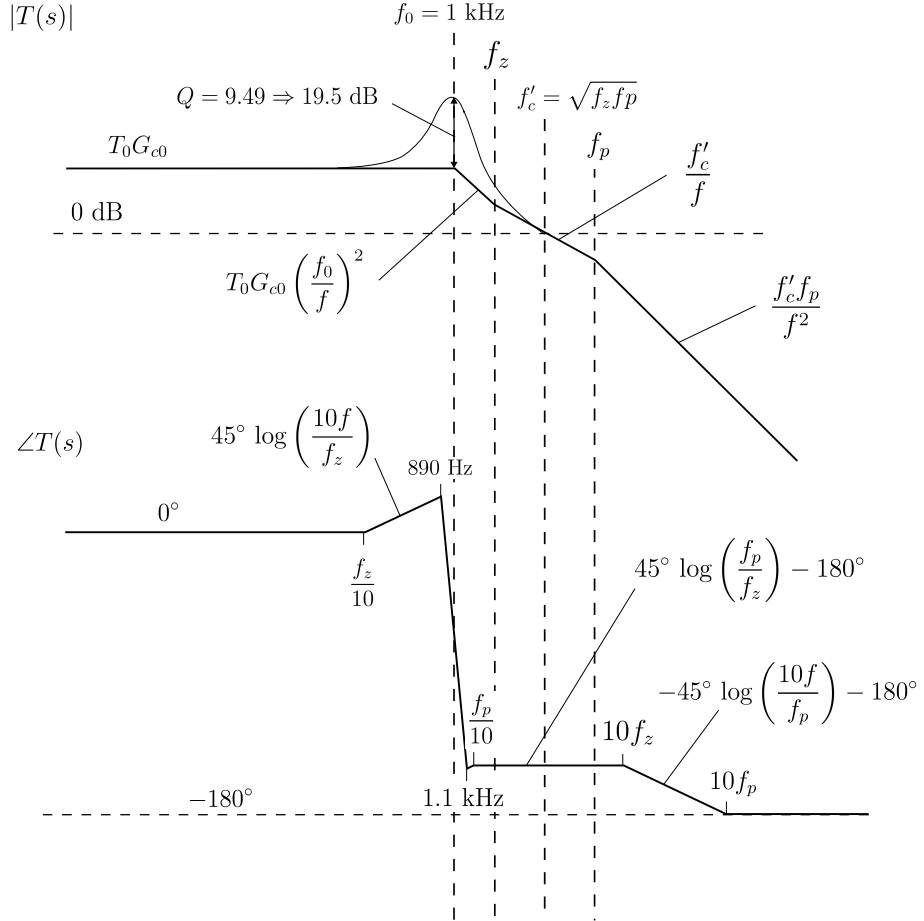
Figure 1.11: Loop gain with lead compensator

converter system becomes

$$T(s) = T_0 G_{c0} \frac{\left(1 + \frac{s}{\omega_z}\right)}{\left(1 + \frac{s}{\omega_p}\right)\left(1 + \frac{s}{Q\omega_0} + \left(\frac{s}{\omega_0}\right)^2\right)} \tag{1.10}$$

The asymptotic Bode plot of this loop gain is shown in Figure 1.11. The expressions shown can be used to place the pole and zero frequencies of the compensator to obtain the desired phase margin and unity-gain crossover. As can be seen, the phase margin of the system is equal to the phase of the lead compensator at the new crossover frequency, f_c'.

$$\phi_M = \text{ Compensator phase at } f_c' = 45° \log\left(\frac{f_p}{f_z}\right)$$

$$45° = 45° \log\left(\frac{f_p}{f_z}\right)$$

$$\frac{f_p}{f_z} = 10^1$$

$$f_p = 10 f_z$$

Also, f_c' will necessarily be the geometric mean of the pole and the zero frequency. Since the phase margin condition gives a relationship between the pole and zero frequencies, this can be used to solve for both.

$$f_c' = \sqrt{f_z f_p}$$

$$5 \text{ kHz} = \sqrt{10 f_z^2}$$

$$f_z = \frac{5 \text{ kHz}}{\sqrt{10}}$$

$$f_z = 1.58 \text{ kHz and } f_p = 15.8 \text{ kHz}$$

These relationships result in the pole and zero frequencies for the lead compensator. To complete the design, the required low-frequency gain G_{c0} of the compensator to place the unity-gain point at the appropriate frequency must be determined. This can be found by equating the values of the gain asymptotes at f_z.

$$T_0 G_{c0} \left(\frac{f_0}{f_z}\right)^2 = \frac{f_c'}{f_z}$$

Substituting the values of f_0 and T_0 for the example converter, and the values of f_z and f_c' as previously calculated, the gain G_{c0} of the compensator is

$$G_{c0} = \frac{1}{T_0} \left(\frac{f_z}{f_0}\right)^2 \frac{f_c'}{f_z}$$

$$G_{c0} = \frac{1}{2.33} \left(\frac{1.58 \text{ kHz}}{1 \text{ kHz}}\right)^2 \frac{5 \text{ kHz}}{1.58 \text{ kHz}}$$

$$G_{c0} = 3.4$$

The resulting compensated system has a phase margin of 45°, as designed for. The gain margin can be found by evaluating the gain at the point the phase crosses $-180°$. This occurs at $10 f_p$.

$$G_M = \text{ Gain below 0 dB at } 10 f_p$$

$$\text{Gain} = \frac{f_c' f_p}{f^2} = \frac{(5 \text{ kHz}) f_p}{(10 f_p)^2} = \frac{5 \text{ kHz}}{100 (15.8 \text{ kHz})}$$

$$\text{Gain} = 0.00317 \Rightarrow -50 \text{ dB}$$

$$G_M = 50 \text{ dB}$$

Since the general desirable gain margin for a stable system is 10 dB, this is quite acceptable. In reality, since the phase only approaches $-180°$, the gain margin of the system will actually be infinite, as in the previous two cases. In any case, this compensated system has very good phase and gain margins.

With all of the parameters of the lead compensator determined, what remains is to implement the compensator using an op-amp circuit and simulate the closed-loop converter to evaluate its performance. A general circuit that can be used to implement any lead or lag compensator is shown in Figure 1.12. The transfer function of this circuit is

$$G_c(s) = -\frac{R_2}{R_1}\left(\frac{R_1 C_1 s + 1}{R_2 C_2 s + 1}\right) \tag{1.11}$$

The resistor ratio sets the low frequency gain, and the two resistor-capacitor pairs set the pole and zero frequencies. Two standard valued resistors that give nearly the required gain are $R_1 = 100$ kΩ and $R_2 = 330$ kΩ. From these values, the capacitor values to set the pole and zero can be calculated.

$$\omega_z = \frac{1}{R_1 C_1} \Rightarrow 2\pi\,(1.58 \text{ kHz}) = \frac{1}{(100 \text{ k}\Omega)\,C_1}$$

$$C_1 = \frac{1}{2\pi\,(1.58 \text{ kHz})\,(100 \text{ k}\Omega)} \Rightarrow C_1 = 1.0 \text{ nF}$$

$$\omega_p = \frac{1}{R_2 C_2} \Rightarrow 2\pi\,(15.8 \text{ kHz}) = \frac{1}{(330 \text{ k}\Omega)\,C_2}$$

$$C_2 = \frac{1}{2\pi\,(15.8 \text{ kHz})\,(330 \text{ k}\Omega)} \Rightarrow C_2 = 33 \text{ pF}$$

It it also necessary to derive a value for the reference voltage on the non-inverting input of the op-amp. The sensed voltage from the output will be 5 V in steady-state as before, and the control voltage should be 2.14 V. Using these in combination with the resistor values for the lead compensator, the reference voltage can be found.

$$V_{ref} = \frac{R_2}{R_1 + R_2}V_{sense} + \frac{R_1}{R_1 + R_2}V_{control}$$

$$V_{ref} = \frac{330 \text{ k}\Omega}{100 \text{ k}\Omega + 330 \text{ k}\Omega}\,(5 \text{ V}) + \frac{100 \text{ k}\Omega}{100 \text{ k}\Omega + 330 \text{ k}\Omega}\,(2.14 \text{ V}) = 4.33 \text{ V}$$

These values were used in the PECS simulator, and the response of the lead-compensated buck converter to a step in the input voltage was simulated as before. The results of the simulation are shown in Figure 1.13. The lead compensator is quite effective in increasing the phase margin of the system. The oscillatory behavior evident in the output voltage of the uncompensated converter is not present, and the magnitude of the steady-state error due to the step is reduced, though not eliminated. Thus, the system with the lead compensator is very stable, but will still exhibit steady-state errors to a step disturbance. To fix this problem, the system type number must be increased by adding a pole at $s = 0$. This is the approach taken in the design of the next and final compensator.
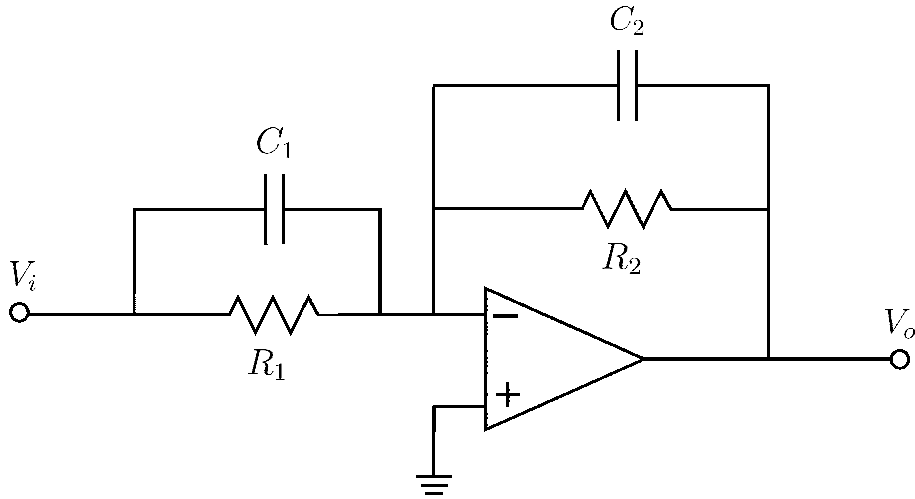
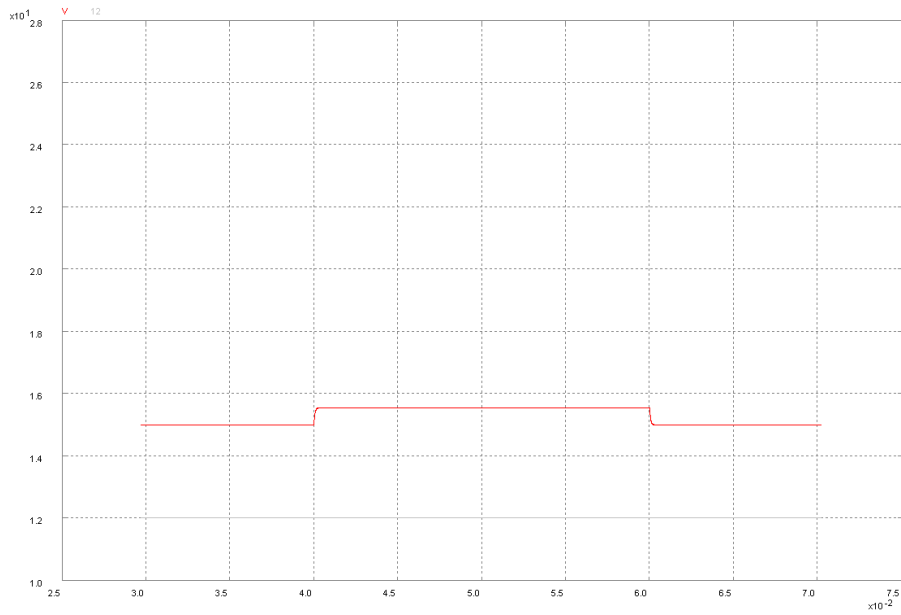Figure 1.12: Op-amp circuit implementation of lead compensator

Figure 1.13: Step response of lead-compensated buck converter

1.5 Combined Lead and PI Compensation

Although both the PI compensator and the lead compensator were able to improve some aspects of the buck converter, neither was able to completely

eliminate its undesirable properties. The lead compensator provided a good transient response, but had a steady-state error to step disturbances, since the compensated loop gain had a type number of 0. The PI compensator had a type number of 1 and thus was able to eliminate steady-state error in response to a step, but had undesirable transient characteristics. By combining the two compensators, one can use the advantages of each to design a more effective compensator. The transfer function for such a combined lead and PI compensator is

$$G_c(s) = \frac{G_{c0}\left(1 + \frac{s}{\omega_{z1}}\right)\left(1 + \frac{s}{\omega_{z2}}\right)}{s\left(1 + \frac{s}{\omega_p}\right)}, \qquad (1.12)$$

where ω_{z2} is the zero introduced by the lead compensator and thus $\omega_{z2} < \omega_p$. Also, to separate the effects of the lead and PI portions of the compensator, it will be assumed here that $\omega_{z1} < \omega_{z2}$. An asymptotic Bode plot of the transfer function of this compensator is shown in Figure 1.14. When ω_{z2} at a frequency 10 times or more greater than ω_{z1}, the design is separated into two essentially independent pieces, the design of a PI compensator at low frequencies and the design of a lead compensator at high frequencies.

A plot of the loop gain of the example converter with a combined lead and PI compensator is shown in Figure 1.15. To determine the design, the two zeros and the pole must be placed. For the phase response of the two compensator portions to have no interaction, ω_{z1} must be two decades below ω_{z2}. For a faster response, it would be good that ω_{z2} be as large as possible, but ω_{z2} should not be too large. The value used here is $f_{z2} = 2$ kHz, and thus $f_{z1} = 20$ Hz. As determined in the design of the lead compensator, to get a phase margin of 45°, $\omega_p = 10\omega_{z2}$, which means that $f_p = 20$ kHz. With the pole and zeros placed, the only factor that remains to determine is the gain. Since it is desirable to have a large gain at low frequencies, the combined compensator will be designed to have the gain factor $G_{c0}T_0$ be 1000. This gives a value of

$$G_{c0}T_0 = 1000 \Rightarrow G_{c0} = \frac{1000}{2.33} \Rightarrow G_{c0} = 430$$

1.6   Performance Evaluation

The gain and phase margins can be found by evaluating the asymptotes at the respective crossover frequencies. The unity-gain crossover frequency is $f_c' = \sqrt{f_{z2}f_p} = 6.32$ kHz. The phase at this frequency is given by

$$\angle T(s) = 45° \log\left(\frac{f_p}{f_{z2}}\right) - 180° = 45° \log\left(\frac{20 \text{ kHz}}{2 \text{ kHz}}\right) - 180° = -135°$$

The phase margin is thus

$$\phi_M = 180° + \angle T(s) = 180° - 135° = 45°$$
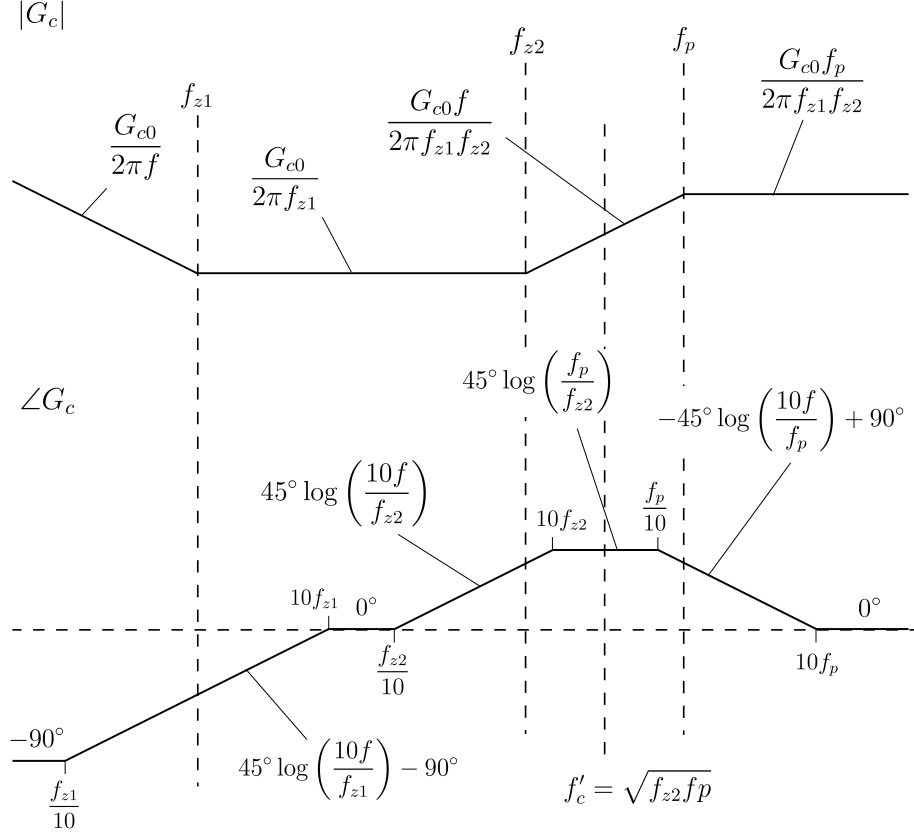
Figure 1.14: Lead and PI compensator transfer function

which is no surprise, since this is what was designed for. A gain margin value could be calculated as before, using $10\omega_p$ as the $-180°$ crossover frequency, but as previously discussed, the actual gain margin will be infinite. Thus, the combined compensator has a $45°$ phase margin, an infinite gain margin, and a pole at $s = 0$. This system should be very stable, exhibit good transient response, and completely compensate for step disturbances with no steady-state error.

The circuit implementation for the lead and PI compensator is simply a lead circuit as shown in Figure 1.12 cascaded with a PI circuit as shown in Figure 1.8. The same expressions given before can be used to find the new component values. The overall gain of the compensator must be 430. For simplicity, the gain of the lead section will be set to 4.3 and the gain of the PI section set to 100. A resistor pair that gives the required gain for the lead section is $R_{L1} = 27$ kΩ and $R_{L2} = 120$ kΩ. Using these values, the capacitor values to place the pole
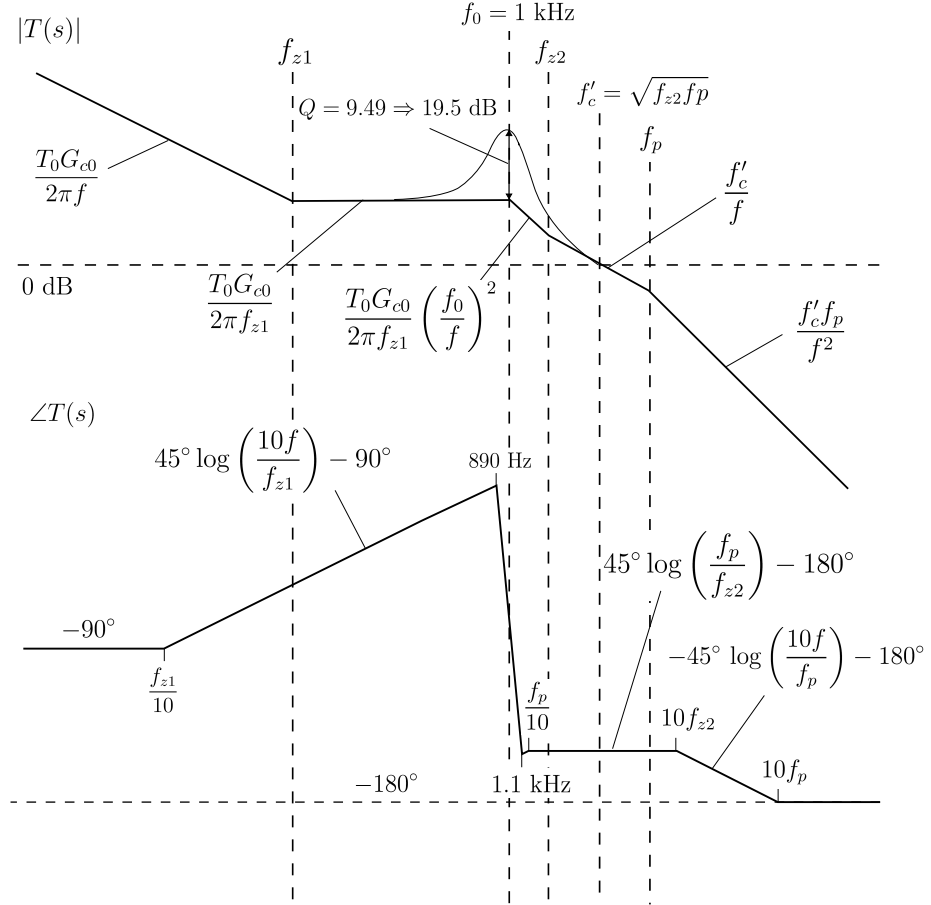
Figure 1.15: Loop gain with lead and PI compensator

and the second zero are simply

$$\omega_{z2} = \frac{1}{R_{L1}C_{L1}} \Rightarrow 2\pi\,(2\text{ kHz}) = \frac{1}{(27\text{ k}\Omega)\,C_{L1}}$$

$$C_{L1} = \frac{1}{(27\text{ k}\Omega)\,(2\pi 2\text{ kHz})} \Rightarrow C_{L1} = 3.0\text{ nF}$$

$$\omega_p = \frac{1}{R_{L2}C_{L2}} \Rightarrow 2\pi\,(20\text{ kHz}) = \frac{1}{(120\text{ k}\Omega)\,C_{L2}}$$

$$C_{L2} = \frac{1}{(120\text{ k}\Omega)\,(2\pi 20\text{ kHz})} \Rightarrow C_{L2} = 68\text{ pF}$$

The PI section must provide a gain of 100 and place ω_{z1} at 20 Hz. If R_{I2} is assumed to be 100 kΩ, then the values of the capacitor and the remaining

resistor can be found.

$$\omega_z = \frac{1}{R_{I2}C_I} \Rightarrow 2\pi \,(20 \text{ Hz}) = \frac{1}{(100 \text{ k}\Omega)\, C_I}$$

$$C_I = \frac{1}{2\pi \,(20 \text{ Hz}) \,(100 \text{ k}\Omega)} \Rightarrow C = 82 \text{ nF}$$

$$G_{I0} = \frac{1}{R_{I1}C_I} \Rightarrow 100 = \frac{1}{R_{I1}\,(82 \text{ nF})}$$

$$R_{I1} = \frac{1}{100 \,(82 \text{ nF})} \Rightarrow R_{I1} = 120 \text{ k}\Omega$$

These values can be used in PECS to simulate the response of the converter. A reference voltage of 5 V can be used, as with the PI compensator.

The simulated response of the combined compensator to the same step disturbance is shown in Figure 1.16. The nature of the improvement is evident. Just as with the PI compensator, the initial disturbance is fully compensated for and the output voltage returns to the set-point value. This is due to the high-low frequency gain, which tends to cause such disturbances to be rejected. As with the lead compensator, the voltage transitions smoothly and with no oscillations, since the phase margin of the system is within the acceptable range. By combining these benefits, this circuit represents a fairly good method of controlling the output of a buck converter
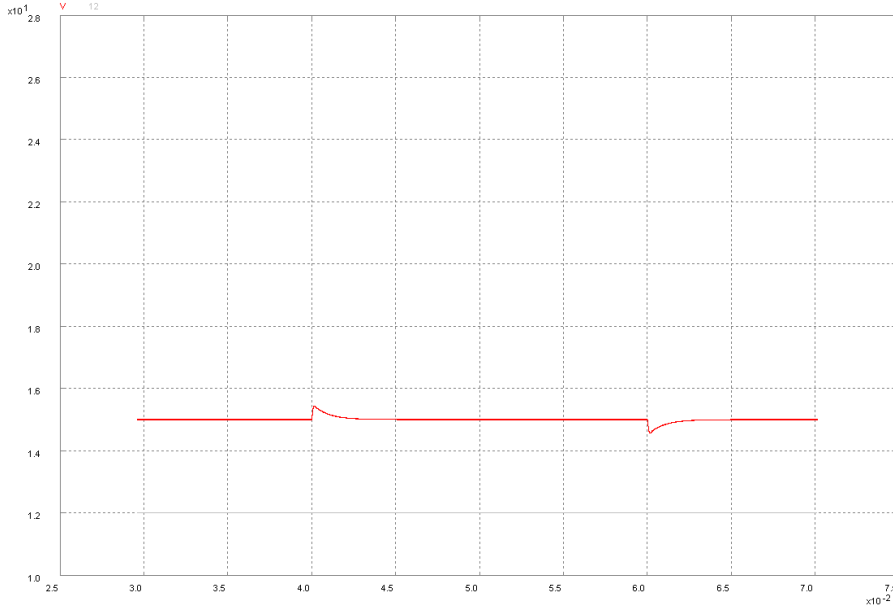
Figure 1.16: Step response of lead- and PI-compensated buck converter

1.7   Conclusion

This chapter has discussed the design of three different compensators for the buck switching converter, and evaluated their performance based on phase margins and the response to an input voltage step. The first design was a PI compensator, which provided good voltage regulation but poor transient performance. The second design was a lead compensator, which by increasing the phase margin of the system yielded very good transient response, but which still demonstrated a steady-state error to a step. By combining these two approaches, the final lead and PI compensator provides an excellent regulator for the buck converter, which keeps the output voltage at the set value despite large changes in the input voltage. These results could be applied to the construction of a practical compensator for an operating buck converter, or as an example of how to design controllers for other switching converter topologies.

Figure 1.17: PECS schematic of PI-compensated buck converter

Figure 1.18: PECS schematic of lead-compensated buck converter

Figure 1.19: PECS schematic of lead - and PI-compensated buck converter

Part II

Modern Control

Chapter 2

Introduction

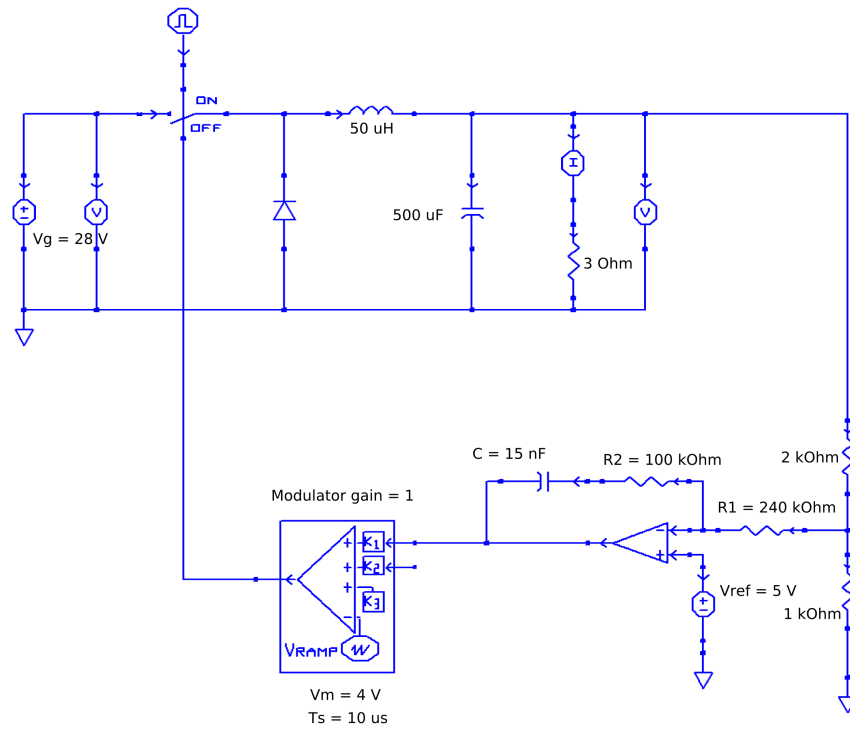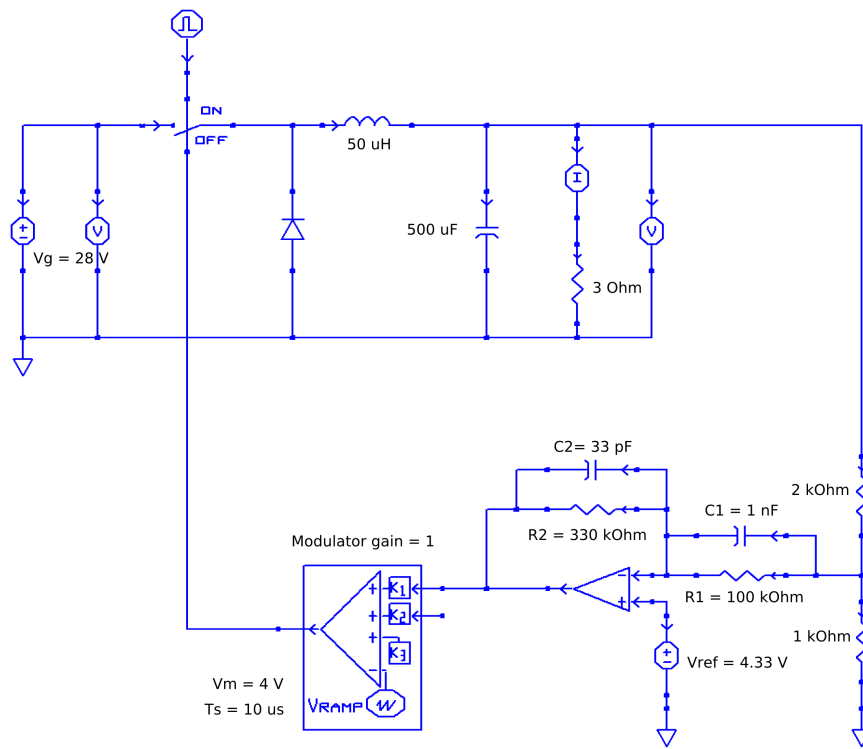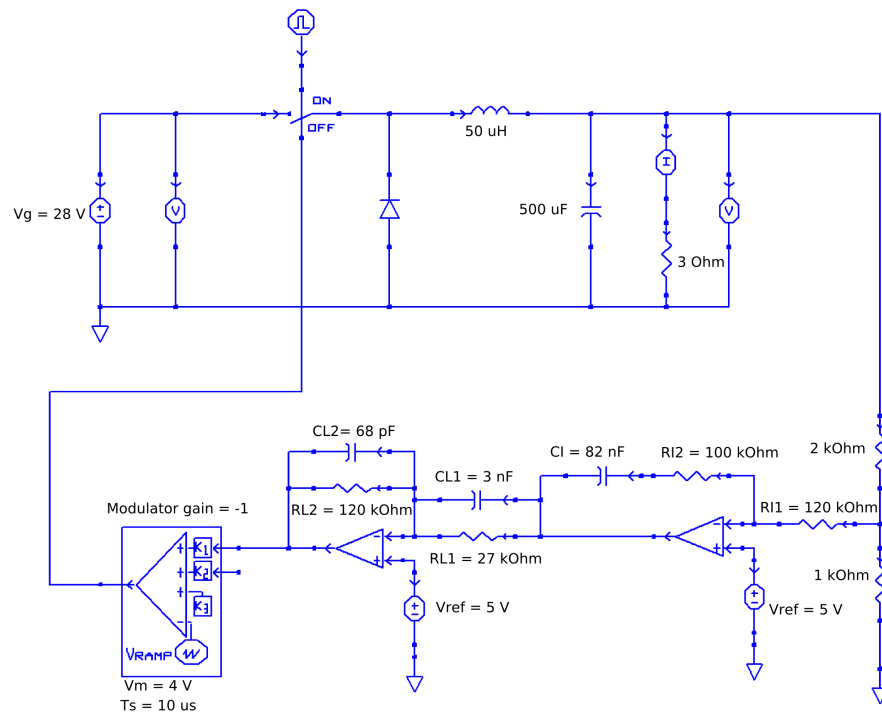There are three main problems that can be examined in the study of systems in the controls context: system dynamics, system identification or modeling, and system control. They develop from the three aspects that are present in the block diagram of a basic system: input, system, and output [3]. Typically, two of the three aspects are known, and the third must be determined from the other two.

In system control, the system is known, and the input to the system that produces a desired output must be determined. Part II focuses on the fundamental control problem of regulation for disturbance rejection as it pertains to DC-DC converters, and uses the Ćuk DC-DC converter as the platform for applying the various design steps, leading up to a mimimal-order compensator design, demonstrated in Chapter 8. It is assumed that the reader of this part of the book is familiar with the classical control system design techniques presented earlier as the modern control design methods build on a classical foundation. Note that for the regulation problem, the desired output value is fixed, whereas in the servo problem, the desired output is to track a changing setpoint.

The Ćuk DC-DC converter was chosen as an example system for two main purposes. This nonlinear switching circuit can act to raise (boost) or lower (buck) the voltage from input to output, making it a generic DC-DC converter (compared to converters that can only boost or buck the input voltage, but not do both). Also, the circuit contains four energy storage devices leading to a fourth-order system, which creates sufficient complexity in an output feedback compensator to require compensator order reduction. This allows an original idea regarding order reduction to be presented. Boost or buck converters are typically implemented with only two energy storage components, and the resulting simplicity in compensators designed using modern control techniques either does not require model reduction or renders one of the techniques presented practically useless.

Analysis of the Ćuk converter circuit begins in Chapter 3. The control system design procedures use MATLAB from The Mathworks, Inc. (See Appendix 11 for code.) The nonlinear Ćuk switching circuit is modeled as a small-

signal continuous linear time invariant (LTI) system using state space averaging. The LTI model to be used during the design process is validated by transient comparison with a nonlinear circuit simulation to justify the assumption that the small-signal model would be adequate. The open-loop performance characteristics are tested, and a set of performance criteria for the closed-loop controlled system are specified.

Chapter 4 covers pole placement using state feedback. This chapter uses desired poles given by a filter prototype that is optimal with respect to an integral performance index and discusses how to select a weighting parameter that determines the closed-loop pole locations.

Integral augmentation of the state feedback architecture is described in Chapter 5. This allows the closed-loop system to completely eliminate steady state error, which could not be accomplished by state feedback alone.

Chapter 6 discusses state estimation using full- and reduced-order observers to allow for the use of output feedback, as state information is not always available to the designer.

Chapter 7 shows the application of optimal control and estimation using linear quadratic methods. These techniques allow the designer to determine optimal controller and optimal estimator gains. Loop transfer recovery is discussed as a means to recover desirable frequency-domain stability margins that are lost when designing an optimal output feedback compensator.

In order to design compensators that can be constructed from a minimum number of components, Chapter 8 covers order reduction methods. First, a reduced-order optimal compensator with recovered loop gain is designed. This step is followed by applying balanced realization and truncation techniques to eliminate states with little effect on performance, resulting in additional compensator order reduction.

Chapter 9 describes how to implement two of the final compensator designs that were created and shows the difference in analog controller circuit complexity that can arise from only one additional order in the compensator.

Finally, Chapter 10 presents the minimal compensator circuit test results from a power electronics simulator that prove the performance of the final controller design exceeded the original design specifications.

Chapter 3

System Analysis

Prior to designing a controller for a system, the control system designer must understand the system's characteristics. For example, is the system open-loop stable? Are there dominant poles? Are there poles that may be neglected during design? Is the system controllable using the selected inputs? Can an estimator be constructed based on the measured outputs? These types of questions should be answered both intuitively and mathematically prior to embarking on an attempt to design a controller for the system.

As stated in Chapter 2, the Ćuk DC-DC converter is used here as the example system for demonstrating the compensator design processes described in Part II. The starting point is the construction of a mathematical model of the system in MATLAB. The model is a mathematical description of some or all of the behavior of the real-world system that is adequate for performing controller design. State space averaging yields a linear small-signal model for the nonlinear switching system (derivations may be found in the Appendix) [4]. Additionally, a nonlinear circuit model was created in the Power Electronics Circuit Simulator (PECS) software package in order to validate the performance of the assumed linear model. PECS uses a schematic-based circuit editor and features its own plotting tool, PECSPLOT.

A note on notation: the zeros, poles, and gains of systems discussed in Part II are in the Evans form, i.e., the coefficient of the highest power of s in each factored term is unity and the stated gain is not the DC gain of the system. This is in contrast to Bode form, where the constant in each factored term is unity and the DC gain is explicitly stated. Evans form was chosen for convenience, as it is the form used by zpk systems in MATLAB.

3.1   The Ćuk Converter

The Ćuk converter is a step-down/step-up converter based on a switching boost-buck topology. Essentially, the converter is composed of two sections, an input stage and an output stage. The schematic of the Ćuk converter is pre-
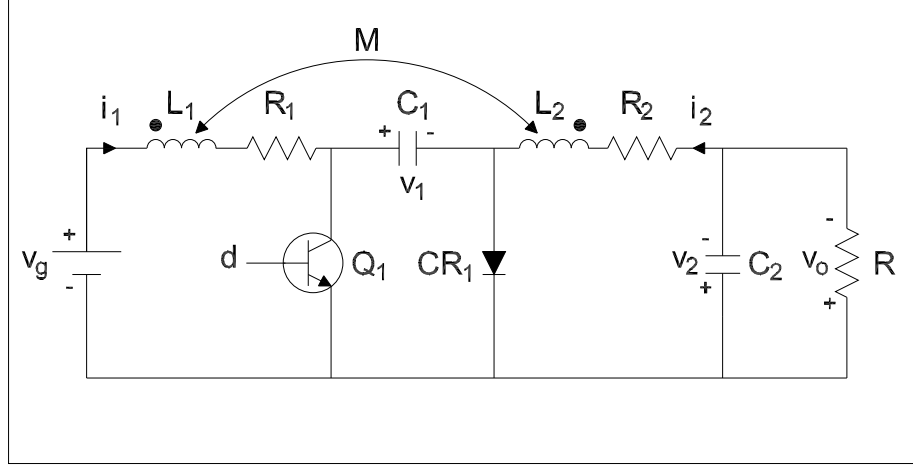
Figure 3.1: Ćuk converter with inductor equivalent series resistances.

sented in Figure 3.1, with component values given in the Appendix. (The lowercase variables indicate small-signal deviations from nominal operating point variables as obtained by linearization.) The input voltage v_g is fed into the circuit via inductor L_1. When transistor Q_1 is on, current i_1 builds the magnetic field of the inductor in the input stage. The diode CR_1 is reverse biased, and energy dissipates from the storage elements in the output stage. When Q_1 turns off, inductor L_1 tries to maintain the current flowing through it by reversing polarity and sourcing current as its magnetic field collapses. It thus provides energy to the output stage of the circuit via capacitor C_1. Both currents i_1 and i_2 must sum to zero in the steady state, since the assumption is that voltage v_1 is essentially constant (given that the voltage across a capacitor cannot change instantaneously and the switching speed of the circuit is high). This provides for the following charge conservation relation:

$$i_1 t_{on} + i_2 t_{off} = 0 \tag{3.1}$$

The inductor currents are the input and output currents, therefore, if the principle of conservation of energy is applied:

$$\frac{v_o}{v_g} = \frac{D_s}{1 - D_s} \tag{3.2}$$

where D_s is the duty cycle of the switch, $D_s \triangleq \frac{t_{on}}{t_{on}+t_{off}}$. Equation 3.2 shows that by controlling the duty cycle of the switch (by small-signal deviation d), the output voltage v_o can be controlled and can be higher or lower than the input voltage v_g. By using a controller to vary the duty cycle during operation, the circuit can also be made to reject disturbances, as will be shown.

3.2 Open Loop Performance of the Ćuk Converter

Before a controller was designed, the performance of the open-loop Ćuk model was examined. A state space block diagram for the open-loop model is shown in Figure 3.2. The state space equations were determined to be:

$$
\begin{aligned}
\dot{x} &= Ax + Bv_g + B_d d \\
v_o &= Cx \\
x &= \begin{bmatrix} v_2 & v_1 & i_2 & i_1 \end{bmatrix}'
\end{aligned}
\tag{3.3}
$$

The state space matrices for the open-loop model from the disturbance input
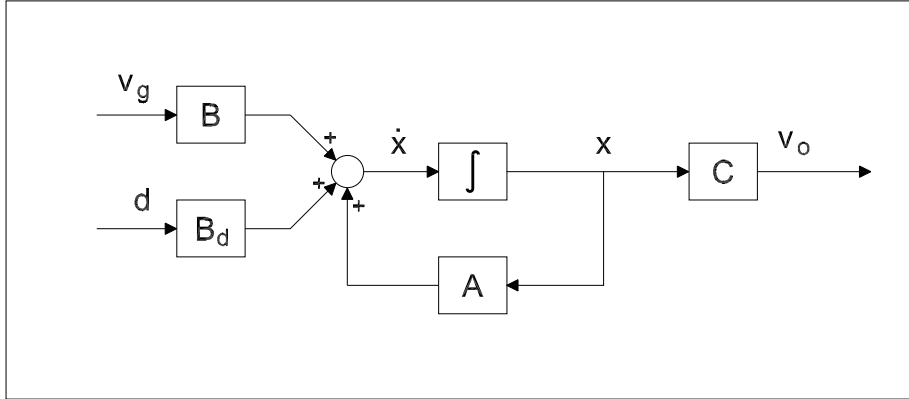
Figure 3.2: State space model of the Ćuk converter.

v_g to the output v_o are the state space averaged matrices $\{A, B, C, D\}$. The state space matrices for the open-loop system from the control input d to the output v_o are the state space averaged matrices $\{A, B_d, C, D\}$. Thus, the model of the Ćuk converter has two inputs (a control input d and a disturbance input v_g) and one output (v_o). (See Appendix for model derivations.)

The MATLAB model open-loop response to a unit step disturbance in v_g is shown in Figure 3.3. By inspection of the plotted response, it was determined that the system reached lightly damped oscillations around a steady state DC value in approximately 20 ms. The steady state value was 26 V, a value predicted from the gain equation for the Ćuk converter:

$$
v_o = \frac{D_s}{1 - D_s} v_g
\tag{3.4}
$$

With nominal duty cycle $D_s = 0.667$, a 1 V step input in v_g produces a 2 V step in the output voltage v_o. This shows that the open-loop system does not reject disturbances on the input voltage v_g. Also, note that the output of the circuit is a lightly damped sinusoid, with an approximate frequency of 1.83 kHz (11.5 krad/s).
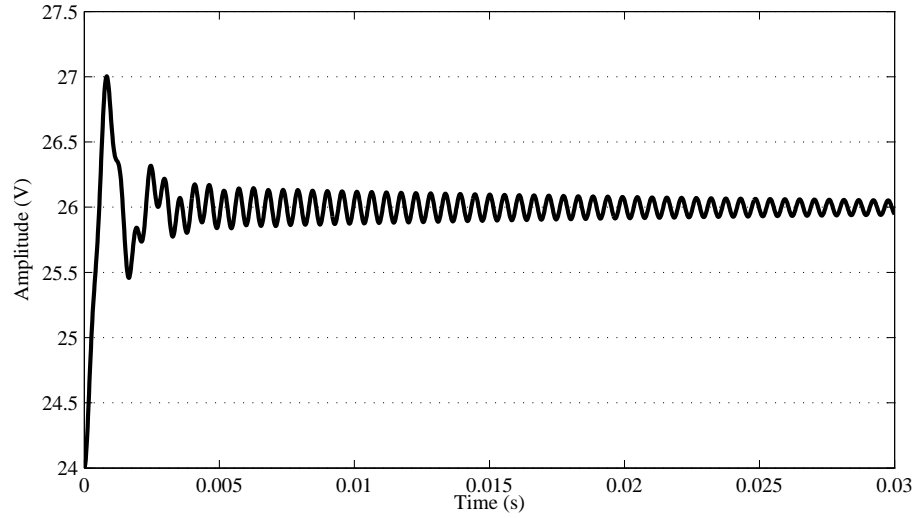
Figure 3.3: Ćuk converter output voltage response to a unit step disturbance in v_g.

The PECS circuit is shown in Figure 3.4. The simulator was set up to check the performance of the nonlinear converter in response to a unit step up in v_g. The PECS plot of these transients is shown in Figure 3.5. Comparison of the MATLAB and PECS plots reveals that the linear model used in MATLAB is an acceptable model of the plant to use for control system design.

The pole-zero plot of $T_{v_o d}$ is shown in Figure 3.6. All poles and zeros are in the LHP, therefore the Ćuk converter is a stable minimum-phase system. The locations for the zeros and poles are:

$$
\begin{aligned}
z &= \begin{bmatrix} -1490 \pm j9000 \end{bmatrix} \\
p &= \begin{bmatrix} -879 \pm j3641, & -40 \pm j11500 \end{bmatrix}
\end{aligned}
$$

The 1.83 kHz ringing in the output transient caused by the unit step disturbance is due to the frequency associated with the dominant pole pair at $-40 \pm j11500$.

3.3   Controllability and Stabilizability

The idea of controllability refers to the ability of the input control u to affect the system dynamics. Controllability is defined as the ability to move the state
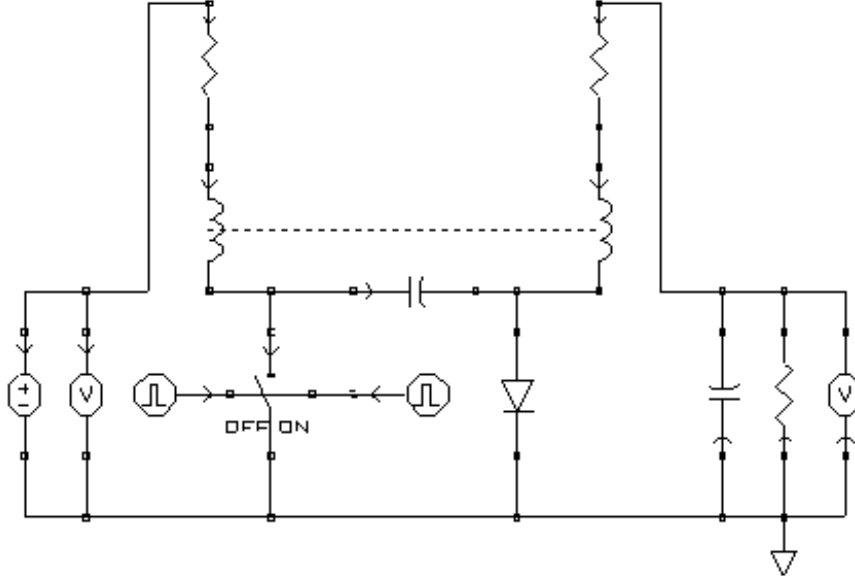
Figure 3.4: The Ćuk converter simulated in PECS.

of a system from an initial value x_0 to any arbitrary state x_f within a finite time period t using the input signal u. (Note that controllability says nothing about the magnitude of the input signal u, i.e., the control effort, nor the time t required to accomplish this transition.) Essentially, it is a test to determine if the closed-loop system poles may be arbitrarily placed in the complex plane.

The controllability matrix M_c is constructed from $(A, \ B)$ in the following manner:

$$M_c = \begin{bmatrix} B & AB & A^2B & \dots & A^{n-1}B \end{bmatrix} \tag{3.5}$$

where n is the order of the system. If M_c is a full rank matrix, the system is fully controllable. The rank deficiency of M_c tells the designer how many modes are uncontrollable. There is no rank deficiency in M_c for the Ćuk converter model, therefore the system is fully controllable.

3.4   Observability and Detectability

Observability refers to the ability to determine any initial state x_0 using only a finite record of the output y between an initial time and a final time. The
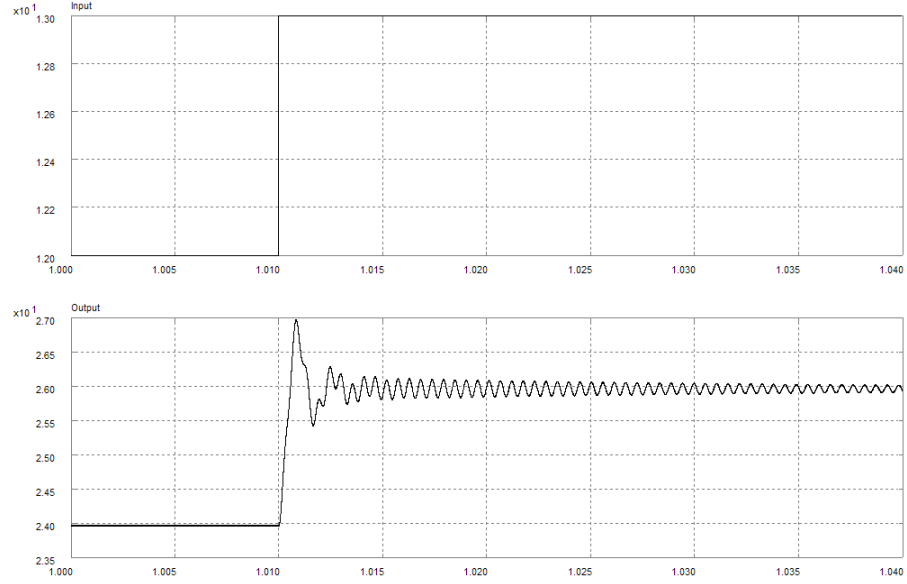
Figure 3.5: Unit step response of the Ćuk converter in PECS.

observability matrix M_o is constructed from $(A,\ C)$ in the following manner:

$$M_o = \begin{bmatrix} C \\ CA \\ CA^2 \\ \vdots \\ CA^{n-1} \end{bmatrix} \tag{3.6}$$

where n is the order of the system. If M_o is a full rank matrix, the system is fully observable. The rank deficiency of M_o tells the designer how many modes are unobservable. The Ćuk converter model is fully observable.

3.5   Controlling the Ćuk Converter

The model used in controller design is a small-signal model, since, like many other methods of linearization, the state-space averaging method only holds for small deviations from the nominal operating point. Most of the equations and figures that follow refer to deviations from the nominal operating point of the system unless otherwise stated or identifiable from context.

The control system designer must always begin with a set of design specifications when starting a project. The specifications are a set of goals for the behavior of the controlled system, and may need to change during the design
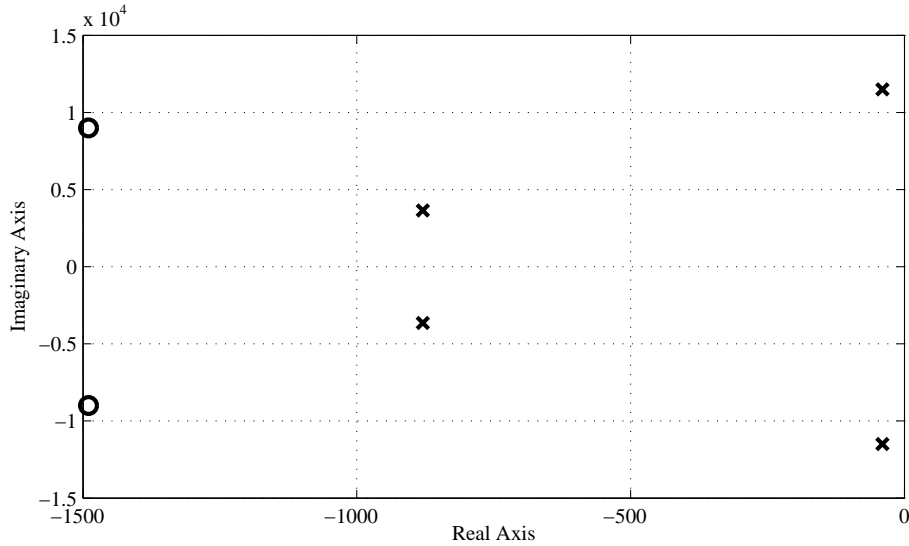
Figure 3.6: Map of the pole and zero locations of $T_{v_o v_g}$.

process if not achievable or as new information becomes available. Specifications generally consider both transient behavior (e.g., rise time, settling time, percent overshoot) and stability margins (e.g., relative stability, gain margin, phase margin).

3.5.1 Time Domain Specifications

Time domain constraints are given by the system performance specifications. The transient response of a regulated system is typically limited in terms of both maximum amplitude deviation from the nominal output and settling time in response to a transient. The goal for the Ćuk converter controller design example is to control the output voltage to within 1% of nominal (i.e., 23.76 to 24.24 V) in response to unit step voltage disturbances in the input. This matches the 1% regulation of standard industrial power supplies sold by a major control system equipment manufacturer. Also, the controller should be able to maintain the nominal output voltage within tolerances as the input varies over a range of 9 to 14 V, though this shall be considered a steady-state, not transient, operating requirement. As a final specification, steady-state error in the output voltage shall be eliminated within 20 milliseconds of the start of a transient.

3.5.2 Frequency Domain Specifications

The frequency response of the transfer function $T_{v_o d}$ should be high at low frequencies for proper regulation and low at high frequencies for adequate noise rejection. The example system base switching frequency is 100 kHz (6.28×10^5

rad/s). As the small signal model breaks down above half of the switching frequency, the loop gain at any frequency above 50 kHz (3.14×10^5 rad/s) should be less than 0 dB. Indeed, there should be a design margin left between this frequency and the gain crossover frequency. A gain margin of at least 20 dB and a phase margin of at least 50° will be sought to ensure stability.

3.5.3   Control Effort Constraints

The Ćuk converter nominal duty cycle is related to the steady-state gain of the converter G by Equation 3.4. Neglecting circuit losses, Equation 3.4 may be rearranged to calculate the duty cycle as a function of the output operating point and input voltages, v_o and v_g:

$$D_s = \frac{v_o}{v_o + v_g} \tag{3.7}$$

Therefore, the nominal duty cycle at the operating point of 24 V for an input of 12 V is determined to be 0.667. However, the purpose of controller design is to ensure the output voltage remains within 1% of 24 V despite disturbances in the input voltage. Since a deviation model is used, the difference between the nominal operating duty cycle and the duty cycle required to keep the output at exactly 24 V may be approximated, and this is shown in Figure 3.7. It is this
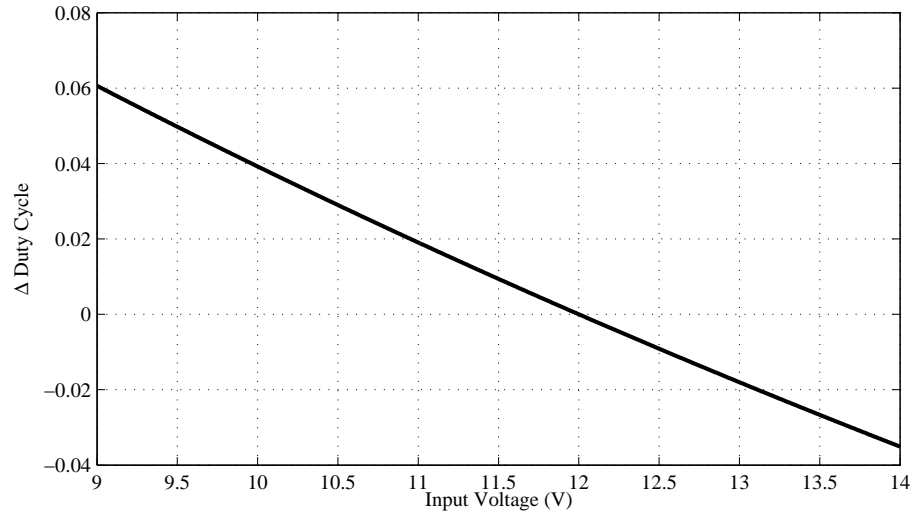

Figure 3.7: The small-signal duty cycle required over the full input voltage range to maintain nominal output voltage.

change in duty cycle that the controller must provide, as the deviation in duty cycle is the small-signal control input of the Ćuk converter. Thus, it can be predicted from Equation 3.7 or Figure 3.7 that the the controller must change

the duty cycle by -0.018 to maintain the output at 24 V for a step disturbance input on v_g from the nominal 12 V to 13 V. This value of -0.018 will be used to verify the correct steady-state control effort in controller design. (Note that Equation 3.7 does not account for any voltage losses within the circuit, so the duty cycle will actually be slightly higher from the calculated value when any resistances are included in the circuit.) The duty cycle is limited to $0 \leq D_s \leq 1$, therefore if the control effort plus the nominal value of 0.667 exceeds these limiting values, the compensator design is not acceptable. This leads to hard limits on the small-signal control effort of $[-0.667, \ 0.333]$, though the inclusion of a design margin to these limits may be desirable. It is up to the individual designer to choose constraints on the control effort, however it is generally best to allow the use of as much of the control effort range as possible.

Chapter 4

Pole Placement

For a system that is completely controllable and where all the states are accessible, feedback of all of the states through a gain matrix can be used to place the poles at any desired location in the complex plane. The control law used for state feedback is:

$$u = -Kx \qquad (4.1)$$

which uses the matrix K to place the poles of the system at desired locations [2]. This type of compensator is said to employ full state feedback (FSFB). A FSFB regulator is shown in Figure 4.1.
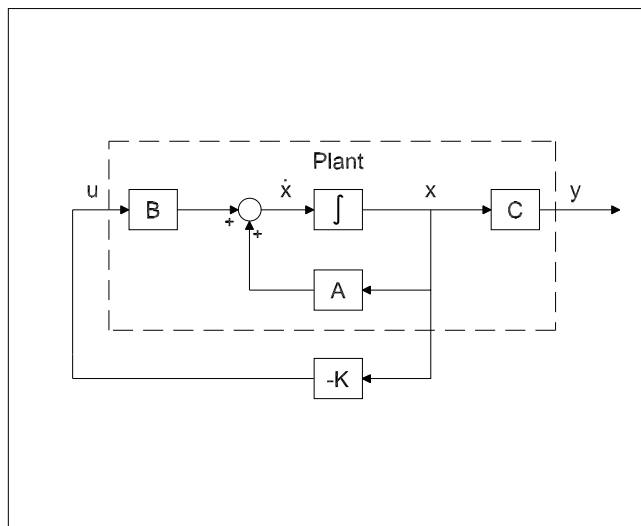

Figure 4.1: State feedback regulation.

4.1 Pole Placement via Ackermann's Formula

Ackermann's formula may be used with single-input, single-output (SISO) systems like the Ćuk converter. Ackermann's formula is:

$$K = \begin{bmatrix} 0 & 0 & \ldots & 1 \end{bmatrix} M_c^{-1}(A^n + \alpha_1 A^{n-1} + \ldots + \alpha_{n-1}A + \alpha_n I) \qquad (4.2)$$

This method of determining K may be used with the system in any representation. It is this method of pole placement that is used in the designs of the state feedback controllers that follow.

4.2 Ćuk Converter with State Feedback Compensator

One problem with pole placement is how to go about selecting desirable pole locations. Two main methods of design are commonly followed [5]:

- Select pole locations such that a dominant complex pole pair exists. This technique is generally used when designing tracking systems, for which the transient time domain requirements (e.g., rise time, overshoot, settling time, etc.) are able to be recast into desired dominant pole locations.

- Select pole locations that have been determined to give a prototype time-domain response, e.g., filter pole locations.

The latter method is used in this chapter for pole placement with full state feedback control.

Graham and Lathrop [6] discuss assigning the system poles of higher-order systems to prototype locations that minimizes a performance index (or cost function) known as the integral of the time-weighted absolute error (ITAE) to an input signal:

$$J_{ITAE} = \int_0^\infty t\,|e(t)|\,dt \qquad (4.3)$$

By placing poles in an ITAE filter pattern to minimize J_{ITAE}, the designer achieves a response that is optimized with respect to deviation from setpoint (provided by the absolute error) and settling time (errors that occur later in the time history contribute more to the J_{ITAE} cost). Since the goal of the control system designer is to regulate the Ćuk converter output voltage with respect to input voltage disturbances, J_{ITAE} provides a scalar figure of merit by which to judge controller performance. For regulator problems, the desired output is rejection of disturbance deviations from the nominal operating point. The error between the desired output and the plant output is defined as $e(t) = r(t) - y(t)$. Since $r(t) = 0$ for all time t in a regulator problem, the error $e(t)$ is simply $-y(t)$.

Table 4.1: Frequency-Normalized Characteristic Equations for ITAE Response

Order	Characteristic Equation
1	$s + \omega$
2	$s^2 + 1.414\omega s + \omega^2$
3	$s^3 + 1.75\omega s^2 + 2.15\omega^2 s + \omega^3$
4	$s^4 + 2.1\omega s^3 + 3.4\omega^2 s^2 + 2.7\omega^3 s + \omega^4$
5	$s^5 + 2.8\omega s^4 + 5\omega^2 s^3 + 5.5\omega^3 s^2 + 3.4\omega^4 s + \omega^5$

The frequency-normalized characteristic equations for minimum ITAE response are given in Table 4.1 up through order five (so that a full-order state feedback controller with an integrator may be applied to the Ćuk converter).

A control system designer can use a computer program (e.g., MATLAB from The Mathworks with the Control Systems Toolbox) to iteratively design and test state feedback controllers over a range of values for the scalar multiplier frequency ω. It is easiest to work with the characteristic equations given in Table 4.1 in MATLAB in a factored format as shown in Table 4.2. The control system designer must determine the value of ω that places the poles in such a way as to achieve the desired time domain response. By using the steady state error

Table 4.2: Frequency-Normalized Pole Locations for ITAE Response

Order	Factored Pole Locations
1	$\omega[-1]$
2	$\omega^2[-0.7071 \pm j0.7071]$
3	$\omega^3[-0.7081, -0.521 \pm j1.068]$
4	$\omega^4[-0.424 \pm j1.263, -0.626 \pm j0.4141]$
5	$\omega^5[-0.8955, -0.3764 \pm j1.292, -0.5758 \pm j0.5339]$

as a measurement metric for each iteration during the design, ω can be chosen that produces a steady state error within the performance specification of 1%. Figure 4.2 shows a plot of steady-state error vs. ω, and this figure was used to select a value of ω that corresponded to 0.24 V (1% voltage regulation). Initially, a wide range of frequencies was selected with a large increment, then the range and the increment were made smaller in order to narrow in on the first frequency with less than 0.24 V of steady state error, which occurs at $\omega = 10.0125$ rad/s. The unit step disturbance response of the system with a full state feedback controller designed in this manner is shown in Figure 4.3. Note that there is 0.24 V of steady-state error to the 1 V step disturbance in input voltage, indicating that the disturbance is rejected to within the performance specifications. The amplitude and settling time of the transient meet design specifications, so this controller has very desirable time-domain response characteristics. The loop gain of the regulated system is shown in Figure 4.4, where the loop is broken at the large X shown on the control input d in Figure 4.5. MATLAB calculations
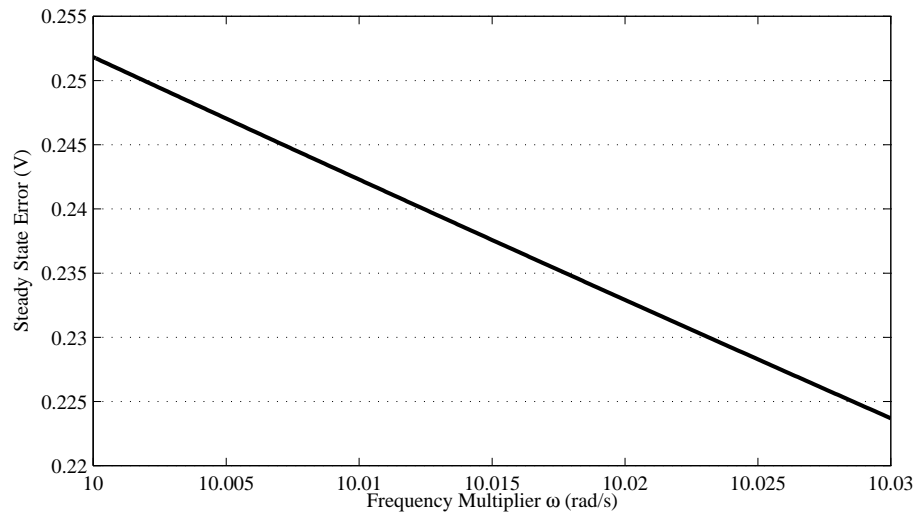
Figure 4.2: Steady state error of unit step disturbance as frequency multiplier is swept.
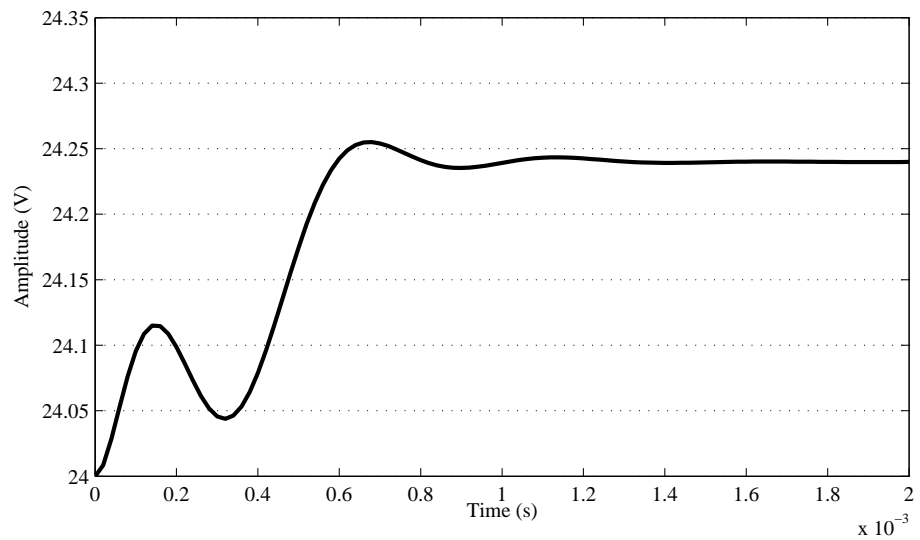
Figure 4.3: Response to unit step disturbance of input voltage.
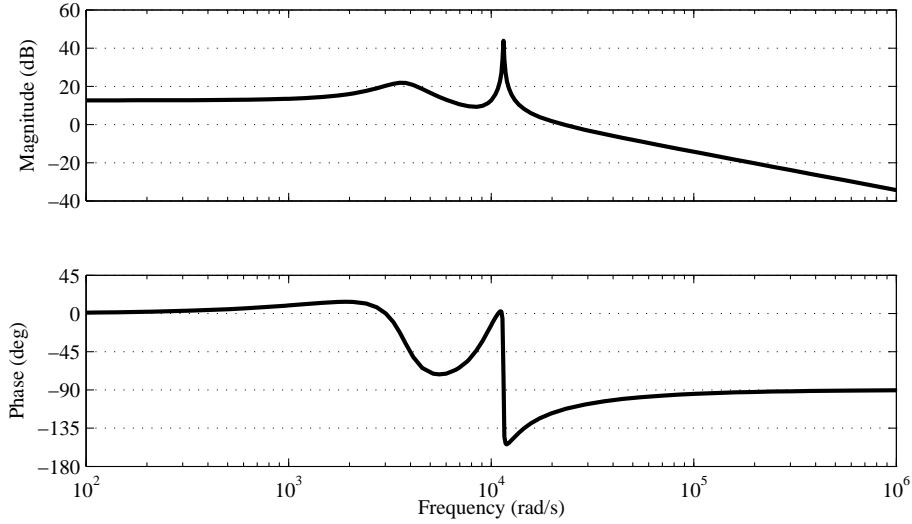
Figure 4.4: Loop gain with the full state feedback controller.

give the gain margin as ∞ and a phase margin of 67°, which are very desirable frequency-domain response characteristics.

Finally, the control effort of the design should be examined. Once again, the control input to the Ćuk converter is the change in duty cycle d used to turn on and off $Q1$. The control effort is plotted in Figure 4.6, and it can be seen that the effort is not approaching the limits assigned to d. It can also be seen that the steady-state deviation control effort is approximately -0.0163, which corresponds roughly to calculations using Equation 3.7.

Figure 4.5: The full state feedback controller applied to the Ćuk converter.

Figure 4.6: Control effort with the full state feedback controller.

Chapter 5

Integral Action

The previous state feedback design for the Ćuk converter resulted in 0.24 V of steady-state error to the 1 V disturbance in input voltage, which is just withi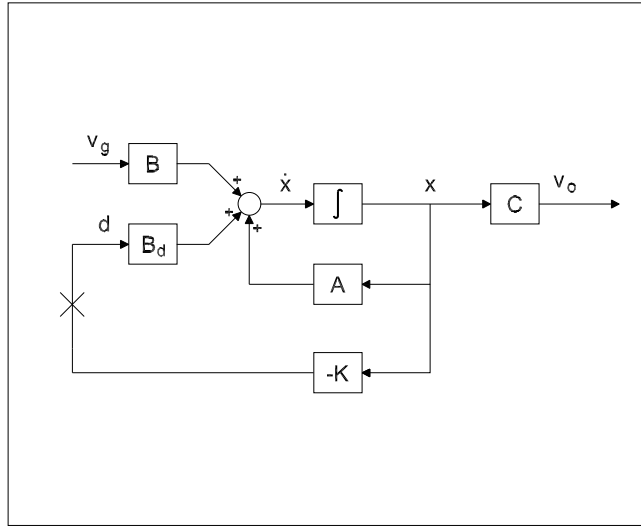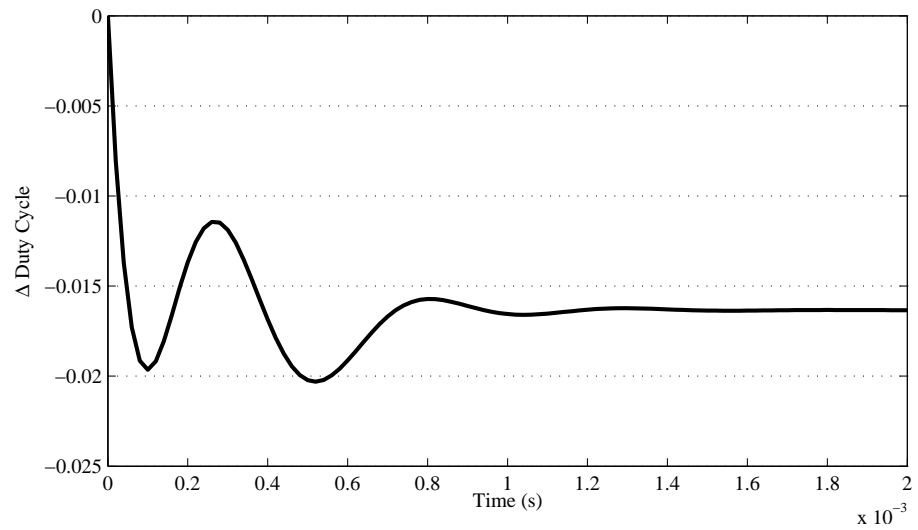n design specifications. Additional gain could reduce this error, though it could never be eliminated, as the Ćuk converter is a type 0 system, which means that there will always be some finite steady-state error to a unit step disturbance or setpoint change, even in a controlled system, no matter how high the gain. However, it is desirable to eliminate steady-state error entirely if possible. The only way to do this is to have the controller raise the type number. Full state feedback does not introduce an integrator into the closed loop, therefore does not change the type number.

5.1   Adding Integrators

In order to eliminate any steady-state offset that may occur, an integrating controller may be added to the controlled system. Integral control is a method of output feedback, as shown in Figure 5.1. The integrating controller integrates the error between any reference signal and the output $e(t) = r(t) - y(t)$ and adds it to the state feedback control effort to eliminate steady-state error. The equation for the integrator is $x_i = \int e\,dt$, or $\dot{x}_i = e$. Since each row in the state space representation is a first-order linear differential equation, and the integrator adds one new differential equation to the system $\dot{x}_i = -y = -Cx$, one new state x_i must be added to the state vector to raise the Ćuk system from type 0 to type 1. The augmented state vector is $[x\ x_i]'$ and the new state
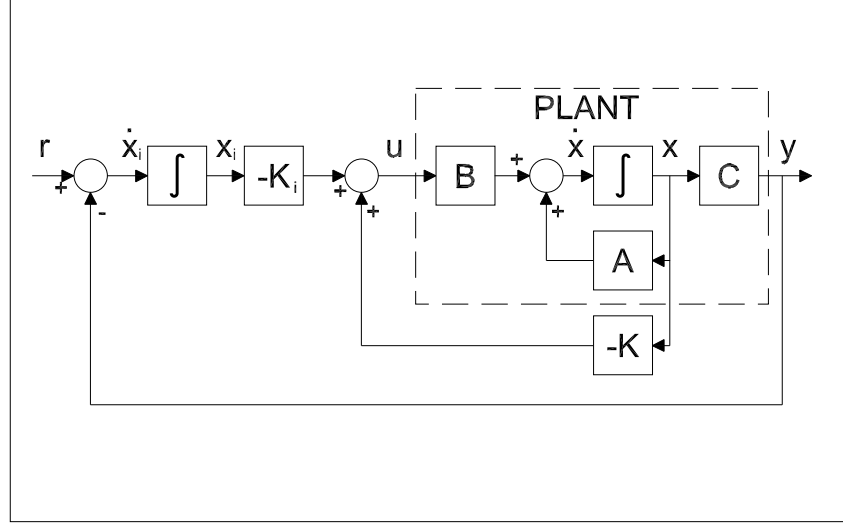
Figure 5.1: Generic system controlled with a FSFB regulator and output integral feedback.

space quadruple is:

$$
\begin{aligned}
A &= \begin{bmatrix} A & 0 \\ -C & 0 \end{bmatrix} \\
B &= \begin{bmatrix} B & 0 \end{bmatrix}' \\
C &= \begin{bmatrix} C & 0 \end{bmatrix} \\
D &= 0
\end{aligned}
\tag{5.1}
$$

The control law for this augmented system is $u = -kx - k_i x_i$. From the above modifications, the desired poles (with an added desired closed-loop pole location to account for the pole associated with the integrator) can be used to determine the state feedback gain, which has the structure $K = [k \;\; k_i]$.

5.2   Ćuk Converter with State Feedback and Integral Compensator

The augmented controlled system of the Ćuk converter is shown in Figure 5.2. This control method is described as full state feedback with an integrator (FSFBI).

The state quadruple for the system augmented with the new state and con-
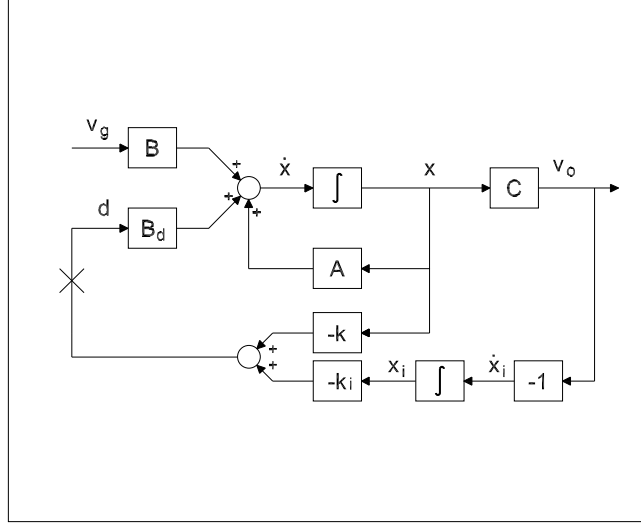
Figure 5.2: System controlled with a FSFBI regulator.

trolled with the new control law may be derived from the block diagram.

$$
\begin{aligned}
\dot{x} &= (A - B_d k)x - B_d k_i x_i + B v_g \\
v_o &= Cx
\end{aligned}
\tag{5.2}
$$

along with the augmented closed-loop state space matrices

$$
\bar{A} = \begin{bmatrix} A - B_d k & -B_d k_i \\ -C & 0 \end{bmatrix}
\tag{5.3}
$$

$$
\begin{aligned}
\bar{B} &= \begin{bmatrix} B & 0 \end{bmatrix}' \\
\bar{C} &= \begin{bmatrix} C & 0 \end{bmatrix} \\
\bar{D} &= [D]
\end{aligned}
$$

The controlled system then becomes:

$$
\begin{aligned}
\dot{x} &= \bar{A}x + \bar{B}v_g \\
v_o &= \bar{C}x
\end{aligned}
\tag{5.4}
$$

A frequency-sweep technique similar to that used for the FSFB controller was used to determine the pole placement for the system augmented with an integrator, and the results are shown in Figure 5.3. However, because the steady state error of a step disturbance response is always zero with a type 1 system, steady state error cannot be used as the performance metric for determining the frequency weighting used with the ITAE filter pole locations given in Table 4.1. Instead, the ITAE value of each unit step transient is calculated, and the

frequency multiplier is found for the transient that has the minimum ITAE value. The frequency multiplier was swept and the minimum ITAE determined to occur at $\omega = 6.564$ rad/s. The step disturbance transient is shown in Figure 5.4. The
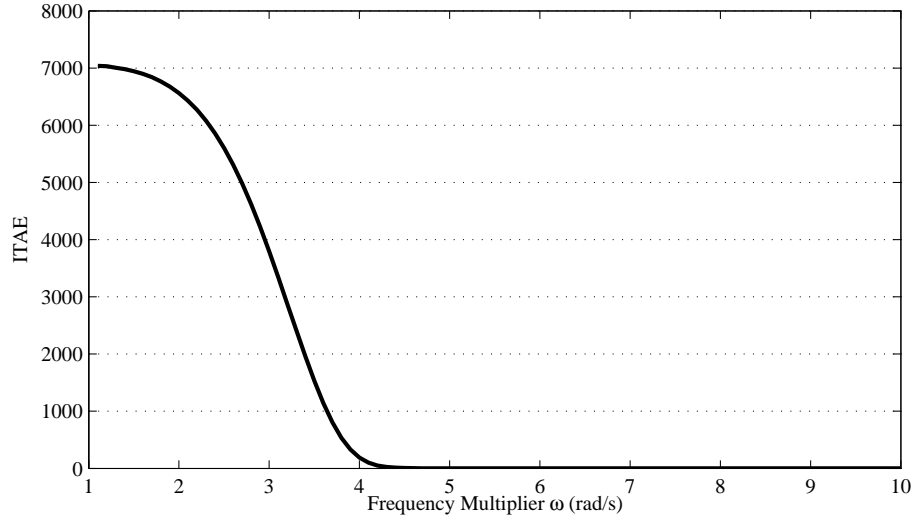
Figure 5.3: ITAE pole frequency multiplier determination.

loop gain of the controlled system may be seen in Figure 5.5, where the loop is broken at the large X shown on the control input d in Figure 5.2. MATLAB calculations give the gain margin as ∞ and a phase margin of $68°$. Figure 5.6 shows the change in duty cycle effected by the FSFBI controller to control the Ćuk converter. Note that the final value of the control effort is -0.018. This is the approximate change in duty cycle that is necessary to completely reject the unit step disturbance in v_g as shown in Figure 3.7.

From this point forward in this paper, all of the example compensator designs will include an integrator term to completely reject the effects of the step disturbance in v_g, and though sometimes not explicitly stated in the compensator name, terms related to the integrator will appear in the state equations as well as the block diagrams relating to control of the Ćuk converter.

Figure 5.4: Unit step disturbance response of system with FSFBI controller.

Figure 5.5: Loop gain of Ćuk converter controlled by FSFBI.

Figure 5.6: Control effort of FSFBI compensator.

Chapter 6

State Estimation

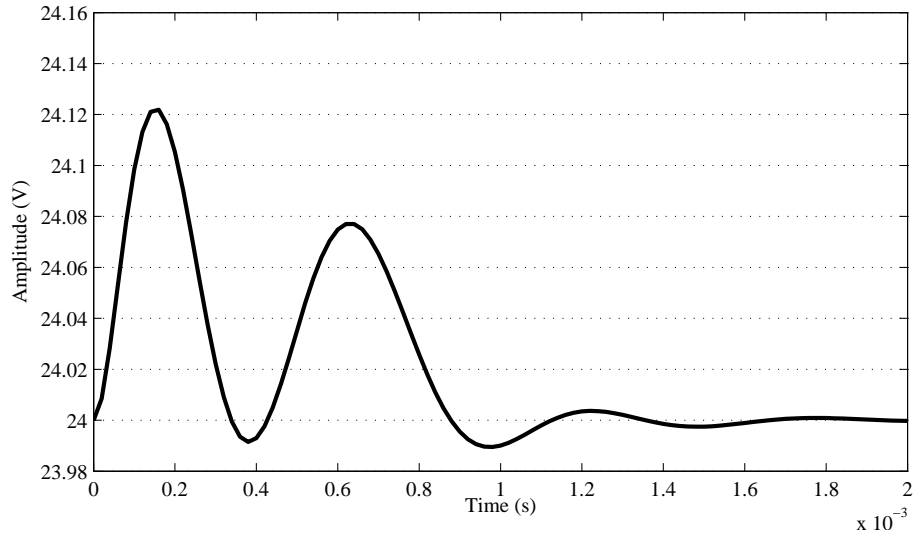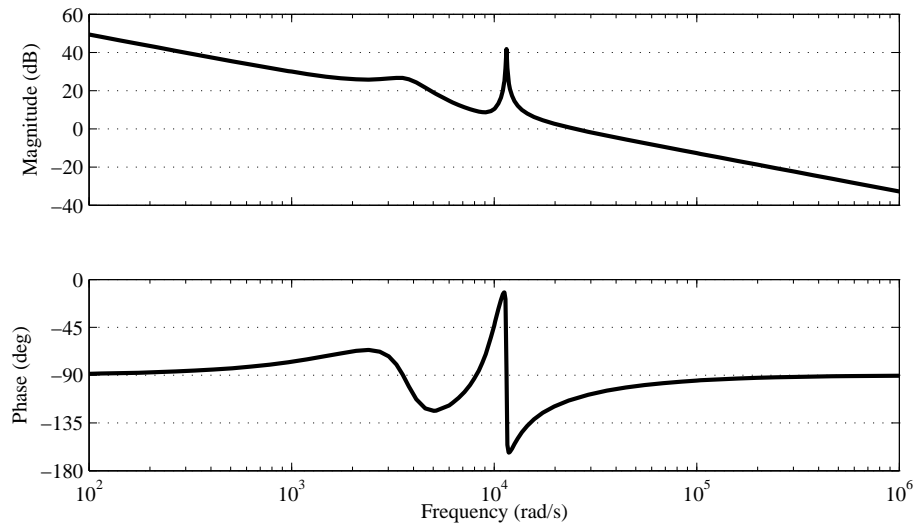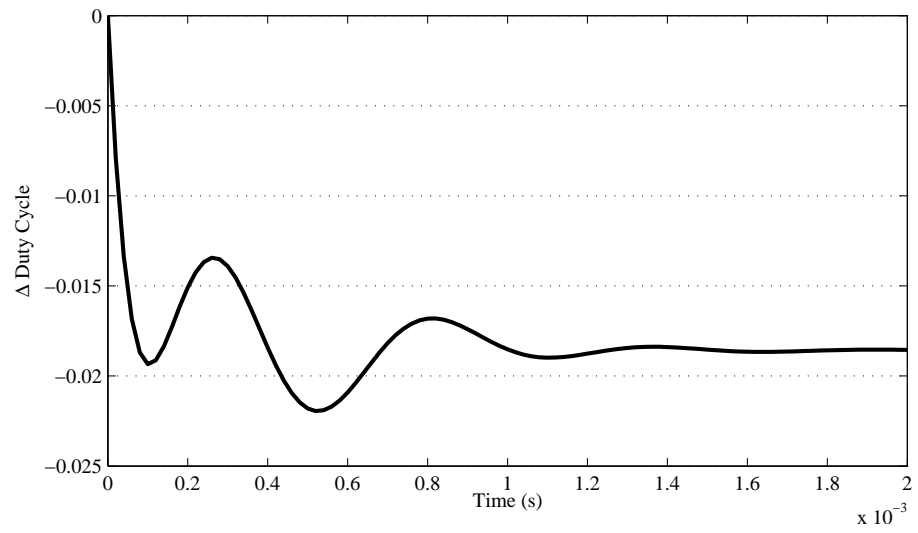Since an n-th order system requires n states be fed back to the gain matrix K to allow pole placement anywhere in the complex plane, this requires at least n measurements of the state variables. This can be prohibitively expensive or complex. In some cases, the internal system states may not even be measurable. In general, only the input and output of a system are available to the control system designer. However, if the system is fully observable, a state estimator (also known as an observer) may be used to provide estimated state values for use in feedback control. The use of an observer requires that the state estimates converge to the actual state values (if starting from different initial states) more rapidly than the system itself responds. The control law used is then:

$$u \quad = \quad -K\hat{x} \tag{6.1}$$

where $\hat{x}$ indicates that the states fed back into the system are estimates.

In order to quickly force the state estimate to converge to the actual values of the state from arbitrary initial conditions, a correction term must be applied to the estimator dynamics such that the error dynamics approach zero rapidly.

6.1   Full-Order State Estimators

A state estimator may be constructed from the same system state space model used for control law gain determination as long as the system is fully observable. The output of the estimator $C\hat{x}$ can be compared to the output of the system, and any difference between them may be multiplied by a gain vector and fed back to the state estimator dynamics. Therefore:

$$
\begin{aligned}
e \quad &= \quad y - C\hat{x} \\
&= \quad C(x - \hat{x})
\end{aligned}
\tag{6.2}
$$

51

Multiplying this error by a gain vector L, the desired state error correction term is formed, which can then be added to the dynamics of the estimator to form:

$$\begin{aligned}
\dot{\hat{x}} &= A\hat{x} + Bu - LC(x - \hat{x}) \\
&= (A - LC)\hat{x} + Bu + LCx
\end{aligned} \tag{6.3}$$

When L is chosen such that the eigenvalues of $A - LC$ lie in the left half of the complex plane, the estimator error $e \to 0$ as $t \to \infty$. Since the state estimate must converge to the controlled state faster than the state itself can change, the eigenvalues of $A - LC$ should be placed farther to the left than the eigenvalues of $A - BK$. A good rule of thumb is to make the estimator dynamics at least twice as fast as the controlled system dynamics.

To form an output feedback compensator based on an estimator, the separation principle of controller design holds, which states that the controller gain K and the observer gain L can be found independently. The proof of this is in many other references (e.g., [2]), so it shall not be repeated here, but application shall be made of the principle in the design examples to follow.

When paired with the linear state feedback control law, the estimator-based compensator is formed. For the case of state feedback without an integral state added, the compensator is given by:

$$\begin{aligned}
\dot{\hat{x}} &= (A - BK - LC)\hat{x} + Ly \\
u &= -K\hat{x}
\end{aligned} \tag{6.4}$$

Where the state of the system has been augmented by an integrator state, the compensator is given by:

$$\begin{aligned}
\begin{bmatrix} \dot{\hat{x}} \\ \dot{x}_i \end{bmatrix} &= \begin{bmatrix} A - Bk - LC & -Bk_i \\ 0 & 0 \end{bmatrix} \begin{bmatrix} \hat{x} \\ x_i \end{bmatrix} + \begin{bmatrix} L \\ -1 \end{bmatrix} y \tag{6.5} \\
u &= \begin{bmatrix} -k & -k_i \end{bmatrix} \begin{bmatrix} \hat{x} \\ x_i \end{bmatrix}
\end{aligned}$$

6.2   Full-Order Estimator-Based Compensator

The block diagram for the Ćuk converter controlled with a full-order state estimator with linear control law and integral action is shown in Figure 6.1, and was used to derive the following closed-loop state equations:

$$\begin{aligned}
\dot{x} &= Ax - B_d k\hat{x} - B_d k_i x_i + Bv_g \tag{6.6} \\
\dot{x}_i &= -Cx \\
\dot{\hat{x}} &= LCx - B_d k_i x_i + (A - B_d k - LC)\hat{x} \\
v_o &= Cx
\end{aligned}$$

and the associated state space matrices:

$$
\begin{aligned}
\bar{A} &= \begin{bmatrix} A & -B_d k_i & -B_d k \\ -C & 0 & 0 \\ LC & -B_d k_i & A - B_d k - LC \end{bmatrix} & (6.7) \\
\bar{B} &= \begin{bmatrix} B & 0 & 0 \end{bmatrix}' \\
\bar{C} &= \begin{bmatrix} C & 0 & 0 \end{bmatrix} \\
\bar{D} &= [D]
\end{aligned}
$$

The step disturbance transient is shown in Figure 6.2. There is more oscillatory
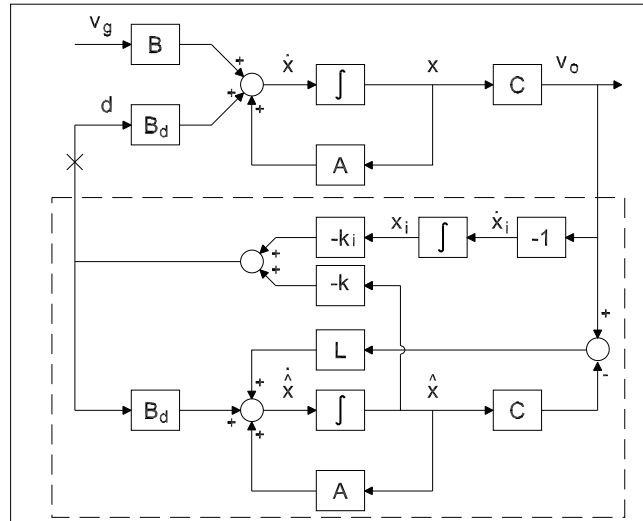
Figure 6.1: An estimated state feedback compensator with integral action.

behavior in the initial part of the transient response compared to the response under FSFBI control. This is likely caused by the initial estimation of states and their convergence to the actual state values. Comparison of the settling times shows that they are approximately the same, and the only transient differences occur early in the transient. The loop gain of the controlled system may be seen in Figure 6.3, where the loop is broken at the large X shown on the control input d in Figure 6.1. MATLAB calculations give the gain margin as 33.6 dB and a phase margin of 105°. Figure 6.4 shows the control effort of the ESFBI controller. Since the Ćuk converter has four states, the observer itself will be a fourth-order system. Along with the integral state, the compensator becomes a fifth-order system. When evaluating desired observer pole locations, keep in mind that the poles of the observer must be placed to the left of the poles of the plant by a large margin to ensure that the state estimator dynamics are faster than those of the plant.
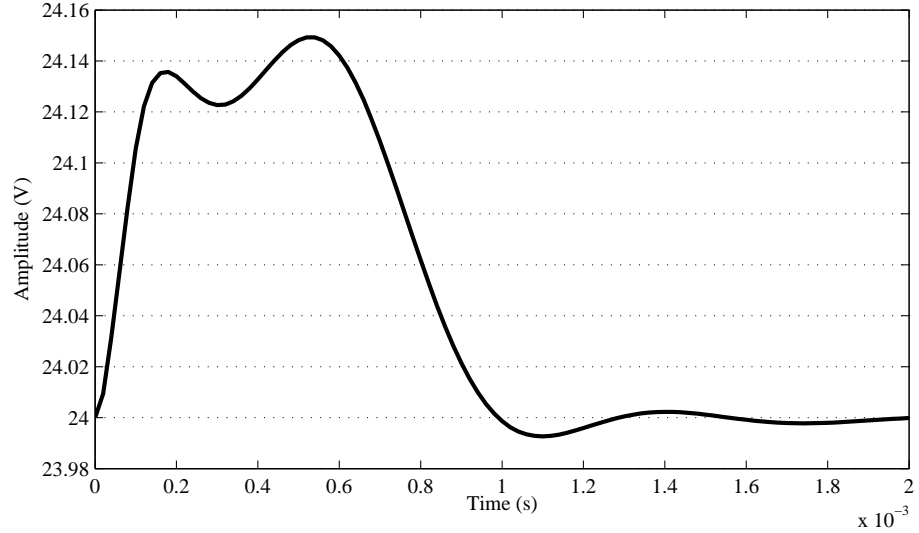
Figure 6.2: Unit step disturbance response of Ćuk converter with ESFBI compensator.

6.3 Reduced-Order State Estimators

If some of the states appear directly in the output as a function of the measurement equation (i.e., are not a linear combination of other states), those states do not need to be estimated. Hence, a reduced-order estimator may be constructed that only estimates the unmeasured states.

If C is a full rank matrix, a nonsingular linear transformation matrix can be formed by choosing a matrix T of dimension $(n - r)$ x n and forming:

$$P \;\; = \;\; \begin{bmatrix} C \\ T \end{bmatrix} \tag{6.8}$$

The matrix T may be any arbitrary matrix that produces a nonsingular P matrix, as P must be invertible.

Applying the standard linear transformation $x = Px$ with Equation (6.8) puts the system into an equivalent representation where C is of the form:

$$\begin{bmatrix} I_r & 0 \end{bmatrix} \tag{6.9}$$

(I is a square identity matrix with dimension r x r, $r < n$). It can be assumed that this representation exists without loss of generality since it is the result of a linear transformation.

The system and feedback gain matrix can now be partitioned into measured

Figure 6.3: Loop gain of Ćuk converter controlled by ESFBI compensator.

and unmeasured portions:

$$
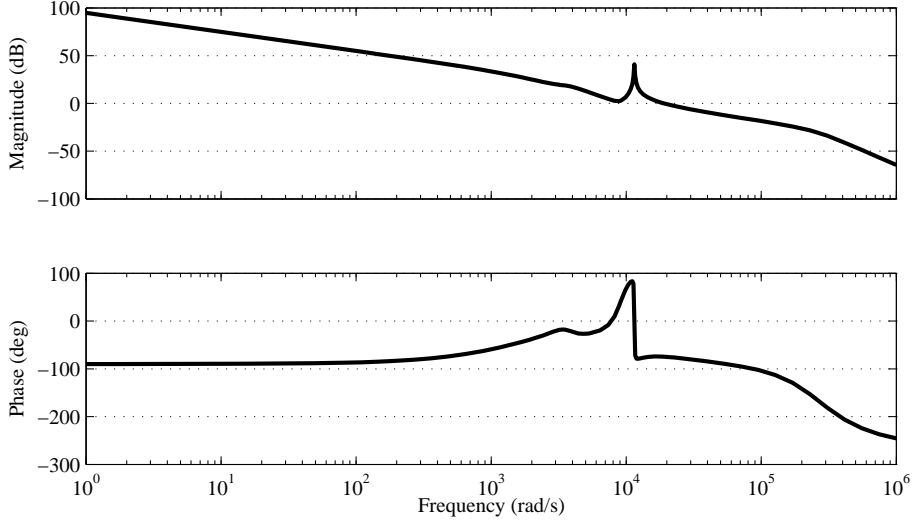\begin{bmatrix} \dot{x}_m \\ \dot{x}_u \end{bmatrix} = \begin{bmatrix} A_{11} & A_{12} \\ A_{21} & A_{22} \end{bmatrix} \begin{bmatrix} x_m \\ x_u \end{bmatrix} + \begin{bmatrix} B_1 \\ B_2 \end{bmatrix} u \tag{6.10}
$$
$$
y = x_m
$$
$$
K = [k_m \; k_u]
$$

Since x_m corresponds to the states that appear in the output of the measurement equation, x_u represents the remaining unmeasured states. As x_m is present in the output, these states do not require estimation. This means that a reduced-order state estimator can be constructed that allows the estimation of x_u in such a manner that all states (either measured or estimated) are available for feedback via a linear control law:

$$
u = -k_m x_m - k_u \hat{x}_u \tag{6.11}
$$

In order to ensure that the reduced-order observer dynamics converge to the true state values of x, the error dynamics must converge to zero. A full-order observer uses a correction term to perform this, which is a gain matrix that multiplies the error between plant output and observer output. Unfortunately, since only the x_m states appear in the plant output, using the plant output contributes no information about the unmeasured states to the estimator and therefore has no dynamic effect on the estimate $\hat{x}_u$. However, a variable change can be performed:
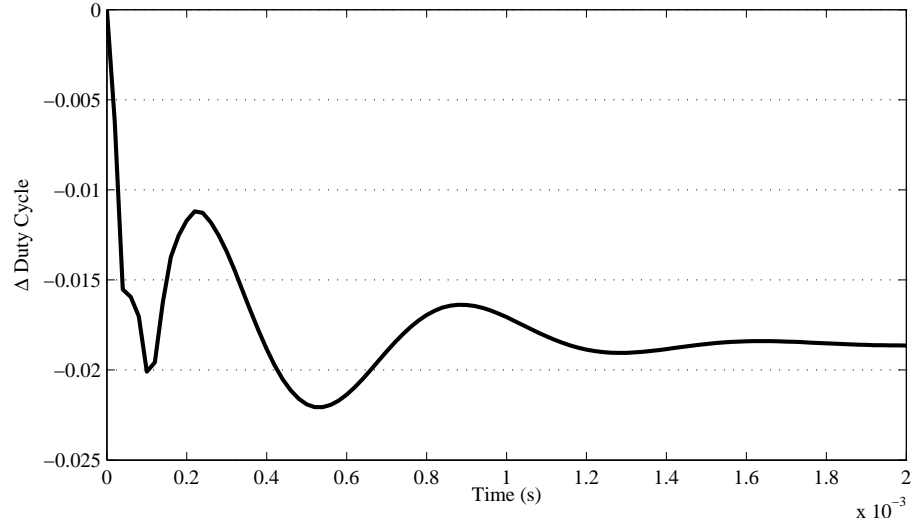
$$
\hat{x}_u = Ly + z \tag{6.12}
$$

Figure 6.4: Control effort of ESFBI compensator.

where z is the output of a system of order $r < n$:

$$\dot{z} = Ez + Fy + Gu \tag{6.13}$$

with E, F, and G and the observer gain L yet to be determined.

Since observer design is concerned with elimination of the error between the actual state and its estimate, the estimation error can be defined as $e_u = x_u - \hat{x}_u$ and the error dynamics will converge to zero if $\hat{x}_u \to x_u$.

Using the partitioned format of x_u from Equation 6.10 along with $\hat{x}_u$ determined from the block diagram in Figure 6.5, it can be shown that:

$$\begin{aligned}
\dot{\hat{x}}_u &= L(A_{11}x_m + A_{12}x_u + B_1u) + E(\hat{x}_u - Lx_m) + Fx_m + Gu \quad (6.14) \\
\dot{x}_u &= A_{21}x_m + A_{22}x_u + B_2u
\end{aligned}$$

Adding zero to the right side of $\dot{\hat{x}}_u$ in the form of $Ex_u - Ex_u$:

$$\begin{aligned}
\dot{\hat{x}}_u &= (LA_{11} - EL + F)x_m + (LA_{12} + E)x_u \ldots \quad (6.15) \\
&\quad + (LB_1 + G)u + E(x_u - \hat{x}_u)
\end{aligned}$$

This gives the following equation for the estimator error dynamics when substituted into the time derivative of the unmeasured error $\dot{e}_u = \dot{x}_u - \dot{\hat{x}}_u$:

$$\begin{aligned}
\dot{e}_u &= (A_{21} - LA_{11} + EL - F)x_m + (A_{22} - LA_{12} - E)x_u \ldots \quad (6.16) \\
&\quad + (B_2 - LB_1 - G)u + Ee_u
\end{aligned}$$

In order for the estimator error dynamics to be independent of the state x, plant output y, and the input u, the first three terms on the right side of Equation 6.16
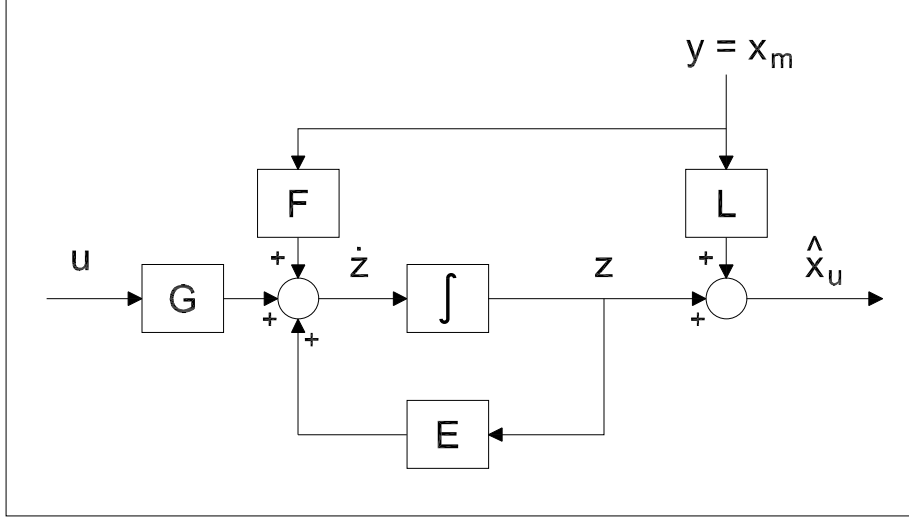
Figure 6.5: Reduced-order estimator construction.

must be zero. This is accomplished by selecting:

$$
\begin{aligned}
E &= A_{22} - LA_{12} \\
F &= A_{21} - LA_{11} + EL \\
G &= B_2 - LB_1
\end{aligned}
\tag{6.17}
$$

This leaves $\dot{e}_u = Ee_u$, which converges to zero when E is an asymptotically stable matrix. Thus, the error dynamics die out, leaving an estimate that equals the state. This means that L must be selected such that $A_{22} - LA_{12} \to 0$ as $t \to \infty$, i.e., the poles of E must lie in the left half of the complex plant. As with the full-order observer, the reduced-order observer poles should be placed such that the estimator dynamics are much more rapid than the controlled plant dynamics.

When paired with the properly-partitioned linear state feedback control law, the reduced-order estimator-based compensator is formed. For the case of state feedback without an integral state added, the reduced-order compensator is given by:

$$
\begin{aligned}
\dot{z} &= (E - Gk_u)z + (F - Gk_uL - Gk_m)y \\
u &= -k_uz + (-k_uL - k_m)y
\end{aligned}
\tag{6.18}
$$

Where the state of the system has been augmented by an integrator state, the

reduced-order compensator is given by:

$$
\begin{bmatrix} \dot{z} \\ \dot{x}_i \end{bmatrix} = \begin{bmatrix} E - Gk_u & -Gki \\ 0 & 0 \end{bmatrix} \begin{bmatrix} z \\ x_i \end{bmatrix} + \begin{bmatrix} F - Gk_uL - Gk_m \\ -1 \end{bmatrix} y \quad (6.19)
$$

$$
u = \begin{bmatrix} -k_u & -k_i \end{bmatrix} \begin{bmatrix} z \\ x_i \end{bmatrix} + (-k_uL - k_m)y
$$

6.4   Reduced-Order Estimator-Based Compensator

For the Ćuk converter model, matrix C is of the form $C = \begin{bmatrix} I & 0 \end{bmatrix}$ therefore v_2 is a measured state, and the unmeasured states are v_1, i_2, and i_1. This means that a reduced order observer may be designed that estimates only the three unmeasured states. The block model for a system controlled by a compensator made of a reduced-order estimator and a linear state feedback law is shown in Figure 6.6, and was used to derive the following state equations:

$$
\begin{aligned}
\dot{x} &= (A - B_dk_uLC - B_dk_mC)\, x - B_dk_ix_i - B_dk_uz + Bv_g \quad (6.20) \\
\dot{x}_i &= -Cx \\
\dot{z} &= (FC - Gk_mC - Gk_uLC)\, x - Gk_ix_i + (D - Gk_u)\, z \\
v_o &= Cx
\end{aligned}
$$

from which were determined the matrices:

$$
\begin{aligned}
\bar{A} &= \begin{bmatrix} A - B_dk_mC - B_dk_uLC & -B_dk_i & -B_dk_u \\ -C & 0 & 0 \\ FC - Gk_mC - Gk_uLC & -Gk_i & E - Gk_u \end{bmatrix} \quad (6.21) \\
\bar{B} &= \begin{bmatrix} B & 0 & 0 \end{bmatrix}' \\
\bar{C} &= \begin{bmatrix} C & 0 & 0 \end{bmatrix} \\
\bar{D} &= [D]
\end{aligned}
$$

where

$$
\begin{aligned}
E &= A_{22} - LA_{12} \quad (6.22) \\
F &= EL + A_{21} - LA_{11} \\
G &= B_{d_2} - LB_{d_1}
\end{aligned}
$$

To determine estimator pole placement, the same type of iterative algorithm used for the full order observer was implemented. The reduced order observer poles were placed to have faster dynamics than the poles of the controlled system.

The step disturbance transient is shown in Figure 6.7. The loop gain of the controlled system may be seen in Figure 6.8, where the loop is broken at
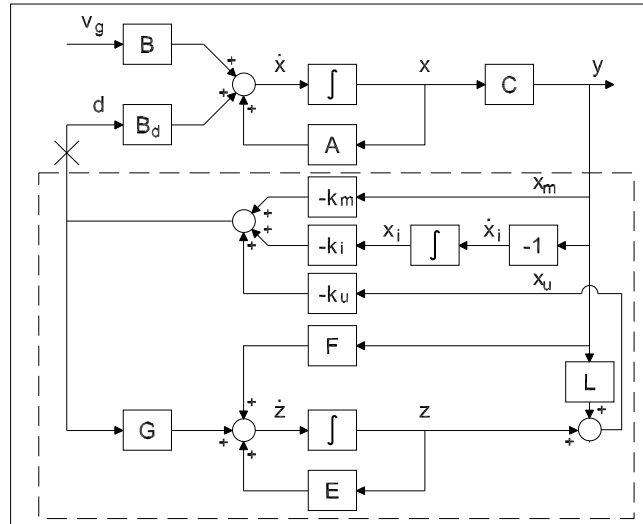
Figure 6.6: A state feedback regulator with integral action based on a reduced-order estimator.

the large X shown on the control input d in Figure 6.6. MATLAB calculations give the gain margin as ∞ dB and a phase margin of 36.5°. The latter clearly does not meet the design specification for phase margin, and uncertainty in the system model may make the controlled system unstable.
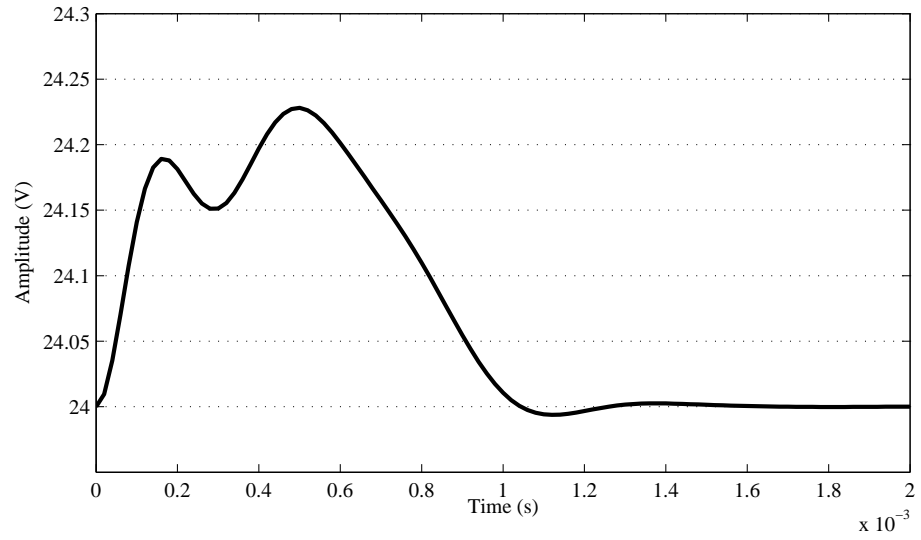
Figure 6.7: Unit step disturbance response of Ćuk converter with ROESFBI compensator.
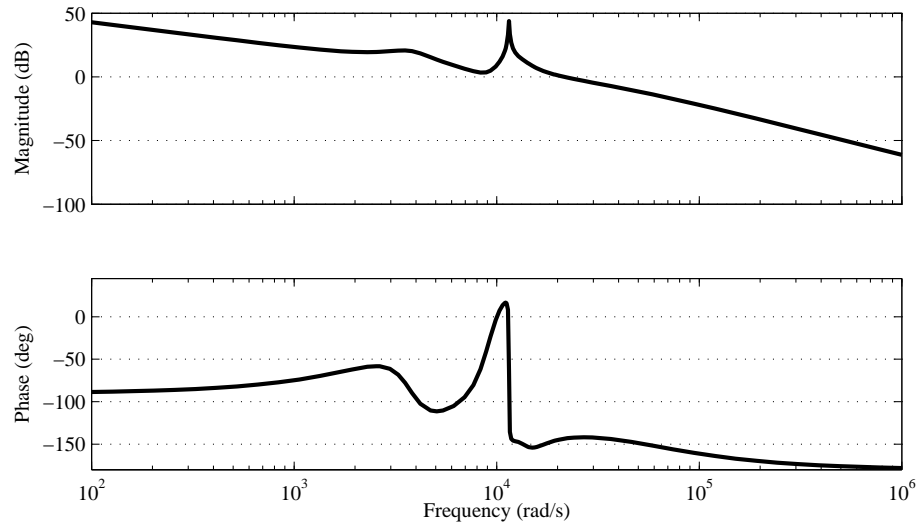
Figure 6.8: Loop gain of Ćuk converter controlled by ROESFBI compensator.

Chapter 7

Linear Quadratic Optimal Control

Linear quadratic optimal control uses penalties on state transients x and control effort u to optimize system performance with respect to a figure of merit determined by a cost function. There is typically a classical trade-off designed into the cost function: one cannot have tight control over state transients with small control effort. In other words, small output transients require large controller gains (and therefore control effort). Additionally, quadratic forms are used to ensure that only the magnitude and not the sign of the transient contributes to the cost determined by the penalty function.

7.1 Linear Quadratic Regulators

To optimally control state transients and control effort within performance specifications, a compensator is sought that seeks to provide a control effort u that minimizes a Lagrangian cost function:

$$J = \int_0^\infty (x^T Q x + u^T R u) dt \tag{7.1}$$

subject to the constraint of the state equation:

$$\dot{x} = Ax + Bu \tag{7.2}$$

This is known as the linear quadratic regulator (LQR) problem. The weight matrix Q is an $n \times n$ positive semidefinite matrix (for a system with n states) that penalizes variation of the state from the desired state. The weight matrix R is an $m \times m$ positive definite matrix that penalizes control effort. Solutions for the constrained optimal system can be found in [7], [8], and [9]. The well-published time invariant solution to this problem is:

$$K = R^{-1} B^T P \tag{7.3}$$

where P is the unique, symmetric, positive definite solution to the steady-state algebraic Riccati equation (ARE):

$$PA + A^T P - PBR^{-1}B^T P + Q = 0 \tag{7.4}$$

The minimum value of the cost function is based on the initial state x_0, and is given by:

$$J_{min} = x_0^T P x_0 \tag{7.5}$$

The LQR designed for a SISO system can be shown to possess very desirable stability properties: it always has a gain margin between {-6 dB, ∞} and a phase margin of at least 60°. However, it has a high frequency roll-off rate of only 20 dB per decade so the open loop frequency response shows susceptibility to high frequency noise.

Since the weight matrices Q and R are both included in the summation term within the cost function, it is really the relative size of the weights within each quadratic form which are important. Simple inspection of the cost function shows that multiplying both weight matrices by the same real constant (e.g., κ) will not affect their ratio. The multiplier κ may be factored out of the integral, thus returning the cost function to its original form. Thus, the problem of minimizing κJ becomes the same as minimizing J. Therefore, holding one weight matrix constant while varying either the individual elements or a scalar multiplier of the other is an acceptable technique for iterative design. It is good for the designer to maintain an understanding of the effects of manipulating individual weights, however. In general, raising the effective penalty a single state or control input by manipulating its individual weight will tighten the control over the variation in that parameter, however it may do so at the expense of larger variation in the other states or inputs.

7.2   Ćuk Converter with LQR Compensator

The fifth-order system formed by augmenting the Ćuk converter with an integral state requires that Q be a five-by-five matrix. To review, the state vector is $[v_2\ v_1\ i_2\ i_1\ x_i]'$, where x_i corresponds to the integral of the reference error e. Since the states have physical significance in this model, it is easy to see that each voltage, current, or error transient may be individually penalized using the diagonal elements of the Q matrix. As the objective of controlling the Ćuk converter is to regulate the output $v_o = v_2$ in the face of disturbances to v_g, penalizing transients that occur on state v_2 is a logical choice, as is penalizing the state x_i associated with the reference error integral as the integral of that error should be minimized to provide for good regulation. Hence, the Q matrix chosen for design of the LQR has two positive entries corresponding to the first (Q_{11}) and last (Q_{55}) entries along the diagonal to ensure it is positive semidefinite. The Ćuk converter has only a single control input, and for initial design R was set equal to 1 arbitrarily. If the control effort exceeds the limitations put on it

(refer to Section 3.5), the value of R may need to be increase to penalize the control effort.

After proceeding through an iterative process where Q_{11} and Q_{55} were varied with R fixed, a finalized design was determined. The step disturbance response of the controlled Ćuk converter is shown in Figure 7.1 The loop gain of the
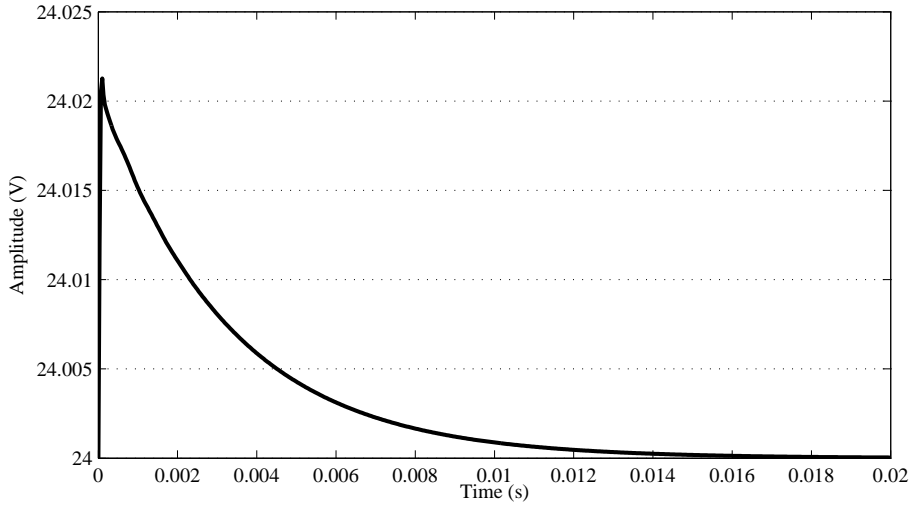

Figure 7.1: Unit step disturbance response of the Ćuk converter controlled by LQR.

controlled system is shown in Figure 7.2, where the loop is broken at the large X shown on the control input d. Figure 7.3 shows the control effort produced by the optimal controller. Note that the time of the unit step disturbance transient with the LQR compensator was significantly longer than the settling times of the previously designed compensators. However, the amplitude deviation was significantly smaller. This is an acceptable design tradeoff since the performance specifications were still met.

7.3 Linear Quadratic Gaussian Regulators

The LQR problem requires that full state feedback be used. This is not always possible, as was discussed in Section 6. The Kalman-Bucy filter is the dual to the LQR problem; it forms an optimal state estimator in the presence of process and measurement noise for a system that is observable. The presence of noise introduces stochastic effects on the state trajectory, therefore, the optimal state estimator must deal with these stochastic effects appropriately by removing them. Since the process of removing noise from a signal is commonly known as filtering, the optimal observer became known as the Kalman filter, or Kalman-Bucy filter, after its creator(s). The Kalman filter is based on essen-
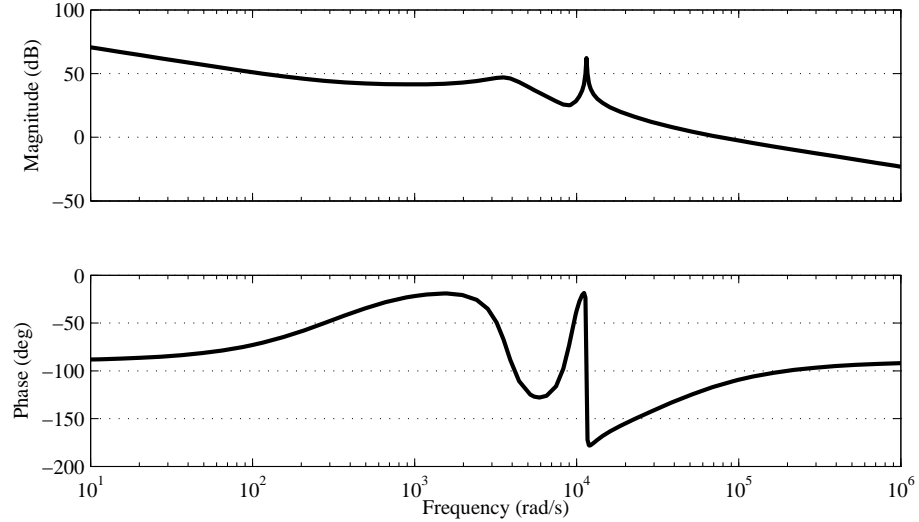
Figure 7.2: Loop gain of Ćuk converter controlled by LQR compensator.

tially the same mathematics as the LQR and, as such, has come to be known as a linear quadratic estimator (LQE). The cost function J_0 that is minimized is the error variance between the state vector and its estimate. LQE calculates the solution to an ARE (which happens to be the error covariance) and uses it to determine L, the estimator gain vector, along the lines of the same equations given for the LQR gain K. Q_0, the covariance matrix of the process noise, and R_0, the covariance matrix of the sensor noise, have to be selected for optimal determination of the observer gain vector L.

When combined, the linear quadratic controller and estimator form a structure known as a linear quadratic Gaussian (LQG) compensator. Once the state variables have been estimated, they are fed back through the controller gain K to close the loop. The separation principle previously mentioned still holds true for LQG design: the LQR and LQE problems can be solved independently via two algebraic Riccati equations.

Adding process disturbances and measurement noise to the state space system description results in:

$$\begin{aligned} \dot{x} &= Ax + Bu + \omega \\ y &= Cx + \nu \end{aligned} \qquad (7.6)$$

where ω is the disturbance signal (typically modeled by Gaussian white noise of spectral density Q_0) and ν is additive measurement noise (Gaussian white noise, with spectral density R_0). Note that the fact that neither ω or ν has a coefficient implies a coefficient of I, meaning each state and output has its own distinct noise [10]. The time invariant solution to the optimal estimator
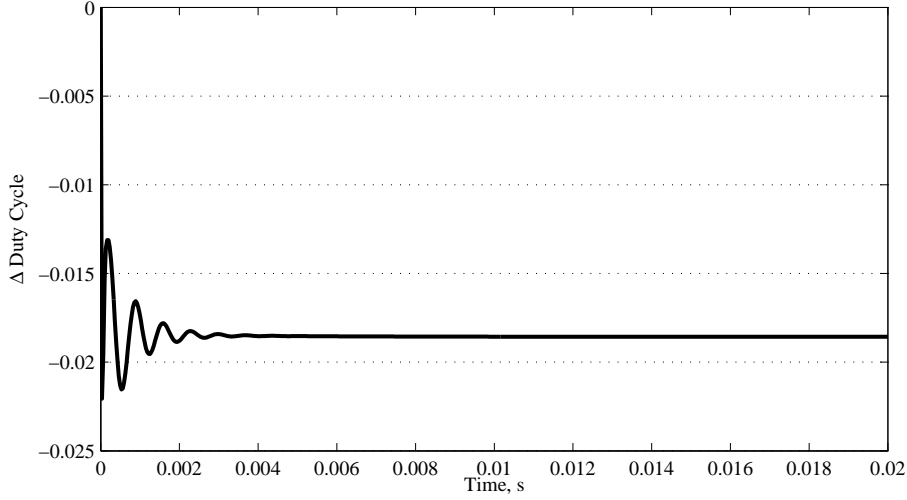
Figure 7.3: LQR control effort.

problem is then:

$$L = P_0 C^T R_0^{-1} \tag{7.7}$$

where P (known as the estimation error variance) is the unique, symmetric, positive definite solution to the steady-state algebraic Riccati equation:

$$AP_0 + P_0 A^T - P_0 C^T R_0^{-1} C P_0 + Q_0 = 0 \tag{7.8}$$

Since the spectral density of the process and measurement noise in a system is typically unknown, designers frequently treat Q_0 and R_0 as additional design parameters that can be manipulated. The bandwidth of the open-loop system frequency response can be controlled using these matrices. This can allow reduction of the susceptibility of the controlled system to noise at higher frequencies.

7.4   Ćuk Converter with LQG Compensator

The unit step response of the Ćuk converter controlled by a LQG compensator is shown in Figure 7.4. A comparison of the loop gains of the LQR and LQG controlled systems is shown in Figure 7.5, where the loop is broken at the control input d. Loss of gain and phase margins has clearly occurred. Figure 7.6 shows the control effort produced by the LQG controller. Minimal discussion is given to this design as it requires the improvements described in the next section.

Figure 7.4: Unit step disturbance response of Ćuk converter controlled by LQG compensator.

7.5   Control with LQG/LTR Compensators
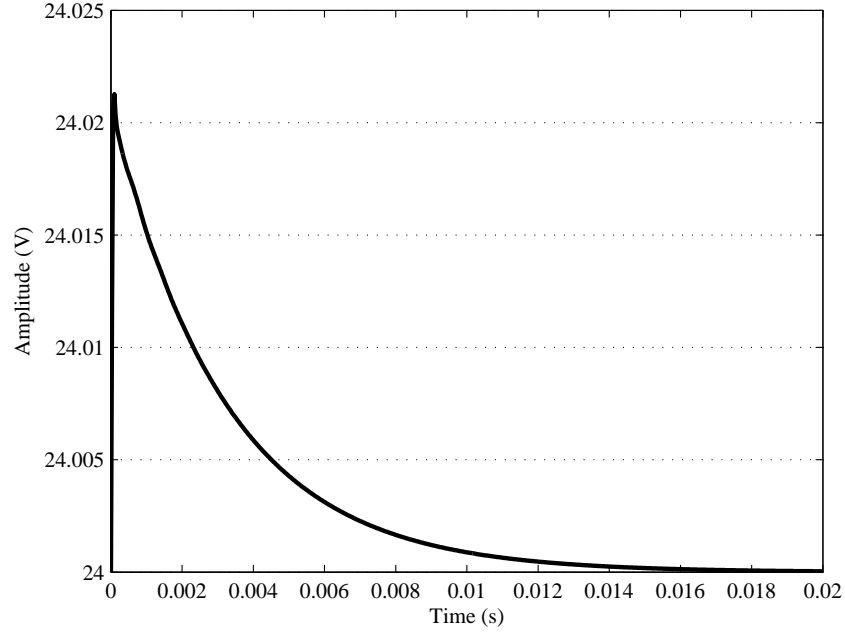
Newcomers to the world of optimal control might think that the pairing of the optimal controller formed by the solution of the LQR problem and the optimal estimator formed by the construction of a Kalman filter would have optimal properties. This is not necessarily the case. Doyle [11] provided an example to show that the LQG design loses the guaranteed stability margins of the LQR design when feeding back estimated states. Doyle and Stein [12] then showed how this problem could be addressed. In order to recover the good stability margins and sensitivity properties of an LQR design, an iterative procedure known as loop transfer recovery (LTR) may be performed during the LQG design. (A variety of other methods for LTR have been presented in the controls literature, including several which require employment of subspace methods or special coordinate bases [13], [14], but these techniques are beyond the scope of this work.) The Doyle-Stein method of LTR is performed by iteratively increasing the intensity of the noise covariance matrices used in Kalman filter design. LTR causes the open loop frequency domain characteristics associated with the LQR design to be either exactly or asymptotically recovered as an input noise matrix weighting parameter q is increased. As $q \to \infty$, the properties of
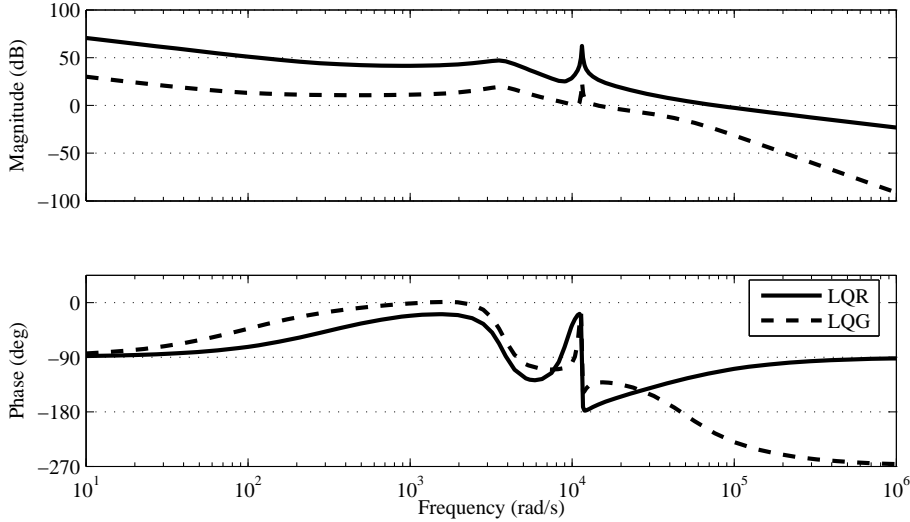
Figure 7.5: Loop gain of Ćuk converter controlled by LQR vs. LQG.

the LQR are recovered. Essentially, LTR produces a state estimator whose estimates $\hat{x}$ are independent of the control input u (or only weakly depended on u) and dependent only on the input provided by the plant output y.

Performing the Doyle-Stein method of asymptotic loop transfer recovery on a full-order compensator requires:

- The system must be minimum-phase and strictly proper.

- $R_o = 1$ and $Q_o = q^2 BB'$

The fact that the plant must be minimum-phase (all poles and zeros in the left half of the complex plane and no pure delays) prevents the compensator designed from being unstable, since the LTR technique moves some of the compensator poles toward the plant zeros where pole-zero cancellation makes them unobservable. (Other LTR methods may be used with nonminimum-phase systems by using subspace [14] or loop-shaping techniques [15].) The remainder of the poles (an excess of poles exists because the plant is strictly proper) move toward infinity in the left-half of the complex plane in a Butterworth filter pattern [16].

The effect of loop transfer recovery is to essentially decouple the observer from the control input u by raising the observer gain L so that the state estimate $\hat{x}$ depends only on the plant output y. This is illustrated in Figure 7.7. The decoupling is accomplished by the increasing noise intensity on u, which causes L to increase such that y has a larger contribution to the state estimate.

In order to accomplish LTR, the loop is broken at the large X on the control input shown in Figure 6.1. The loop is explicitly shown in Figure 7.8. The frequency response of the loop from d to d' is driven to asymptotically approach the frequency response of the system with LQR control. Figure 7.9 shows the
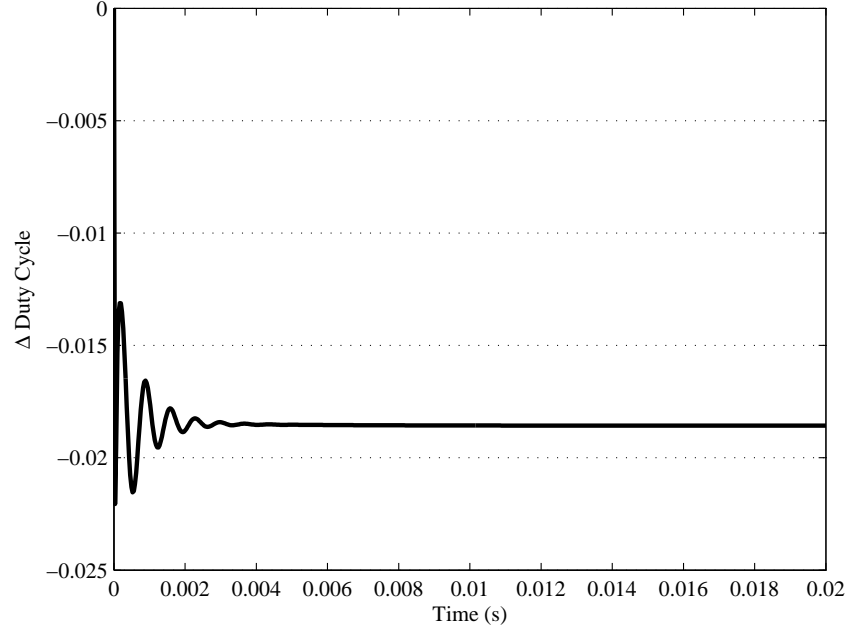
Figure 7.6: LQG control effort.

LQGI/LTR iterative design process applied to the Ćuk converter. Initial LQGI design resulted in a gain margin reduction from infinity to 28.2 dB and a loss of phase margin from $65.4°$ to $32.7°$. The iterative loop transfer recovery process resulted in a controlled system gain margin of 30.2 dB and phase margin of $61.7°$. Iteration was stopped at that point since these margins are adequate. Further iterations would result in larger observer gains that may be undesirable during implementation, and recovery of the undesirable high frequency characteristics of the LQR compensator has already begun.
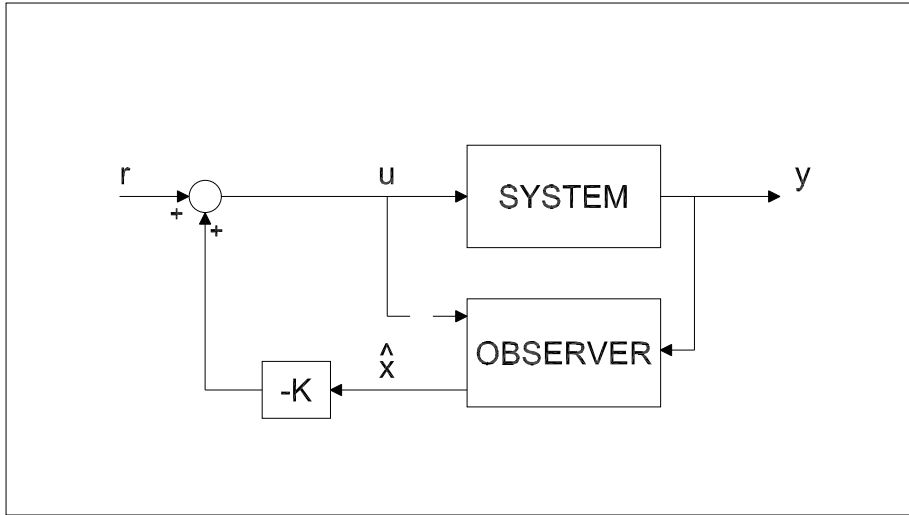
Figure 7.7: Input decoupling effect of loop transfer recovery.
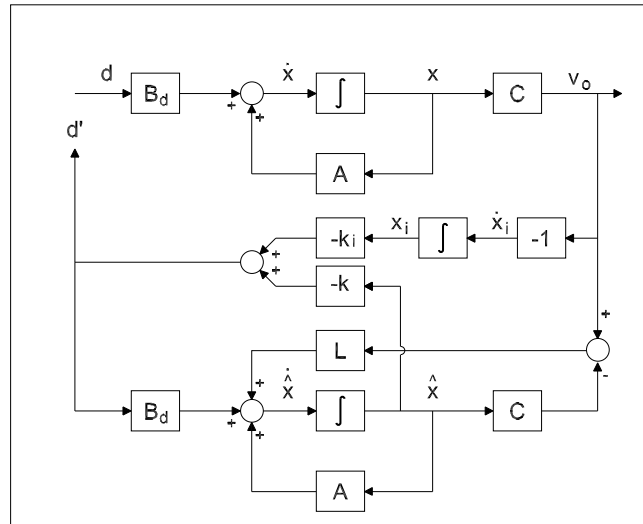
Figure 7.8: The loop to be recovered during loop transfer recovery with a full-order observer.

Figure 7.9: Loop transfer recovery of an LQGI compensator.

Chapter 8

Compensator Order Reduction

With the advent of computer control of systems, high-order system models can be created that allow model-based control methods (such as observer-based compensators) to be easily implemented. These digital controller implementations have many advantages over analog controllers, which may be considered to be outdated. However, analog control can often still be performed at the circuit level with a few discrete components and may be more cost-effective to implement when compared to a microproce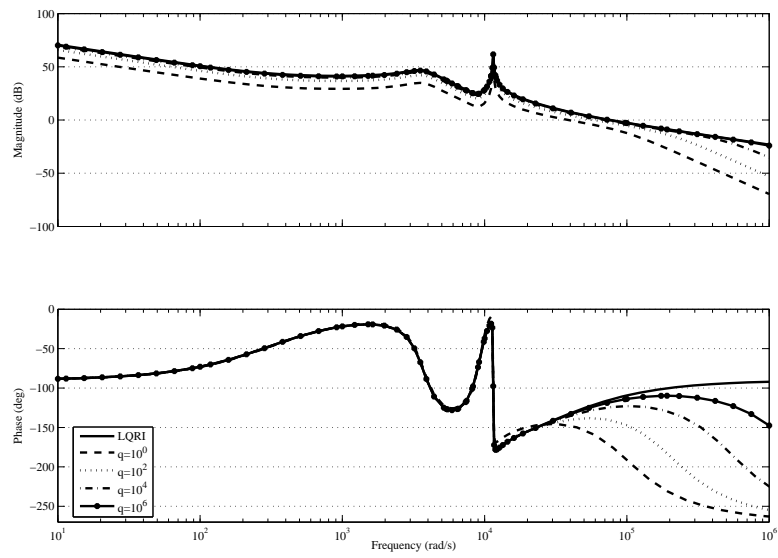ssor and its associated support circuitry and programming. Thus, this section examines the idea of controller order reduction for use with analog circuitry. It focuses first on reducing the order of an LQGI/LTR compensator using model reduction techniques, then design of an LQGI/LTR compensator using a reduced-order Kalman filter (ROKF), and finally, application of model reduction techniques to the ROKF-based compensator. This final two-step order reduction technique has not been previously seen in the literature.

8.1 Model Reduction of the LQGI/LTR Compensator

Model reduction (MR) may be accomplished by creating a balanced realization (i.e., equal and diagonal controllability and observability Gramian matrices) of the system to be reduced using a linear transformation such as the *balreal* command in MATLAB [17]. Examination of the eigenvalues of the Gramian matrix of the balanced realization allows the designer to identify states that are weakly coupled to both the input and output of the compensator. These states, which are at once both weakly controllable and weakly observable, have small Hankel singular values associated with them. Hankel singular values are determined by taking the square root of the product of the eigenvalues of the

controllability and observability Gramian matrices. In a balanced realization, the Hankel singular values are the diagonal entries of the common controllability/observability Gramian matrix, and the states are ordered from highest to lowest Hankel singular value [18]. Compensator states with small Hankel singular values may be eliminated with little impact to the performance of the compensator using the *modred* command in MATLAB.

In this case, the system to be reduced is the compensator. The *balreal* command identifies only two states that may be eliminated from the LQGI/LTR compensator designed previously without significant loss of accuracy, as may be predicted by the information provided from the pole-zero plot in Figure 8.1. Model reduction resulted in the addition of a high-frequency zero for this particular compensator. This zero was a simulation artifact created by the *modred* command, therefore it was removed by truncation.

Examination of the LQGI/LTR compensator poles, zeros, and gain of the transfer function yields:

$$p = \begin{bmatrix} -1490 \pm j9000 & -1129500 \pm j1129500 & 0 \end{bmatrix} \qquad (8.1)$$
$$z = \begin{bmatrix} -32410 & -319 & -1440 \pm j9090 \end{bmatrix}$$
$$k = 7.195 \times 10^7$$
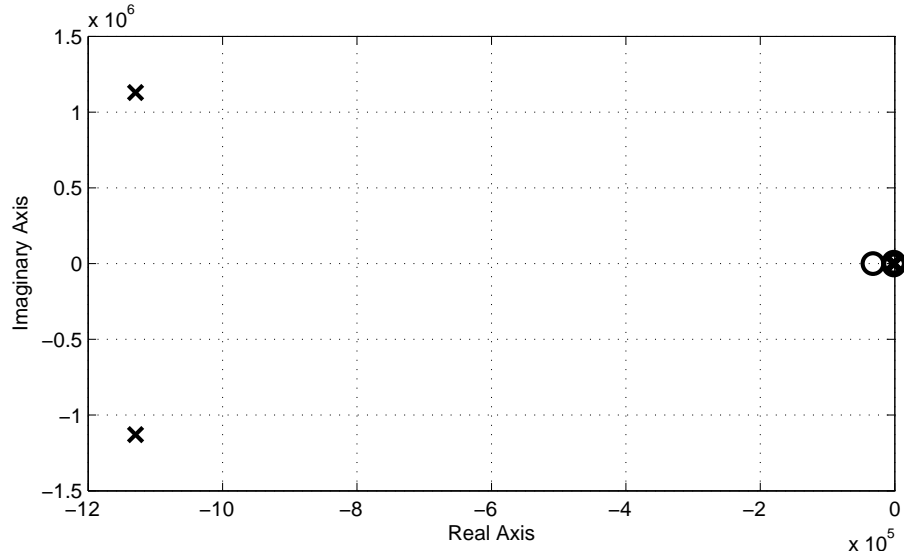
Figure 8.1: Pole-zero plot of the LQGI/LTR compensator.

By comparing the frequencies at which the poles and zeros occur and their complex plane locations, it can be seen that a complex pair of zeros at $-1490 \pm j9000$ essentially cancels out a complex pair of poles at $-1440 \pm j9090$. This is more readily viewed in the close-up view of the pole-zero plot in Figure 8.2. Examination of the compensator after model reduction methods yields:
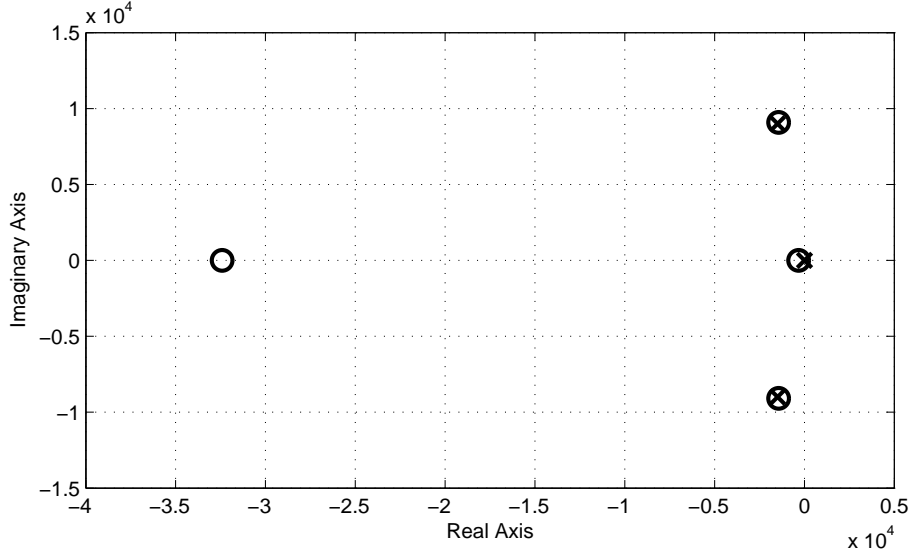
Figure 8.2: Compensator pole-zero plot showing likely pole-zero pair cancellation.

$$
\begin{aligned}
pr &= \begin{bmatrix} 0 & -1126800 \pm j1132300 \end{bmatrix} \\
zr &= \begin{bmatrix} -319.5 & -33035 \end{bmatrix} \\
kr &= 7.18 \times 10^7
\end{aligned}
\tag{8.2}
$$

Once model reduction has been accomplished, validation must occur to verify that significant differences do not exist between the full-order and model-reduced compensators. Comparison of the full-order and model-reduced compensator frequency responses is shown in Figure 8.3. Based on this diagram, it is readily apparent that the model-reduced compensator may be used to replace the full-order compensator without significant difference, thus reducing the controller order. The MRLQGI/LTR compensator can then be achieved with less analog circuitry than the LQGI/LTR yet still perform adequately, and therefore may be selected for implementation.

Care must be taken when performing model reduction to ensure desirable stability margins are not lost. Comparable frequency responses between the full-order and model-reduced compensators tell the designer that margins will probably not change appreciably during model reduction. Verification of margins was performed for system with the MRLQGI/LTR compensator; no change in gain margin resulted but phase margin was reduced to 61.2°, a loss of 0.5°, which is not a significant difference.

The step disturbance response for the model-reduced compensator is shown in Figure 8.4. The step disturbance input is attenuated well, with a maximum deviation of just over 20 mV. This would be a perfectly acceptable controller
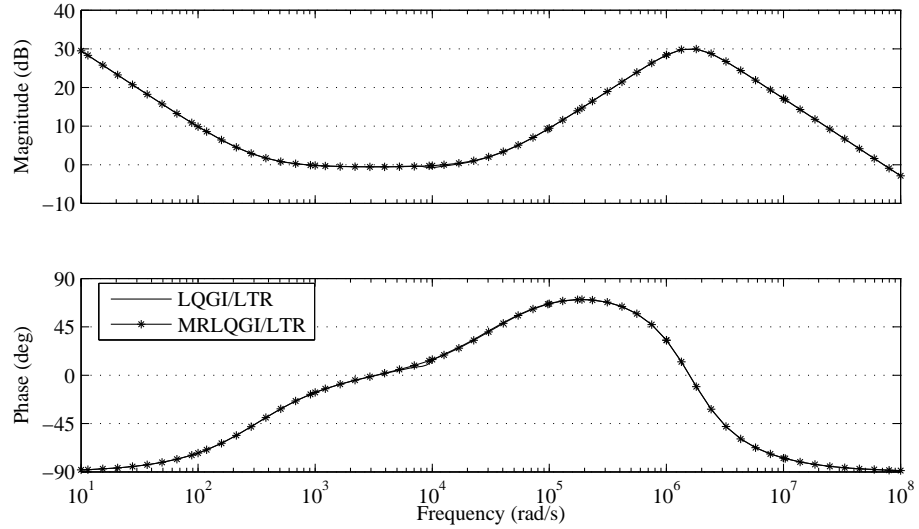
Figure 8.3: Compensator frequency response comparison following model reduction.

for the Ćuk converter, however, additional order reduction (though impossible to achieve in this controller incarnation without significantly impacting performance) would be desirable and is explored in the next section.

8.2   A Reduced-Order LQGI/LTR Compensator

The model-reduced compensator designed in Section 8.1 is based on pole-zero cancellation in a balanced state-space realization of the Kalman filter and truncation to remove a high-frequency zero. However, a compensator based on a LQRI paired with a reduced-order Kalman filter (ROKF) can be designed and the LTR technique applied during the design process in order to develop a ROLQGI/LTR compensator. Madiwale and Williams [19] described the mathematics necessary for performing loop transfer recovery with reduced-order linear quadratic compensators and provided proofs that the equations used in this section achieve LTR.

The design of the ROLQGI/LTR compensator begins with construction of a linear quadratic regulator. Once the regulator gain K has been determined, the system matrices and K are partitioned to form a reduced-order observer as in Equation 6.10.

Consider a minimum phase system with process noise ω (with positive definite Gaussian spectral density matrix V) that is distributed into the state dynamics by W and let the system be free from measurement noise in the measured
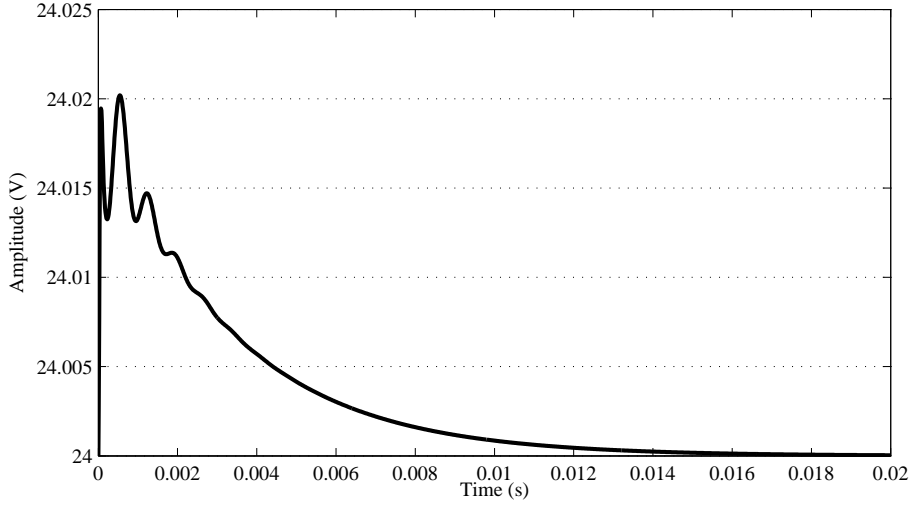
Figure 8.4: Unit step disturbance response of Ćuk converter - MRLQGI/LTR compensator.

state vector x_m:

$$
\begin{aligned}
\dot{x} &= Ax + Bu + W\omega \\
y &= x_m
\end{aligned}
\tag{8.3}
$$

Process noise characteristics are usually difficult to determine or unknown. Thus, both W and the corresponding noise spectral density V are manipulated as design parameters for determining the optimal reduced-order estimator gain L in a manner similar to the manipulation of Q_0 and R_0 in full-order estimator design methods. Both W and V are also partitioned as in Equation 6.10 in order to form the reduced-order Kalman filter. Let:

$$
\begin{aligned}
V_{11} &= W_1 V_1 W_1' + q^2 B_1 V_2 B_1' \\
V_{12} &= W_1 V_1 W_2' + q^2 B_1 V_2 B_2' \\
V_{22} &= W_2 V_1 W_2' + q^2 B_2 V_2 B_2'
\end{aligned}
\tag{8.4} \tag{8.5} \tag{8.6}
$$

Then with:

$$
\begin{aligned}
\bar{A} &= A_{22} - V_{12}' V_{11}^{-1} A_{12} \\
\bar{V} &= V_{22} - V_{12}' V_{11}^{-1} V_{12}
\end{aligned}
\tag{8.7}
$$

where V_{11} is nonsingular, the following ARE is solved for for Q_o:

$$
\bar{A}Q_o + Q_o\bar{A}' - Q_o A_{12}' V_{11}^{-1} A_{12} Q_o + \bar{V} = 0
\tag{8.8}
$$

The Kalman filter gain L can then be determined from:

$$
L = (Q_o A_{12}' + V_{12}') V_{11}^{-1}
\tag{8.9}
$$

Now, as q is increased in Equations 8.4-8.6, the target feedback loop of the LQR controller is recovered.

Once again, the loop is broken at the large X on the control input as shown in Figure 6.6. The open loop is shown explicitly in Figure 8.5. The frequency response of the loop from d to d' is again driven to asymptotically approach the frequency response of the system with LQR control as shown in Figure 8.6, which is a plot of the iterative LTR process for this reduced-order compensator and the Ćuk converter.
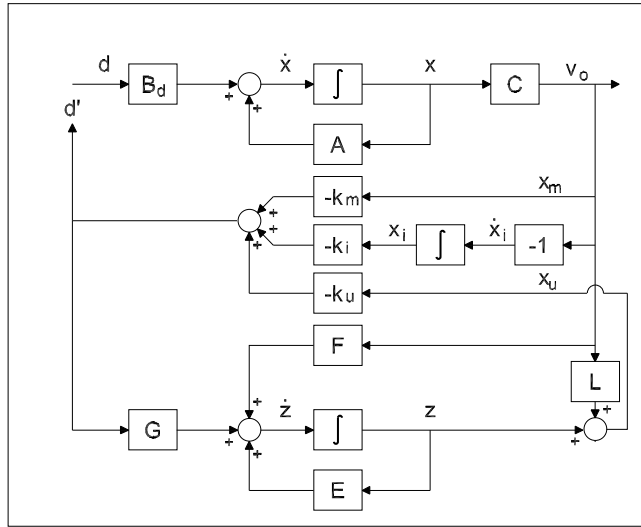
Figure 8.5: Loop transfer recovery with a reduced-order observer.

During simulation, it was found that the original matrices selected to represent the process noise had values that were too large. The initial results showed loop transfer recovery had already occurred, therefore the noise values had to be made smaller to verify that LTR was taking place. For the model of the Ćuk converter to be controlled, the following partitions of the W and V matrices were used to simulate the fictitious noise:

$$W_1 = \begin{bmatrix} 1 \times 10^{-4} & 0 & 0 \end{bmatrix}, W_2 = \begin{bmatrix} 1 \times 10^{-5} & 0 & 0 \\ 0 & 1 \times 10^{-5} & 0 \\ 0 & 0 & 1 \times 10^{-5} \end{bmatrix}$$

$$V_1 = \begin{bmatrix} 1 \times 10^{-5} & 0 & 0 \\ 0 & 1 \times 10^{-5} & 0 \\ 0 & 0 & 1 \times 10^{-5} \end{bmatrix}, V_2 = 1 \times 10^{-5}$$

The scalar q was allowed to vary from 1×10^{-10} to 1×10^{-7} during the recovery process.
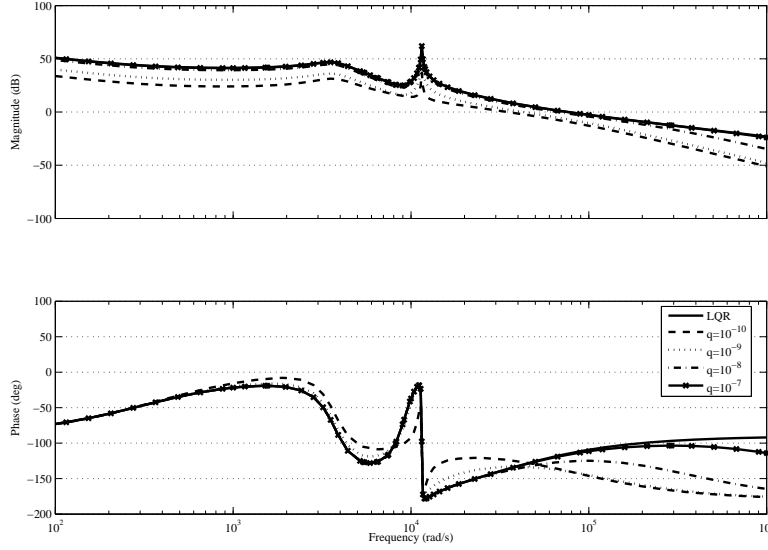
Figure 8.6: Loop transfer recovery of a ROKF-based LQGI compensator.

Examination of the ROLQGI/LTR compensator transfer function yields:

$$
\begin{aligned}
pr &= \begin{bmatrix} -1490.0 \pm j9000.0 & -2466000.0 & 0.0 \end{bmatrix} \quad\quad (8.10) \\
zr &= \begin{bmatrix} -32990.0 & -319.2 & -1442.0 \pm j9087.0 \end{bmatrix} \\
kr &= 70.74
\end{aligned}
$$

which shows a pole-zero pair that could possibly be canceled via model reduction methods. The balanced realization approach to model reduction discussed in Section 8.1 was applied. Comparison of the Hankel singular values produced by the *balreal* command revealed that only two states could be eliminated without significant loss of accuracy in the controller model. Elimination of these states resulted in a second-order compensator that had the following characteristics for its transfer function:

$$
\begin{aligned}
pr &= \begin{bmatrix} 0.0 & -2469000.0 \end{bmatrix} \quad\quad (8.11) \\
zr &= \begin{bmatrix} -319.4 & -33570.0 \end{bmatrix} \\
kr &= 70.76
\end{aligned}
$$

This model-reduced compensator has a pole at the origin and two zeros on the negative real axis left of the pole, which is a classical PID controller. It also has another pole on the negative real axis beyond the zeros, which corresponds to high frequency low-pass filtering. It may therefore be thought of as a feedback

PID compensator with the derivative term acted upon by a first-order low-pass filter. This type of filtered derivative action is implemented in PID controllers to reduce the bandwidth of the controller and associated undesirable amplification of high-frequency noise, as well as to make them implementable (the ideal PID equation is non-causal due to the fact that there is an excess of zeros). This PID controller is very simple to implement with a single inverting operational amplifier configuration. A second inverter buffer stage is needed to eliminate the undesirable inversion caused by the first stage.

A frequency response comparison of the two compensators designed in this section is shown in Figure 8.7. There is excellent correlation between the Bode plots, showing that the MRROLQGI/LTR compensator performance will be almost exactly the same as the ROLQGI/LTR compensator.
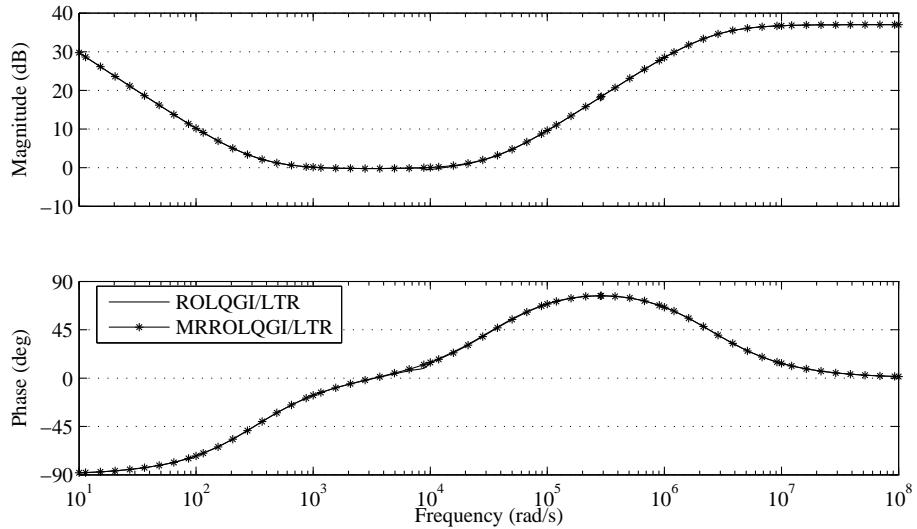
Figure 8.7: Comparison of compensator frequency response - ROLQGI/LTR and MRROLQGI/LTR.

Initial ROLQGI design resulted in no gain margin reduction from infinity but had a loss of phase margin from $65.4°$ to $56.3°$. The iterative loop transfer recovery process resulted in a controlled system phase margin of $63.7°$. Further iterations would result in larger observer gains that may be undesirable during implementation. Verification of margins was performed for system with the MRROLQGI/LTR compensator; no change in gain margin resulted but phase margin was reduced to $63.3°$, a loss of $0.4°$. Again, this is not a significant difference.

The step disturbance response for the model-reduced compensator is shown in Figure 8.8. The step disturbance input is attenuated well, with a maximum deviation of less than 20 mV. This is a perfectly acceptable controller for the Ćuk converter.
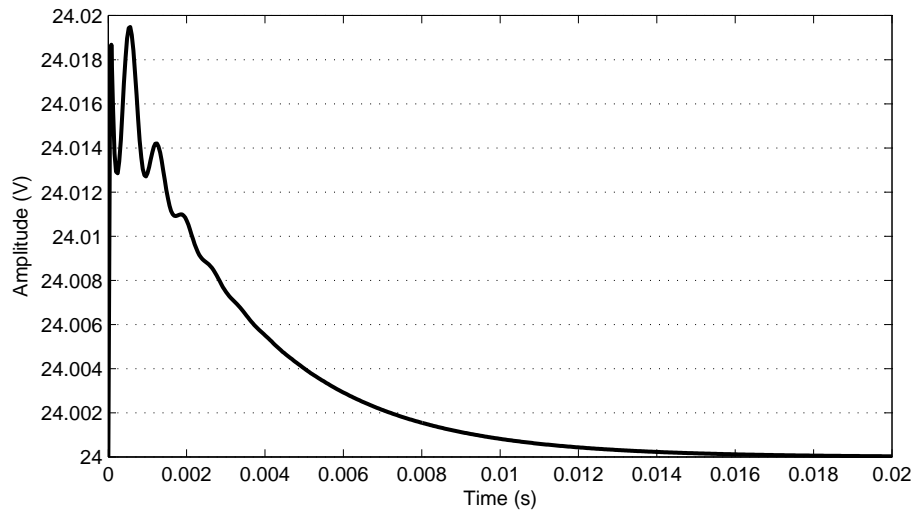
Figure 8.8: Unit step v_g response of Ćuk converter - MRROLQGI/LTR compensator

Chapter 9

Compensator Implementation

At this point, four optimal compensator designs that rely on output feedback and state estimation have been developed. The initial design of the optimal compensator began with a fifth-order controller, with estimated states for each of the four states in the plant and an augmented integral state (LQGI/LTR). Model reduction techniques applied directly resulted in a third-order controller (MRLQGI/LTR), which was a significant improvement in terms of minimizing the circuitry for implementation. The final design began with a fourth-order compensator based on three states from a reduced-order observer augmented by an integral state (ROLQGI/LTR), to which model reduction techniques were applied to form a second-order transfer function (MRROLQGI/LTR). This final regulator had the form of a classical PID controller. The final design had a significant reduction in circuitry yet maintained excellent performance in both the time and frequency domains.

The reduced-order compensators developed in Chapter 8 using model reduction techniques can be implemented with analog circuits using operational amplifiers. The goal is to use the minimum amount of components and circuitry for control (to minimize manufacturing costs) while maintaining adequate controller performance.

9.1 MRLQGI/LTR Compensator Construction

The model-reduced compensator designed in Section 8.1 has two zeros on the negative real axis, a LHP pair of complex poles, and a pole at the origin. This compensator can be implemented by a PI compensator cascaded with a Tow-Thomas biquadratic filter as seen in Figure 9.1. The Tow-Thomas filter is a general second-order filter able to implement low-pass, high-pass, band-pass, notch, and all-pass filters with appropriate choices of coefficients of the filter

transfer function [20]:

$$T_b(s) = \frac{a_2 s^2 + a_1 s + a_0}{b_2 s^2 + b_1 s + b_0} \tag{9.1}$$

The biquad filter section is used to implement the second-order denominator term with a simple zero by setting $a_2 = 0$. The PI section is used to implement the other real zero and the pole at the origin. For both sections, it is desirable to keep the poles and zeros within a certain frequency tolerance of each other to keep the component values reasonable in size. The transfer function of the
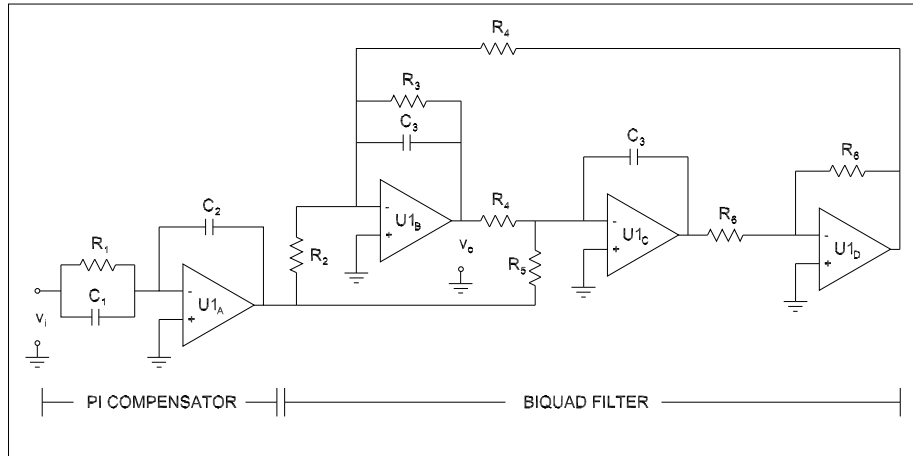
Figure 9.1: The MRLQGI/LTR compensator implemented using operational amplifiers.

PI section is given by:

$$T_p(s) = -\frac{\frac{C_1}{C_2}(s + \frac{1}{C_1 R_1})}{s} \tag{9.2}$$

The transfer function of the biquad filter section is given by:

$$T_b(s) = -\frac{\frac{1}{C_3 R_2} s + \frac{1}{C_3^2 R_4 R_5}}{s^2 + \frac{1}{C_3 R_3} s + \frac{1}{C_3^2 R_4^2}} \tag{9.3}$$

9.2 MRROLQGI/LTR Compensator Construction

A practical example of the MRROLQGI/LTR compensator requires fewer components to implement than the MRLQGI/LTR circuit. It is simply an
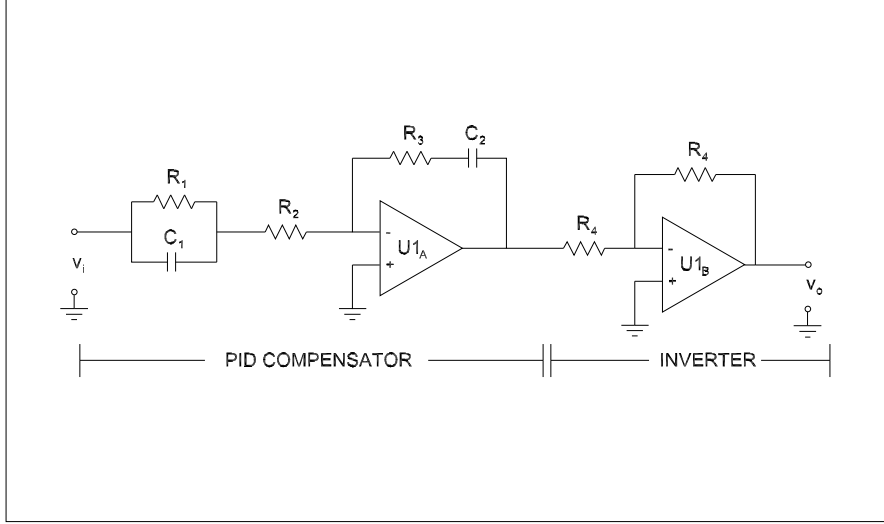
Figure 9.2: The analog MRROLQGI/LTR compensator implementation.

analog PID controller with a filtered derivative term [21]. Consider the circuit in Figure 9.2. With the inverting opamp configuration and some algebraic manipulation, the transfer function is shown to be:

$$T(s) = \frac{\frac{R_3}{R_2}(s + \frac{1}{C_2 R_3})(s + \frac{1}{R_1 C_1})}{s(s + \frac{R_2 + R_1}{R_1 R_2 C_1})} \tag{9.4}$$

which shows the following zeros, poles, and gain:

$$poles = \begin{bmatrix} 0 & \frac{-(R_2 + R_1)}{R_1 R_2 C_1} \end{bmatrix} \tag{9.5}$$
$$zeros = \begin{bmatrix} \frac{-1}{C_2 R_3} & \frac{-1}{R_1 C_1} \end{bmatrix}$$
$$gain = \frac{R_3}{R_2}$$

Component values may be determined by equating the expressions in 9.5 with the compensator values given in 7.11. Since there are fewer equations than unknowns, one of the component values must be fixed before the other component values may be determined. The final design used the component values given in Table 9.1.

Table 9.1: Component values for MRROLQGI/LTR compensator implementation.

Component	Value
R_1	100 $k\Omega$
R_2	1.4 $k\Omega$
R_3	100 $k\Omega$
C_1	0.29 nF
C_2	31.3 nF

Chapter 10

Power Electronic Circuit Simulation

The MRROLQGI/LTR compensator required the least amount of circuitry and was therefore selected for implementation and testing in PECS. The PECS environment provides for relatively short run times compared to SPICE-based circuit simulation environments since power electronics circuits can typically be simulated with simpler component models than other types of analog circuits.

10.1 Simulating the Controlled Ćuk Converter in PECS

The PECS implementation of the MRROLQGI/LTR compensator design from Section 9.2 connected to the Ćuk converter can be seen in Figure 10.1.

First, the small-signal operation was tested using a step disturbance in v_g as was used during controller design. A simulation was set up to provide for input voltage steps up and down from the nominal 12 V using a unit step to 13 V on the Ćuk input. The simulation used a time step of 1 μs and a run time of 0.1 s. The results of this simulation are shown in Figure 10.2. The maximum deviation in the output voltage is only 0.022 V in response to a step input of 1 V. (Note that ripple voltage exists in the simulation which is not present in the state space averaged model simulations in MATLAB. Neglecting the ripple did not pose a problem, however, during the control system design process.)

Next, a large-signal simulation was set up to provide for input voltage steps up and down from the nominal 12 V through a specified operating range of 9-14 V on the Ćuk input. The results of the large-signal simulation are shown in Figure 10.3. The maximum deviation of 0.11 V in the output voltage occurred when the input voltage drops sharply from 14 V to 9 V but is rapidly brought back under control. This value is well within the 0.24 V tolerance that was specified for controller performance.
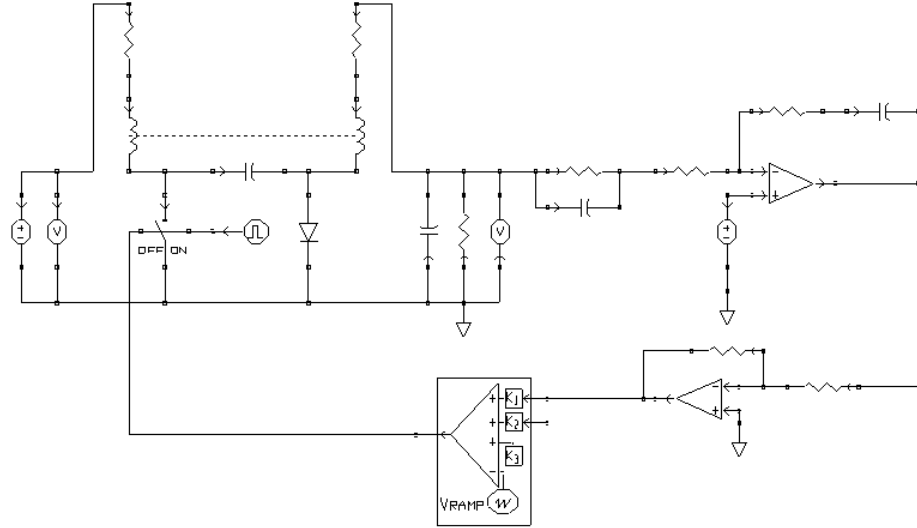
Figure 10.1: PECS simulation of Ćuk converter - MRROLQGI/LTR compensator.

Finally, a simulation was set up to provide for 25% load current steps (0.214 A) around the nominal load current of 0.857 A. The results of this simulation are shown in Figure 10.4. The maximum deviation of 0.175 V in the output voltage occurred when the load current dropped sharply from 1.071 A to 0.643 A, but this is within the transient design specification of regulation to within 1% of the nominal output voltage.

The ability to reject large scale input voltage and load disturbances shows that the compensator design is excellent. The MRROLQGI/LTR controller allowed the system to not only meet the performance specifications, but to exceed them, and achieved these results after two separate reduction of order techniques (reduced-order observer and model reduction) were applied during the design process.
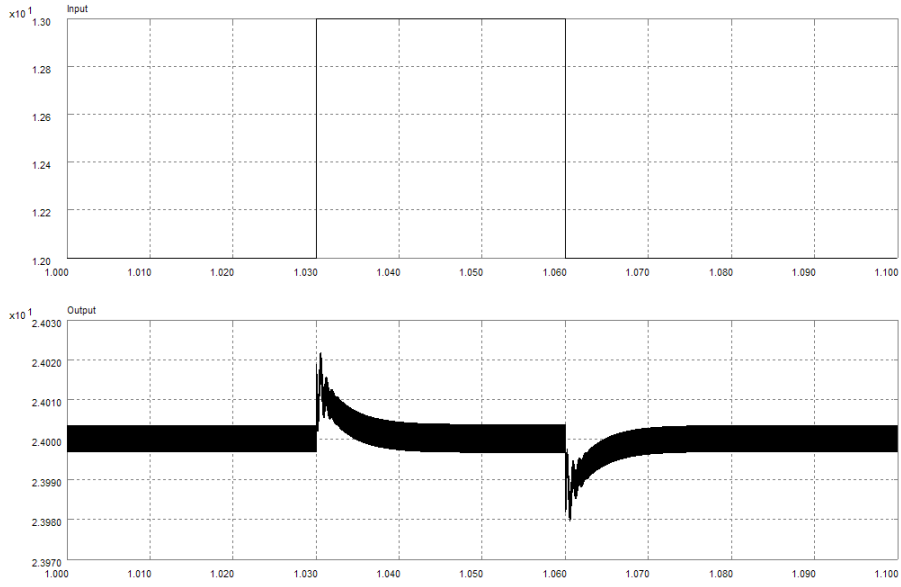
Figure 10.2: Unit step v_g disturbances and v_o response - MRROLQGI/LTR compensator.
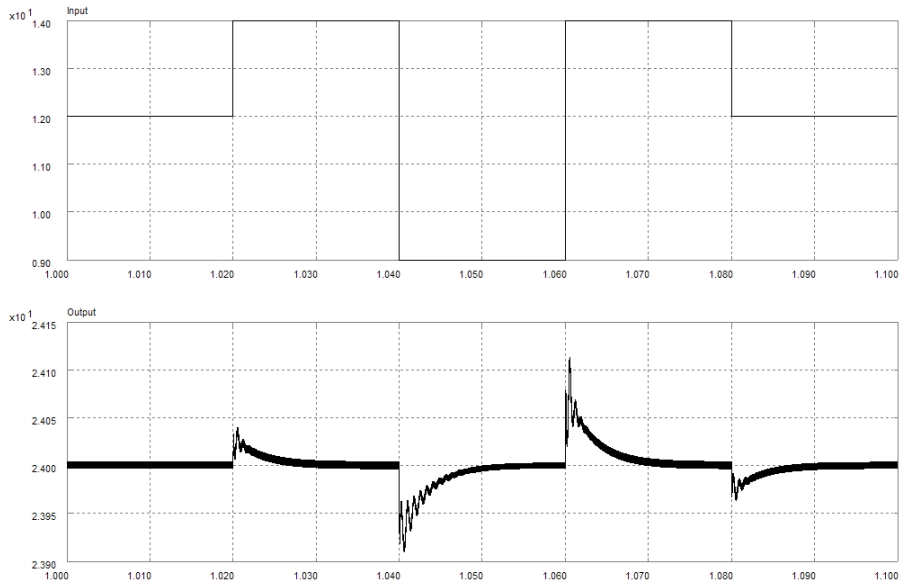
Figure 10.3: Large signal v_g disturbances and v_o response - MRROLQGI/LTR compensator.
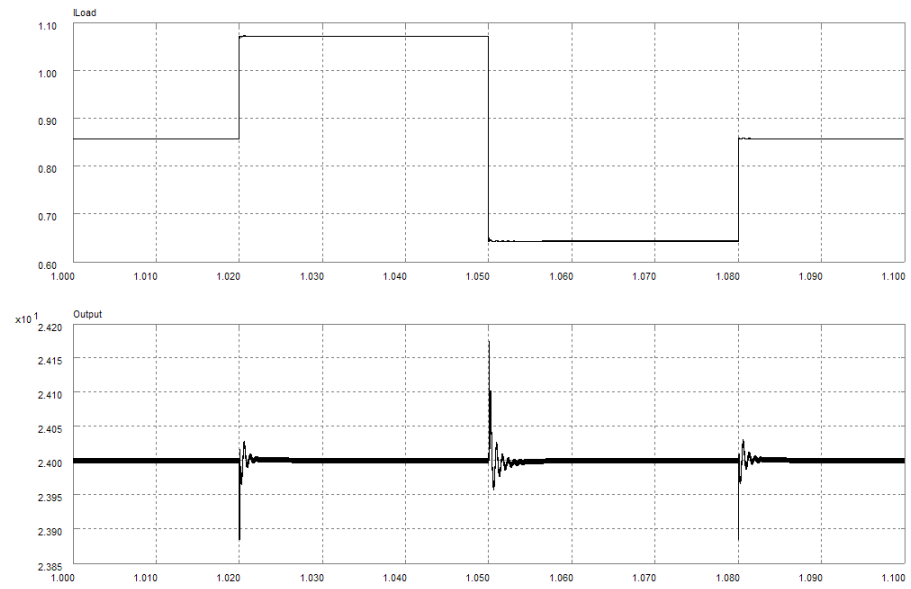
Figure 10.4: Load current disturbance and v_o response - MRROLQGI/LTR compensator.

Chapter 11

Conclusion

Part II demonstrated the process of applying modern control design methods to regulator design for DC-DC converters, and prototypically, to a Ćuk DC-DC converter. Full state feedback control for pole placement was applied - first without integral effort, then with an integrator added. Output compensation using state estimation techniques with full- and reduced-order observers was discussed and simulated. LQR and LQG/LTR techniques were then used to design compensators that were optimized with respect to quadratic performance indices based on state and control effort transients. Balanced realization of the LQGI/LTR compensator identified weakly controllable/observable states, which were then removed using truncation to create a third-order compensator (MR-LQGI/LTR) that could be implemented with a combination PI/Tow-Thomas biquad circuit.

The steps up to this point were typical application of modern state space control methods found in most textbooks. The method that followed (in Section 8.2) resulted in a minimal-order compensator. Namely, when the reduced-order Kalman filter-based compensator design (ROLQGI/LTR) was combined with model reduction using a balanced realization, the result was a second-order compensator (MRROLQGI/LTR) that could be implemented by an analog PID circuit. This MRROLQGI/LTR controller was applied to the Ćuk converter in a power electronics modeling environment and showed excellent input voltage and load current disturbance rejection abilities. The two-step order reduction combination of reduced-order observer design and truncated balanced realization is a novel design method that, while applied to one of the more complex DC-DC converters, appears to be applicable to compensator design in general.

Bibliography

[1] R. W. Erickson and D. Maksimović, *Fundamentals of Power Electronics*, 2nd ed.

[2] R. T. Stefani, B. Shahian, C. J. Savant, Jr., and G. H. Hostetter, *Design of Feedback Control Systems*, 4th ed.   New York, NY: Oxford University Press, 2002.

[3] B. A. Ogunnaike and W. H. Ray, *Process Dynamics, Modeling, and Control.* New York, NY: Oxford University Press, 1994.

[4] G. C. Verghese, "Dynamic modeling and control in power electronics," in *The Control Handbook*, W. S. Levine, Ed.   Boca Raton, FL: CRC Press LLC, 1996, ch. 78.1, pp. 1413–1424.

[5] G. F. Franklin, J. D. Powell, and A. Emami-Naeini, *Feedback Control of Dynamic Systems*, 3rd ed.   Boston, MA: Addison-Wesley, 1993.

[6] D. Graham and R. C. Lathrop, "The synthesis of optimum transient response: Criteria and standard forms," *Trans. AIEE*, vol. 72, pp. 273–288, Nov. 1953.

[7] B. N. Datta, *Numerical Methods for Linear Control Systems.*   San Diego, CA: Elsevier Academic Press, 2004.

[8] R. C. Dorf and R. H. Bishop, *Modern Control Systems*, 10th ed.   Upper Saddle River, NJ: Pearson Prentice Hall, 2005.

[9] B. D. O. Anderson and J. B. Moore, *Optimal Control: Linear Quadratic Methods.*   Englewood Cliffs, NJ: Prentice Hall, Inc., 1990.

[10] G. M. Siouris, *An Engineering Approach to Optimal Control and Estimation Theory.*   New York, NY: Wiley, 1996.

[11] J. C. Doyle, "Guaranteed margins for LQG regulators," *IEEE Trans. Automat. Contr.*, vol. 23, pp. 756–757, Aug. 1978.

[12] J. C. Doyle and G. Stein, "Robustness with observers," *IEEE Trans. Automat. Contr.*, vol. 24, pp. 607–611, Aug. 1979.

[13] B. M. Chen, "Theory of loop transfer recovery for multivariable linear systems," Ph.D. dissertation, Washington State Univ., Pullman, WA, Dec. 1991.

[14] A. Saberi and P. Sannuti, "Observer design for loop transfer recovery and for uncertain dynamical systems," *IEEE Trans. Automat. Contr.*, vol. 35, pp. 878–897, Aug. 1990.

[15] G. Stein and M. Athans, "The LQG/LTR procedure for multivariable feedback control design," *IEEE Trans. Automat. Contr.*, vol. 32, pp. 105–114, Feb. 1987.

[16] B. Friedland, *Control System Design: An Introduction to State-Space Methods.* New York, NY: McGraw-Hill, 1986.

[17] *MATLAB Control Systems Toolbox 6.0 User's Guide*, The Mathworks, 2004.

[18] R. S. Sánchez-Peña and M. Sznaier, *Robust Systems: Theory and Applications.* New York, NY: Wiley, 1998.

[19] A. N. Madiwale and D. E. Williams, "Some extensions of loop transfer recovery," in *Proc. of the American Control Conference (ACC'85)*, Boston, MA, June 1985, pp. 790–795.

[20] R. C. Jaeger, *Microelectronic Circuit Design.* Boston, MA: McGraw-Hill, 1997.

[21] W. J. Palm, *Control Systems Engineering.* New York, NY: Wiley, 1986.

The Ćuk Converter Model Derivations

Component Values

Ćuk converter circuit component values used in this paper:

$$
\begin{aligned}
L_1 &= 0.5\,mH \\
R_1 &= 0.01\,\Omega \\
L_2 &= 7.5\,mH \\
R_2 &= 0.01\,\Omega \\
M &= -1.5\,mH \\
C_1 &= 2.0\,\mu F \\
C_2 &= 20\,\mu F \\
R &= 28\,\Omega \\
V_g &= 12\,V \\
d &= 0.667 \\
f &= 100\,kHz
\end{aligned}
$$

Analysis of Inductors with Mutual Coupling and Equivalent Series Resistances

The equations for the voltage across two inductors L_1 and L_2 joined by mutual coupling are:

$$
\begin{aligned}
v_{L_1} &= L_1 \frac{di_1}{dt} + M \frac{di_2}{dt} \\
v_{L_2} &= M \frac{di_1}{dt} + L_2 \frac{di_2}{dt}
\end{aligned}
$$

The solutions of the two simultaneous equations are:

$$\frac{di_1}{dt} = \frac{L_2}{L_1 L_2 - M^2} v_{L_1} + \frac{-M}{L_1 L_2 - M^2} v_{L_2}$$

$$\frac{di_2}{dt} = \frac{-M}{L_1 L_2 - M^2} v_{L_1} + \frac{L_1}{L_1 L_2 - M^2} v_{L_2}$$

For the circuit with equivalent series resistances included in the inductor models when Q_1 conducts:

$$v_{L_1} = v_g - i_1 R_1$$

$$v_{L_2} = v_1 - v_2 - i_2 R_2$$

therefore:

$$\frac{di_1}{dt} = \frac{M}{\sigma^2} v_2 + \frac{-M}{\sigma^2} v_1 + \frac{MR_2}{\sigma^2} i_2 + \frac{-L_2 R_1}{\sigma^2} i_1 + \frac{L_2}{\sigma^2} v_g$$

$$\frac{di_2}{dt} = \frac{-L_1}{\sigma^2} v_2 + \frac{L_1}{\sigma^2} v_1 + \frac{-L_1 R_2}{\sigma^2} i_2 + \frac{MR_1}{\sigma^2} i_1 + \frac{-M}{\sigma^2} v_g$$

with $\sigma^2 = L_1 L_2 - M^2$.
When Q_1 does not conduct:

$$v_{L_1} = v_g - i_1 R_1 - v_1$$

$$v_{L_2} = -v_2 - i_2 R_2$$

therefore:

$$\frac{di_1}{dt} = \frac{M}{\sigma^2} v_2 + \frac{-L_2}{\sigma^2} v_1 + \frac{MR_2}{\sigma^2} i_2 + \frac{-L_2 R_1}{\sigma^2} i_1 + \frac{L_2}{\sigma^2} v_g$$

$$\frac{di_2}{dt} = \frac{-L_1}{\sigma^2} v_2 + \frac{M}{\sigma^2} v_1 + \frac{-L_1 R_2}{\sigma^2} i_2 + \frac{MR_1}{\sigma^2} i_1 + \frac{-M}{\sigma^2} v_g$$

with $\sigma^2 = L_1 L_2 - M^2$.

The State Space Averaged Model

State space averaging is a well-known method used in modeling switching converters. For a system with a single switching component with a nominal duty cycle, a model may be developed by determining the state and measurement equations for each of the two switch states, then calculating a weighted average of the two sets of equations using the nominal values of the time spent in each state as the weights. To develop the state space averaged model, the equations for the rate of inductor current change derived in the preceding section are used along with the equations for the rate of capacitor voltage change that may be

derived from the Ćuk converter circuit. For the purposes of modeling, the state vector is given by:

$$x = \begin{bmatrix} v_2 & v_1 & i_2 & i_1 \end{bmatrix}'$$

When Q_1 conducts, the following state space matrices result:

$$A_1 = \begin{bmatrix} -\frac{1}{RC_2} & 0 & \frac{1}{C_2} & 0 \\ 0 & 0 & \frac{-1}{C_1} & 0 \\ -\frac{L_1}{\sigma^2} & \frac{L_1}{\sigma^2} & -\frac{L_1 R_2}{\sigma^2} & \frac{M R_1}{\sigma^2} \\ \frac{M}{\sigma^2} & -\frac{M}{\sigma^2} & \frac{M R_2}{\sigma^2} & -\frac{L_2 R_1}{\sigma^2} \end{bmatrix}$$

$$B_1 = \begin{bmatrix} 0 \\ 0 \\ -\frac{M}{\sigma^2} \\ \frac{L_2}{\sigma^2} \end{bmatrix}$$

$$C_1 = \begin{bmatrix} 1 & 0 & 0 & 0 \end{bmatrix}$$

$$D_1 = [0]$$

When Q_1 is not conducting, the circuit model is represented by the following state space matrices:

$$A_2 = \begin{bmatrix} -\frac{1}{RC_2} & 0 & \frac{1}{C_2} & 0 \\ 0 & 0 & 0 & \frac{-1}{C_1} \\ -\frac{L_1}{\sigma^2} & \frac{M}{\sigma^2} & -\frac{L_1 R_2}{\sigma^2} & \frac{M R_1}{\sigma^2} \\ \frac{M}{\sigma^2} & -\frac{L_2}{\sigma^2} & \frac{M R_2}{\sigma^2} & -\frac{L_2 R_1}{\sigma^2} \end{bmatrix}$$

$$B_2 = \begin{bmatrix} 0 \\ 0 \\ -\frac{M}{\sigma^2} \\ \frac{L_2}{\sigma^2} \end{bmatrix}$$

$$C_2 = \begin{bmatrix} 1 & 0 & 0 & 0 \end{bmatrix}$$

$$D_2 = [0]$$

By representing the duty cycle of the switch as D_s, the following results may be obtained for a state space averaged model of the Ćuk converter:

$$D'_s \triangleq 1 - D_s$$

$$\frac{V_o}{V_g} = \frac{D_s}{1 - D_s} = \frac{D_s}{D'_s}$$

$$A = D_s A_1 + D'_s A_2$$
$$B = D_s B_1 + D'_s B_2$$
$$C = D_s C_1 + D'_s C_2$$
$$D = D_s D_1 + D'_s D_2$$
$$X = -A^{-1} B V_g$$
$$B_d = (A_1 - A_2) X + (B_1 - B_2) V_g$$
$$D_d = (C_1 - C_2) X + (D_1 - D_2) V_g$$

$$\dot{\tilde{x}} = A\tilde{x} + B\tilde{v}_g + B_d\tilde{d}$$
$$\tilde{v}_o = C\tilde{x} + D\tilde{v}_g + D_d\tilde{d}$$

where the tilde (˜) indicates a small signal deviation from nominal, and:

$$x = X + \tilde{x}$$
$$v_g = V_g + \tilde{v}_g$$
$$d = D_s + \tilde{d}$$
$$v_o = V_o + \tilde{v}_o$$

$$A = \begin{bmatrix} -\dfrac{1}{RC_2} & 0 & \dfrac{1}{C_2} & 0 \\[2mm] 0 & 0 & -\dfrac{D_s}{C_1} & \dfrac{1-D_s}{C_1} \\[2mm] -\dfrac{L_1}{L_1\,L_2-M^2} & \dfrac{D_s\,L_1+M-D_s\,M}{L_1\,L_2-M^2} & 0 & 0 \\[2mm] \dfrac{M}{L_1\,L_2-M^2} & \dfrac{-D_s\,M-L_2+L_2\,D_s}{L_1\,L_2-M^2} & 0 & 0 \end{bmatrix}$$

$$B = \begin{bmatrix} 0 \\[2mm] 0 \\[2mm] -\dfrac{M}{L_1\,L_2-M^2} \\[2mm] \dfrac{L_2}{L_1\,L_2-M^2} \end{bmatrix}$$

$$C = \begin{bmatrix} 1 & 0 & 0 & 0 \end{bmatrix}$$

$$D = [0]$$

$$B_d = \begin{bmatrix} 0 \\[2mm] -\dfrac{D_s\,V_g}{R(1-D_s)^2\,C_1} \\[2mm] \dfrac{V_g\,(L_1-M)}{(1-D_s)(L_1\,L_2-M^2)} \\[2mm] \dfrac{V_g\,(-M+L_2)}{(1-D_s)(L_1\,L_2-M^2)} \end{bmatrix}$$

$$D_d = [0]$$

The equilibrium state vector is:

$$X = \begin{bmatrix} V_2 \\[2mm] V_1 \\[2mm] I_2 \\[2mm] I_1 \end{bmatrix} = \begin{bmatrix} \dfrac{D_s\,V_g}{1-D_s} \\[2mm] \dfrac{V_g}{1-D_s} \\[2mm] \dfrac{D_s\,V_g}{R(1-D_s)} \\[2mm] \dfrac{D_s{}^2\,V_g}{R(1-D_s)^2} \end{bmatrix}$$

MATLAB Code

The SSA Ćuk Circuit Model

```matlab
% cuk_parameters.m
% Defines the state space averaged model for the Cuk converter

% Define physical inputs
clear
close all

Vg = 12;
Vo = 24;
r = 28;
c1 = 2*10^-6;
c2 = 2*10^-5;
d = Vo/(Vg+Vo);
l1 = 5*10^-4;
r1 = 0.01;
l2 = 7.5*10^-3;
r2 = 0.01;
m = -1.5*10^-3;

% Calculate state variables for each switch position
s2 = l1*l2-m^2;
A1 = [-1/(r*c2) 0        1/c2         0;
      0         0        -1/c1        0;
      -l1/s2    l1/s2    -l1*r2/s2    m*r1/s2;
      m/s2      -m/s2    m*r2/s2      -l2*r1/s2];
B1= [0; 0; -m/s2; l2/s2];
B2 = B1;
A2 = [-1/(r*c2) 0        1/c2         0;
      0         0        0            1/c1;
      -l1/s2    m/s2     -l1*r2/s2    m*r1/s2;
      m/s2      -l2/s2   m*r2/s2      -l2*r1/s2];
C1 = [1 0 0 0];
```

```matlab
C2 = C1;
D = 0;

% Calculate combined state variables given duty cycle d
d1 = 1-d;
A = d*A1+d1*A2;
B = d*B1+d1*B2;
C = d*C1+d1*C2;

% Calculate B matrix for control input - Bd
X = -A^-1*B*Vg;
Bd = (A1-A2)*X;

% Define the state space model from vg to vo
SYS = ss(A,B,C,D);

% Define the state space model from d to vo
SYSd = ss(A,Bd,C,D);

% Unit step response from disturbance input vg to vo
figure;
[y t] = step(SYS,0.03);
plot(t, 24+y);
xlabel('Time (s)');
ylabel('Amplitude (V)');

% Pole-zero map from d to vo
figure;
pzmap(SYSd);

% Open-loop Bode Plot from d to vo
figure;
bode(SYSd);

clear A1 A2 B1 B2 C1 C2 X s2 r c1 c2 l1 l2 m d1
```

Duty Cycle Calculations

```matlab
% duty_cycle_vs_input_v.m
% Plot the desired duty cycle to maintain output voltage
% at the nominal value as the input voltage varies

clc
clear all
close all
```

```
cuk_parameters;
vg = 9:0.01:14;

d_new = Vo./(vg + Vo);
delta_d = d_new-d;

% Plot change in duty cycle as vg is swept to keep Vo at 24 V
figure;
plot(vg, delta_d);
xlabel('Input Voltage (V)');
ylabel('\Delta Duty Cycle');
axis([9 14 -.04 .08]);
grid on

figure;
plot(vg, d_new);
xlabel('Input Voltage (V)');
ylabel('Duty Cycle');
axis([9 14 .62 .74]);
grid on
```

Full State Feedback

```
% fsfb.m
% Design of a Full State Feedback compensator for pole placement

cuk_parameters;

% Sweep scaling frequency and find frequency of
% steady state error <= 0.24
w0 = [10:.0001:10.03];
w0_length = length(w0);
sserr = zeros(size(w0));

wb = waitbar(0,'Sweeping ITAE Filter Scaling Frequency...');

for index = 1:length(w0);
    P = (w0(index))^4 * [-0.4240+1.2360i, -0.4240-1.2360i,...
        -0.6260+0.4141i, -0.6260-0.4141i];
k = place(A,Bd,P);
Abar = [A - Bd * k];
    SYS1 = ss(Abar,B,C,D);
    [y t] = step(SYS1,0.003);
    sserr(index) = abs(y(end));
```

```
    waitbar(index/w0_length, wb)
end
close(wb);

% figure;
% plot(w0,sserr);
% xlabel('Frequency Multiplier \omega (rad/s)');
% ylabel('Steady State Error (V)');

z = find(sserr<=.24);
w = w0(z(1,1));

% Use first frequency of steady state error <= 0.24 to scale the
% ITAE filter pole positions
P = w^4 * [-0.4240+1.2360i, -0.4240-1.2360i, ...
    -0.6260+0.4141i, -0.6260-0.4141i];
k = place(A,Bd,P);
Abar = [A-Bd*k];
SYS_FSFB = ss(Abar,B,C,D);

% Plot closed-loop system response to a unit step
% disturbance input
[y t x] = step(SYS_FSFB,0.002);
figure;
plot(t, 24+y);
xlabel('Time (s)');
ylabel('Amplitude (V)');

% System Loop Gain Plot
figure;
bode(A, Bd, k, 0);

% Control Effort Plot
figure;
plot(t, -k*x');
xlabel('Time (s)');
ylabel('\Delta Duty Cycle');
```

Full State Feedback with Integral Action

```
% fsfbi.m
% Design of a Full State Feedback compensator for pole placement
% with output integrator augmentation

cuk_parameters;
```

```
% Sweep frequency scalar and find frequency of minimum ITAE
w0 = [4:0.01:7];
w0_length = length(w0);
err_ITAE = zeros(size(w0));

wb = waitbar(0,'Sweeping ITAE Filter Scaling Frequency...');

for index = 1:length(w0);
    P = (w0(index))^5 * [-0.8955, ...
-0.3764+1.2920i,...
-0.3764-1.2920i,...
-0.5758+0.5339i,...
-0.5758-0.5339i];
    A_prime = [A zeros(size(B));C zeros(size(D))];
    Bd_prime = [Bd; 0];
    K = place(A_prime,Bd_prime,P);
    k = K(1:4);
    ki = K(end);
    Abar = [A-Bd*k, -Bd*ki; C, 0];
    Bbar = [B; 0];
    Cbar = [C 0];
    SYS1 = ss(Abar,Bbar,Cbar,D);
    [y t] = step(SYS1,0.005);
    err_ITAE(index) = sum(t.*abs(y));
    waitbar(index/w0_length, wb)
end

close(wb);

% Plot the ITAE as a function of the frequency multiplier
figure;
h = plot(w0,err_ITAE);
set(h, 'LineWidth', 2);
xlabel('Frequency Multiplier \omega (rad/s)');
ylabel('ITAE');

[ITAEmin n] = min(err_ITAE);
sprintf('Minimum ITAE error: %1.5f at %4.4f rad/s',ITAEmin,w0(n))

% Use frequency of minimum ITAE to scale the
% ITAE filter pole positions
P = (w0(n))^5 * [-0.8955, ...
-0.3764+1.2920i,...
-0.3764-1.2920i,...
-0.5758+0.5339i,...
```

```
-0.5758-0.5339i]];
A_prime = [A zeros(size(B));-C zeros(size(D))];
Bd_prime = [Bd; 0];
K = place(A_prime,Bd_prime,P);
k = K(1:4);
ki = K(end);

Abar = [A-Bd*k, -Bd*ki; -C, 0];
Bbar = [B; 0];
Cbar = [C 0];
SYS_FSFBI = ss(Abar,Bbar,Cbar,D);

% Plot closed-loop system response to a unit step
% disturbance input
[y t x] = step(SYS_FSFBI,0.002);
figure;
plot(t, 24+y);
xlabel('Time (s)');
ylabel('Amplitude (V)');

% System Loop Gain Plot
figure;
bode(A_prime, Bd_prime, K, 0);

% Control Effort Plot
figure;
plot(t, -K*x');
xlabel('Time (s)');
ylabel('\Delta Duty Cycle');
```

Estimated State Feedback with Integral Action

```
% esfbi.m
% Design of an Estimated State Feedback compensator
% for pole placement with output integrator augmentation
clc
clear
close all
cuk_parameters;

% Sweep scaling frequency and find frequency of minimum ITAE
w0 = [9.1:.001:9.2];
w0_length = length(w0);
err_ITAE = zeros(size(w0));
```

```
wb = waitbar(0,'Sweeping ITAE Filter Scaling Frequency...');
for index = 1:length(w0);
    Pk = (w0(index))^5 * [-0.8955, ...
-0.3764+1.2920i,...
-0.3764-1.2920i,...
-0.5758+0.5339i,...
-0.5758-0.5339i];
    Pl = (w0(index))^4 * [-0.4240+1.2360i, -0.4240-1.2360i, ...
        -0.6260+0.4141i, -0.6260-0.4141i];
    A_prime = [A zeros(size(B));-C zeros(size(D))];
    Bd_prime = [Bd; 0];
    C_prime = [C 0];
    K = place(A_prime,Bd_prime,Pk);
    k = K(1:4);
    ki = K(end);
    L = place(A', C', Pl)';
    Abar = [A,    -Bd*ki, -Bd*k;
            -C,   0, zeros(1,length(A));
            L*C, -Bd*ki, A-Bd*k-L*C];
    Bbar = [B; 0; zeros(4,1)];
    Cbar = [C 0 zeros(size(C))];
    SYS_ESFBI = ss(Abar,Bbar,Cbar,D);
    [y t] = step(SYS_ESFBI,0.003);
    err_ITAE(index) = sum(t.*abs(y));
    waitbar(index/w0_length, wb)
end
close(wb);

% Plot the ITAE value versus the scaling frequency for the ITAE
% filter pole locations
figure;
plot(w0,err_ITAE);
axis tight
xlabel('Scalar Multiplier \omega');
ylabel('ITAE');

[ITAEmin n] = min(err_ITAE);
w0(n);

% Use frequency of minimum ITAE to scale the ITAE filter
% pole positions for both controller and estimator
Pk = (w0(n))^5 * [-0.8955, ...
-0.3764+1.2920i,...
-0.3764-1.2920i,...
-0.5758+0.5339i,...
-0.5758-0.5339i];
```

```
Pl = w0(n)^4 * [-0.4240+1.2360i, -0.4240-1.2360i,...
        -0.6260+0.4141i, -0.6260-0.4141i];
A_prime = [A zeros(size(B));-C zeros(size(D))];
Bd_prime = [Bd; 0];
C_prime = [C 0];
K = place(A_prime,Bd_prime,Pk);
k = K(1:4);
ki = K(end);
L = place(A', C', Pl)';
Abar = [A,    -Bd*ki, -Bd*k;
        -C,   0, zeros(1,length(A));
        L*C, -Bd*ki, A-Bd*k-L*C];
Bbar = [B; 0; zeros(4,1)];
Cbar = [C 0 zeros(size(C))];
SYS_ESFBI = ss(Abar,Bbar,Cbar,D);

% Plot closed-loop system response to a unit step
% disturbance input
[y t x] = step(SYS_ESFBI,0.002);
figure;
plot(t, 24+y);
xlabel('Time (s)');
ylabel('Amplitude (V)');

%  System Loop Gain Plot
A1 = [A, zeros(4,1), zeros(4,4);
      -C, 0, zeros(1,4);
      L*C, -Bd*ki, A-Bd*k];
Bd1 = [Bd;0;zeros(4,1)];
C1 = [zeros(1,4), ki, k];
D1 = 0;
sys1 = ss(A1,Bd1,C1,D1);
figure;
bode(sys1,{1,1e6});

% Control Effort Plot
figure;
x = [x(:,6:end), x(:,5)];
plot(t, -K*x');
xlabel('Time (s)');
ylabel('\Delta Duty Cycle');
```

Reduced-Order Estimated State Feedback with Integral Action

```
% roesfbi.m
% Design of a Reduced-Order Estimated State Feedback compensator
% with output integral augmentation

cuk_parameters;

A11 = A(1,1);
A12 = A(1,2:4);
A21 = A(2:4,1);
A22 = A(2:4,2:4);

B1 = B(1);
B2 = B(2:4);

Bd1 = Bd(1);
Bd2 = Bd(2:4);

% Sweep scaling frequency and find frequency of minimum ITAE
w0 = [1:1:21];
w0_length = length(w0);
err_ITAE = zeros(size(w0));

wb = waitbar(0,'Sweeping ITAE Filter Scaling Frequency...');

for index = 1:length(w0);
    Pk = 6.564^5 * [-0.8955, ...
-0.3764+1.2920i,...
-0.3764-1.2920i,...
-0.5758+0.5339i,...
-0.5758-0.5339i];
    Pl = (w0(index))^3*[-0.7081, -0.5210+1.068i, -0.5210-1.068i];
    A_prime = [A zeros(size(B));-C zeros(size(D))];
    Bd_prime = [Bd; 0];
    C_prime = [C 0];
    K = place(A_prime,Bd_prime,Pk);
    km = K(1);
    ku = K(2:4);
    ki = K(end);
    L = place(A22', A12', Pl)';

    E = A22 - L*A12;
    F = E*L + A21 - L*A11;
```

```
    G = Bd2 - L*Bd1;

    Abar = [A-Bd*km*C-Bd*ku*L*C, -Bd*ki, -Bd*ku;
            -C,  zeros(1,4) ;
            F*C-G*km*C-G*ku*L*C, -G*ki, E-G*ku];
    Bbar = [B; 0; zeros(3,1)];
    Cbar = [C 0 zeros(1,3)];
    SYS1 = ss(Abar,Bbar,Cbar,D);
    [y t] = step(SYS1,0.003);
    err_ITAE(index) = sum(t.*abs(y));
    waitbar(index/w0_length, wb)
end
close(wb);

% Plot the ITAE value versus the scaling frequency for the ITAE
% filter pole locations
figure;
plot(w0,err_ITAE);
axis tight
xlabel('Scalar Multiplier \omega');
ylabel('ITAE');

[ITAEmin n] = min(err_ITAE);
w0(n);

% Determine controller and observer gains
Pk = 6.564^5 *[-0.8955, -0.3764+1.2920i, -0.3764-1.2920i,...
        -0.5758+0.5339i, -0.5758-0.5339i];
Pl = (w0(n))^3*[-0.7081, -0.5210+1.068i, -0.5210-1.068i];
A_prime = [A zeros(size(B));-C zeros(size(D))];
Bd_prime = [Bd; 0];
C_prime = [C 0];
K = place(A_prime,Bd_prime,Pk);
km = K(1);
ku = K(2:4);
ki = K(end);
L = place(A22', A12', Pl)';

E = A22 - L*A12;
F = E*L + A21 - L*A11;
G = Bd2 - L*Bd1;

Abar = [A-Bd*km*C-Bd*ku*L*C, -Bd*ki, -Bd*ku;
        -C,  zeros(1,4) ;
        F*C-G*km*C-G*ku*L*C, -G*ki, E-G*ku];
Bbar = [B; 0; zeros(3,1)];
```

```
Cbar = [C 0 zeros(1,3)];
SYS_ROESFBI = ss(Abar,Bbar,Cbar,D);

% Plot closed-loop system response to a unit step input
[y t] = step(SYS_ROESFBI,0.002);
figure;
plot(t, 24+y);
xlabel('Time (s)');
ylabel('Amplitude (V)');

% System Loop Gain Plot
A1 = [A, zeros(4,1), zeros(4,3);
      -C, 0, zeros(1,3);
       F*C-G*ku*L*C-G*km*C, -G*ki, E-G*ku];
Bd1 = [Bd; 0; zeros(3,1)];
C1 = [km*C+ku*L*C, ki, ku];
D = 0;
sys1 = ss(A1, Bd1, C1, D);
figure;
bode(sys1,{1e2,1e6});
```

Linear Quadratic Regulator with Integral Action

```
% lqri.m
% Designs a linear quadratic regulator for the
% Cuk converter with output integrator augmentation

cuk_parameters;

Cq = [C 0];
Q = Cq'*Cq;
Q(1,1) = 1;
Q(2,2) = 0;
Q(3,3) = 0;
Q(4,4) = 0;
Q(5,5) = 100000;
R = 1;

A_prime = [A zeros(size(B));-C zeros(size(D))];
Bd_prime = [Bd; 0];
B_prime = [B;0];
C_prime = [C 0];

% LQR System design
K = lqr(A_prime,Bd_prime,Q,R);
```

```
k = K(1:4);
ki = K(end);

Abar = [A - Bd * k, -Bd * ki; -C, 0];
Bbar = [B; 0];
Cbar = [C 0];

SYS_LQR = ss(Abar,Bbar,Cbar,D);

% LQR Step Response
[y t x] = step(SYS_LQR,0.02);
figure;
plot(t, 24+y, 'b');
xlabel('Time (s)');
ylabel('Amplitude (V)');

% LQR Loop Gain Plot
figure;
bode(A_prime, Bd_prime, K, 0);

% Control Effort Plot
figure;
plot(t, -K*x');
xlabel('Time, s');
ylabel('\Delta Duty Cycle');
```

Linear Quadratic Gaussian with Integral Action

```
% lqgi.m
% Design of a Linear Quadratic Gaussian Compensator
% with output integral augmentation

% Design of LQR compensator
lqri;

% LQG Design
Q0 = 1e6*eye(size(A));
R0 = 1;

[L,P,E] = lqe(A,eye(size(A)),C,Q0,R0);

% Construct the closed-loop system for time-domain
% response testing
Abar = [A,   -Bd*ki, -Bd*k;
        -C,  0, zeros(1,4);
```

```
        L*C, -Bd*ki, A-Bd*k-L*C];
Bbar = [B; 0; ones(4,1)];
Cbar = [C 0 zeros(size(C))];
SYS_LQG = ss(Abar,Bbar,Cbar,D);

% LQG Step Response
[y t x] = step(SYS_LQG, 0.02);
figure;
plot(t, 24+y, 'b');
xlabel('Time (s)');
ylabel('Amplitude (V)');

% LQR vs. LQG System Loop Gain Plot
A1 = [A, zeros(4,1), zeros(4,4);
      -C, 0, zeros(1,4);
      L*C, -Bd*ki, A-Bd*k];
B1 = [Bd;0;zeros(4,1)];
C1 = [zeros(1,4), ki, k];
D1 = 0;
figure;
sys_lqr = ss(A_prime, Bd_prime, K, 0);
sys_lqg = ss(A1, B1, C1, D1);
bode(sys_lqr,sys_lqg)
legend('LQRI','LQGI')

% Control Effort Plot
figure;
x1 = [x(:,6:end), x(:,5)];
h = plot(t, -K*x1');
xlabel('Time (s)');
ylabel('\Delta Duty Cycle');
```

Model-Reduced LQGI/LTR Design

```
% mrlqgi_ltr.m
% Designs LQGI/LTR and MRLQGI/LTR compensators
% for the Cuk converter
clc

% Design the LQR compensator
lqri;

R0 = 1;
% Open loop frequency response information - LQR
olsys = ss(A_prime,Bd_prime,K,0);
```

```matlab
% figure;
% % bode(olsys,{1e1,1e7});

% Plot the magnitude of the open loop LQR
figure;
bode(A_prime, Bd_prime, K, 0);
hold on

% Loop transfer recovery
q = [1,1e2,1e4,1e6];
for n = 1:length(q)
    Q0 = q(n)*Bd*Bd';
    [L,P,E] = lqe(A,eye(size(A)),C,Q0,R0);
    Aol = [    A, zeros(4,1),  zeros(4,4);
             -C,          0,   zeros(1,4);
           L*C,     -Bd*ki, A-Bd*k-L*C];
    Bol = [Bd; 0; zeros(4,1)];
    Col = [zeros(1,4), ki, k];
    sysol = ss(Aol,Bol,Col,D);

    % Plot the magnitude of the open loop LQGI/LTR
    bode(Aol, Bol, Col, D);
end
hold off
legend('LQRI','q=10^{0}','q=10^{2}','q=10^{4}',...
'q=10^{6}','Location','SouthWest')

% Compensator
Ao = [A-Bd*k-L*C, -Bd*ki;
      zeros(1,4),      0];
Lo = [L; -1 ];
focomp = ss(Ao,Lo,K,0);
[zc,pc,kc]=ss2zp(Ao,Lo,K,0);
focomp = zpk(zc,pc,kc)

% Pole-zero plot of full-order compensator
figure;
pzmap(focomp);

% Close-up
figure;
pzmap(focomp)
axis([-4e4,0.5e4,-1.5e4,1.5e4]);

% Reduce the order of the compensator
[focomp,g] = balreal(focomp);
```

```
g
elim = (g<5e-2)
mrcomp = modred(focomp,elim);
[zrc prc krc] = ss2zp(mrcomp.a,mrcomp.b,mrcomp.c,mrcomp.d);
% An added high-frequency zero results from model reduction.
% Restore the system gain prior to removing the high frequency
% zero using truncation.
krc = krc*abs(zrc(1,1));
zrc = zrc(2:3,1);
mrcompzp = zpk(zrc,prc,krc)
[mrcomp.a,mrcomp.b,mrcomp.c,mrcomp.d]  = zp2ss(zrc,prc,krc)

% Compensator Comparison Bode Plot
figure;
bode(focomp,mrcomp);
legend('LQGI/LTR','MRLQGI/LTR','Location','NorthWest');

% Plot step disturbance response with MRLQGI/LTR compensator
figure;
sys = ss(A,[B,Bd],C,D);
syscl = feedback(sys,mrcomp,[2],[1]);
[y,t,x] = step(syscl,0.02);
plot(t, 24+y(:,1,1));
```

Model-Reduced ROLQGI/LTR Design

```
% mrrolqgi_ltr.m
% Designs ROLQGI/LTR and MRROLQGI/LTR compensators
% for the Cuk converter
clc

% Design the LQR compensator
lqri;

% Partition the system in terms of measured and unmeasured states
A11 = A(1,1);
A12 = A(1,2:4);
A21 = A(2:4,1);
A22 = A(2:4,2:4);

Bd1 = Bd(1);
Bd2 = Bd(2:4);

% Partition the gain vector determined by linquadreg.m
k = K(1:4);
```

```matlab
km = K(1);
ku = K(2:4);
ki = K(end);

% Form the open-loop LQR system and plot the frequency response
olsys = ss(A_prime,Bd_prime,K,0);
[gm1 pm1 wgc1 wpc1] = margin(A_prime,Bd_prime,K,0);
gm1 = 20*log10(gm1);
figure;
bode(olsys,{1e1,1e7});
hold on

% Noise distribution matrices
F1 = 1e-4*eye(1,3);
F2 = 1e-5*diag([1,1,1]);

% White noise vector intensity
V1 = 1e-5*diag([1,1,1]);
V2 = 1e-5*1;

% Loop transfer recovery
q = [1e-10,1e-9,1e-8,1e-7];
for n = 1:length(q);
    V11 = F1*V1*F1'+q(n)^2*Bd1*V2*Bd1';
    V12 = F1*V1*F2'+q(n)^2*Bd1*V2*Bd2';
    V22 = F2*V1*F2'+q(n)^2*Bd2*V2*Bd2';

    Abar = A22-V12'*inv(V11)*A12;
    Vbar = V22-V12'*inv(V11)*V12;

    [Q,M,X] = care(Abar',A12',Vbar,V11);

    L = (Q*A12'+V12')*inv(V11);

    E = A22-L*A12;
    F = E*L+A21-L*A11;
    G = Bd2-L*Bd1;

    % Build open loop system with plant, observer, and state
    % feedback law
    Aol = [A, zeros(4,1), zeros(4,3);
            -C, 0, zeros(1,3);
            F*C-G*km*C-G*ku*L*C, -G*ki, E-G*ku];
    Bol = [Bd; 0; zeros(3,1)];
    Col = [km*C+ku*L*C, ki, ku];
    sysol = ss(Aol,Bol,Col,D);
```

```
    % Plot the frequency response of the open loop system
    bode(sysol,{1e1,1e7});
end
hold off
legend('LQRI','q=10^{-10}','q=10^{-9}','q=10^{-8}',...
'q=10^{-7}','Location','SouthWest')

% Define the reduced order compensator design
Ar = [E-G*ku, -G*ki;
      zeros(1,3), 0];
Br = [F-G*ku*L-G*km; -1];
Cr = [ku ki];
Dr = ku*L+km;
[zr pr kr] = ss2zp(Ar,Br,Cr,Dr);
rocomp = zpk(zr,pr,kr);

% Apply model reduction techniques
[rocomp,g] = balreal(rocomp);
g
elim = (g<5e-2)
mrrocomp = modred(rocomp,elim);
[zrr prr krr]=ss2zp(mrrocomp.a,mrrocomp.b,mrrocomp.c,mrrocomp.d);
mrrocompzp = zpk(zrr,prr,krr)

% Compensator Comparison Bode Plot
figure;
bode(rocomp,mrrocomp);

% Plot step disturbance response
figure;
sys = ss(A,[B,Bd],C,D);
syscl = feedback(sys,mrrocomp,[2],[1]);
[y,t,x] = step(syscl,0.02);
plot(t, 24+y(:,1,1));
xlabel('Time (s)');
ylabel('Amplitude (V)');

% Calculate component values for the MRROLQGI/LTR compensator
% There are five free parameters to find and four equations.
% Arbitrarily assign R3, calculate the remaining
% component values.
R3 = 100000
R2 = R3/krr
C2 = 1/(R3*abs(zrr(1,1)))
R1 = R2*abs(prr(2,1))/abs(zrr(2,1))-R2
```

```
C1 = 1/(R1*abs(zrr(2,1)))
```